SILVER(I) COMPLEXES AS MODEL CATALYSTS IN OLEFIN HYDROFORMYLATION

by

GERTRUIDA JACOBA SUSANNA VENTER

DISSERTATION

Submitted in accordance with the requirements for the degree

MASTER OF SCIENCE

at the

FACULTY OF NATURAL AND AGRICULTURAL SCIENCE

DEPARTMENT CHEMISTRY

at the

UNIVERSITY OF THE FREE STATE

SUPERVISOR: PROF A. ROODT
CO-SUPERVISOR: DR R. MEIJBOOM

November 2007

Preface

My dankbetuigings aan:

My Hemelse Vader vir die talente wat hy aan my gegee het, wat dit vir my moontlik gemaak het om hierdie projek aan te pak.

Prof. André Roodt vir die ongelooflike geleenthede wat hy nie net vir my nie, maar die hele groep skep, en op `n gereelde basis. Baie dankie vir die geleentheid wat ek kon kry om mense regoor die wêreld te ontmoet, en om kulture van ander lande te kon beleef. Dit was `n belewenis wat ek altyd sal koester.

Reinout Meijboom, vir jou insette gedurende my projek en die bystand wat jy verleen het met die skryf van verskillende tekste.

Die anorganiese groep van die Universiteit van die Vrystaat, in besonder die dames in kamer 15A. Julle is meer as kollegas, julle is vriende. Ek is ook baie dank verskuldig aan Fanie, Inus en Leo vir kristallografiese data en hulp met die verfyning van die kristaldata, asook aan Gideon vir alle KMR spektra.

Prof Ola Wendt and his group at the Chemistry department at the University of Lund, Sweden, as well as the organic group at this department, for the opportunity to study with you for two months and learn an enormous amount.

*The DST-NRF Centre of Excellence in Catalysis (c*change), the Research Fund of the University of the Free State, SASOL, THRIP, and the NRF for financial assistance.*

My ouers, Henk en Fransina, vir al die opofferings wat julle gemaak het sodat ek hierdie mylpaal kon bereik. Ek sal altyd alles waardeer wat julle vir my gedoen het, en

steeds doen. Ook wil ek dankie sê aan my ouma Truida, my sussie Celia en boeties Jaco en Willem, asook my skoonsus Hielien, vir hulle ondersteuning en liefde.

Al my maters, van die wat ek van kleins af ken, tot my koshuisvriende, lede van PSMK en ander voortrekkers en mense met wie ek `n huis gedeel het. Julle gee lewe aan my lewe!

I dedicate this study to God, without Whom nothing is possible.

Table of Contents

Table of Contents

Table of Contents

Abbreviations and Symbols

BINAP	2,2'-bis(diphenylphosphino)-1,1'-binaphthyl
Bu	Butyl
c	cyclo
cm	centimetre
CP/MAS	Cross-Polarization/Magic Angle Spinning
Cy	Cyclohexane
dm	decimetre
eq	equivalents
Et	Ethyl
g	gram
L	ligand
m	meta
Me	Methyl
mes	mesitylene
NMR	Nuclear Magnetic Resonance
o	ortho
OMe	Methoxy
p	para
Ph	Phenyl
Pr	Propyl
Pz	Pyrazolyl
T or temp	temperature
tol	tolyl
UV	Ultraviolet
Vis	Visible
X	halide, pseudo-halide

Abstract

Keywords: silver, phosphine, characterization, ligand exchange, kinetics, CO coordination, hydroformylation, magnetization transfer, X-ray, high-pressure infrared.

The aim of this study was to synthesize Ag(I) complexes of the type $[AgXL_n]$ (L = tertiary phosphine; n = 1-4; X = coordinating or non-coordinating anion) and explore the olefin hydroformylation activity and ligand exchange rates of these complexes.

Tertiary phosphine complexes of Ag(I) of the type $[AgXL_n]$ (L = P(*p*-tol)$_3$; n = 1-4; X = Br^-, ClO_4^-, PF_6^-) were synthesized and characterized through X-ray crystallography. Selected crystal data is shown in Table 1.

Table 1 Selected crystal data as obtained for the three Ag(I) crystal structures solved in this study.

Complex identification	**$[Ag\{P(p\text{-}tol)_3\}_4]PF_6$**	**$[Ag\{P(p\text{-}tol)_3\}_3]ClO_4 \cdot CH_3COCH_3$**	**$[Ag_4\{P(p\text{-}tol)_3\}_4Br_4] \cdot CH_3COCH_3$**
Space group	$P2_13$ (198)	$Pna2_1$ (33)	$R\bar{3}$ (148)
Crystal system	Cubic	Orthorhombic	Trigonal
$(Ag\text{-}P)_{max}$ (Å)	2.6142 (7)	2.485 (1)	2.408 (2)
$(Ag\text{-}P)_{min}$ (Å)	2.567 (1)	2.461 (1)	2.400 (1)
Maximum effective cone angle (°)	148.4	167.6	161.8

These complexes are comparable to similar complexes containing transition metals, other phosphine ligands or different counterions. Occurrences of similar structures in literature, however, were limited, indicating a field open to study. The behavior of Ag/PX_3 complexes in solution are not yet explored, due to, amongst others, rapid and complex kinetics, and could be expanded on in future.

The coordination of CO to these complexes for application as hydroformylation catalysts were investigated through high-pressure infrared spectroscopy. No evidence could be obtained through high-pressure infrared of coordination of CO to Ag(I) complexes. The aversion of the silver molecule to coordinate the CO molecule could be attributed to the coordination of bulky phosphine ligands, which could prevent the coordination of CO ligand to the metal centre, as well as the absence of a strong electron-accepting ligand, for example boron- or nitrogen-containing ligands. Another explanation is the high electron

density surrounding the silver atom, which prevents π-back bonding from the silver atom to the CO molecule.

Kinetics of the exchange rate between coordinated phosphine ligands in these complexes and free phosphine is important, as this exchange rate could have an influence on the coordination of other ligands on the silver atom. The exchange rate was investigated using a NMR technique called magnetic spin transfer, or spin saturation transfer. In this method, the sample is saturated at a specific frequency, and through the relaxation of the peak at that frequency the exchange between free and coordinated phosphine could be established. The sample was investigated for different concentrations, shown in Table 2 with the calculated values of the rate of exchange.

Table 2 Calculated values for k_{obs} and T_1

$[PPh_3]_{Total}$ (mM)	$[PPh_3]_{Free}$ (mM)	$[AgPF_6]$ (mM)	k_{obs} (s^{-1}) [a]	$\sigma(k_{obs})$ (s^{-1})	$T_{1,Free}$ (s) [a]	$T_{1,\ Coord}$ (s)
20.0	17.81	0.5411	7.167	1.595	8.285	0.5867
10.0	8.92	0.4270	7.609	1.444	4.808	0.8704
5.0	3.16	0.4624	6.640	1.341	4.049	0.6332

a) No e.s.d.'s were obtained from the fitting program, but are estimated to be ca. 10%.

The rate of exchange at different concentrations is shown in Figure 1.

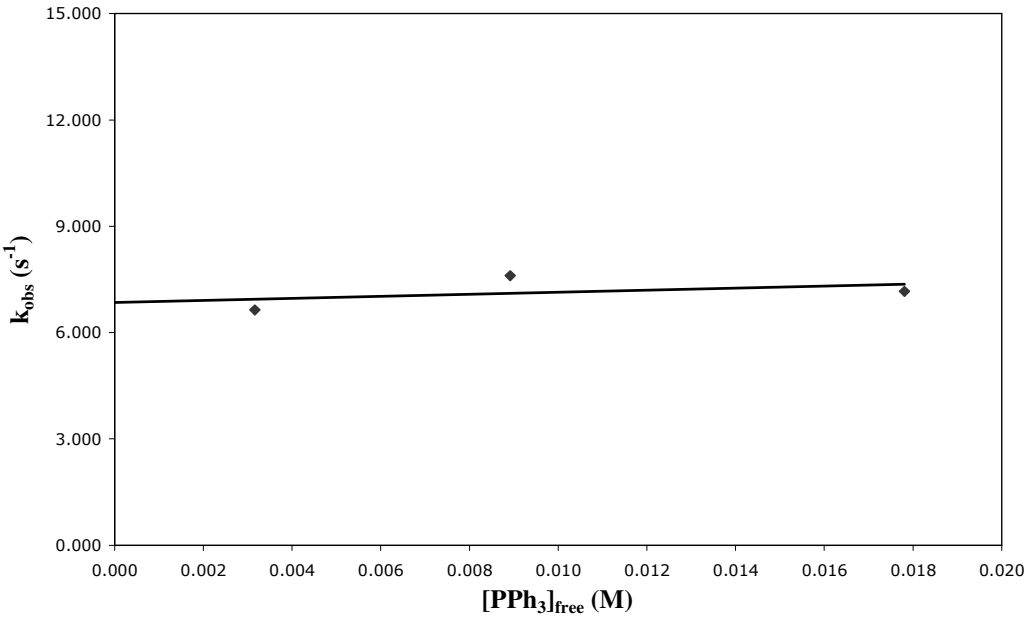

Figure 1 Rate of exchange vs. $[PPh_3]_{Free}$

Abstract

The observed rate of exchange of free phosphine with coordinated phosphine is fast, in ca. 7 s^{-1} at -80 °C, with an average value of 29±60 $mM^{-1}.s^{-1}$ for k_1 and 6.9±0.7 s^{-1} for k_{-1}. The rate of exchange between coordinated and free phosphine has been found to be independent of the concentration of phosphine, indicating a dissociative mechanism.

Since no evidence could be obtained of coordination of CO to the metal centre, application of complexes of Ag(I) of the type $[AgXL_n]$ (L = tertiary phosphine; n = 1-4; X = coordinating or non-coordinating anion) as hydroformylation catalysts does not seem feasible.

Opsomming

Die doel van hierdie studie was die sintese van Ag(I) komplekse van die tipe [$AgXL_n$] (L = tersiêre fosfien; n = 1-4; X = koördinerende of nie-koördinerende anioon) en verkenning van die olefien hidroformileringsaktiwiteit en liganduitruilings-tempo's van hierdie komplekse.

Tersiêre fosfien komplekse van Ag(I) van die tipe [$AgXL_n$] (L = P(*p*-tol)$_3$; n = 1-4; X = Br^-, ClO_4^-, PF_6^-) is gesintetiseer en gekarakteriseer deur X-straal kristallografie. Gekose kristaldata word in Tabel 1 aangedui.

Tabel 1 Gekose kristaldata soos verkry vir die drie Ag(I) kristalstukture bespreek in hierdie studie.

Kompleks identifikasie	**[Ag{P(*p*-tol)$_3$}$_4$]PF_6**	**[Ag{P(*p*-tol)$_3$}$_3$]ClO_4 ·CH_3COCH_3**	**[Ag_4{P(*p*-tol)$_3$}$_4Br_4$] ·CH_3COCH_3**
Ruimtegroep	$P2_13$ (198)	$Pna2_1$ (33)	$R\bar{3}$ (148)
Kristalstelsel	Kubies	Ortorombies	Trigonaal
$(Ag\text{-}P)_{maks}$ (Å)	2.6142 (7)	2.485 (1)	2.408 (2)
$(Ag\text{-}P)_{min}$ (Å)	2.567 (1)	2.461 (1)	2.400 (1)
Maksimum effektiewe keël hoek (°)	148.4	167.6	161.8

Hierdie komplekse is vergelykbaar met soortgelyke komplekse wat oorgangsmetale, ander fosfien ligande of verskillende teenione bevat. Die voorkoms van soortgelyke strukture in literatuur is egter beperk, wat `n gunstige area vir verdere studie aandui. Die gedrag van Ag/PX_3 komplekse in oplossing is nog nie verken nie, as gevolg van, onder andere, vinnige en ingewikkelde kinetika, en kan uitgebrei word in die toekoms.

Die koördinasie van hierdie komplekse met CO, vir toepassing as hidroformileringskataliste, is ondersoek deur middel van hoëdruk infrarooi spektroskopie. Geen bewyse van koördinering van CO met Ag(I) komplekse kon egter deur hoëdruk infrarooi spektroskopie gevind word nie. Die antipatie van die silwer molekule om die CO molekule te koördineer kan toegeskryf word aan die koördinasie van lywige fosfien ligande, wat die koördinasie van CO ligande aan die metaal senter kan verhoed, asook die afwesigheid van 'n sterk elektron-ontvangende ligand, byvoorbeeld boor- of

stikstofbevattende ligande. Nog `n verduideliking is die hoë elektrondigtheid wat die silwer atom omring en π-terugbinding van die silwer atoom na die CO molekule verhoed.

Kinetika van die tempo van uitruiling tussen gekoördineerde fosfiene in die kompleks en vry fosfien is belangrik, aangesien hierdie uitruilingstempo moontlik `n invloed kan hê op die koördinering van die silwer atoom met ander ligande. Die uitruilingstempo is ondersoek deur middel van `n KMR tegniek genaamd magnetiese spin oordrag, of spin versadigingsoordrag. Met hierdie metode word die monster by `n spesifieke frekwensie versadig, en deur die ontspanning van die piek by daardie frekwensie kan die uitruiling tussen vry en gekoördineerde fosfien bestudeer word. Verskillende konsentrasies van die monster is ondersoek, wat saam met die berekende waardes van die tempo van uitruiling in Tabel 2 verskyn.

Tabel 2 Berekende waardes vir k_{obs} en T_1

$[PPh_3]_{Totaal}$ (mM)	$[PPh_3]_{Vry}$ (mM)	$[AgPF_6]$ (mM)	k_{obs} (s^{-1}) [a]	$\sigma(k_{obs})$ (s^{-1})	$T_{1,Vry}$ (s) [a]	$T_{1,Koörd}$ (s)
19.97	17.81	0.5411	7.167	1.595	8.285	0.5867
10.00	8.92	0.4270	7.609	1.444	4.808	0.8704
5.01	3.16	0.4624	6.640	1.341	4.049	0.6332

a) Geen geskatte standaardafwykings is verkry uit die berekeningsprogram nie, maar word geskat as ca. 10%.

Die tempo van uitruiling vir die verskillende konsentrasies word aangedui in Figuur 1.

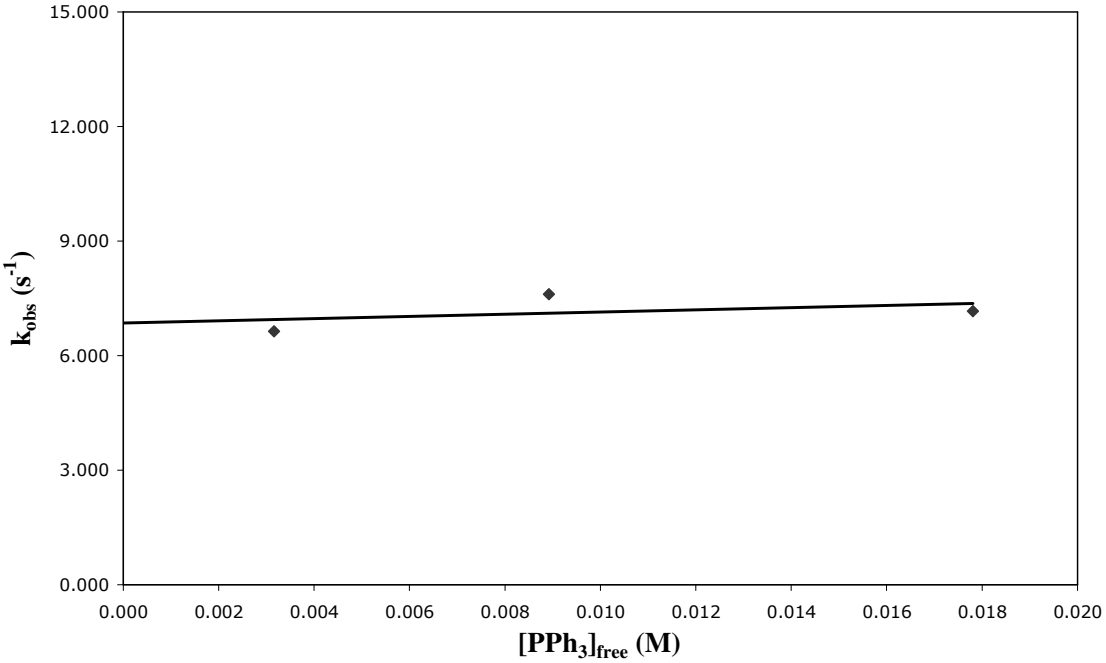

Figuur 1 Tempo van uitruling teenoor $[PPh_3]_{Vry}$

Die waargeneemde tempo van uitruiling van die vry fosfien met die gekoördineerde fosfien is vinnig, ca. 7 s^{-1} by -80 °C, met `n waarde van 29±60 $mM^{-1}.s^{-1}$ vir $k_1$ en 6.9±0.7 $s^{-1}$ vir $k_{-1}$. Die tempo van uitruiling is onafhanklik van die konsentrasie van die fosfien, wat `n dissosiatiewe meganisme aandui.

Aangesien geen bewyse gevind kon word van koordinasie van CO aan die metaal senter nie, is die toepassing van komplekse van Ag(I) van die tipe $[AgXL_n]$ (] (L = tersiêre fosfien; n = 1-4; X = koördinerende of nie-koördinerende anioon) as hydroformileringskataliste nie uitvoerbaar nie.

1 Introduction

1.1 Introduction

1.1.1 SILVER

Silver has the symbol Ag, which stems from the Latin word Argentum. It is a soft white lustrous transition metal that occurs both in minerals and free form and is used in coins, jewellery, tableware, photography and mirrors. The electrical conductivity of silver is the highest of all metals with σ = 63 106 $m^{-1}.\Omega^{-1}$, even higher than copper with σ = 59.6106 $m^{-1}.\Omega^{-1}$, but its tarnishability and greater cost prevents it from being used for electrical purposes instead of copper[1].

Pure silver also has the highest thermal conductivity (429 $W.m^{-1}.K^{-1}$), high optical reflectivity (although it is a poor reflector of ultraviolet light), and the lowest contact resistance of any metal. It is stable in pure air and water, but does tarnish when it is exposed to ozone, hydrogen sulphide, or sulphur-containing air. The most common oxidation state of silver is +1, though a few +2 and +3 compounds are also known.

Silver can be found in native form or combined with sulphur, arsenic, antimony, or chlorine and in various ores such as argentite (Ag_2S) and horn silver (AgCl). The principal sources of silver are copper, copper-nickel, gold, lead and lead-zinc ores obtained from Mexico (historically Batopilas), Peru, Australia, China and Chile, with the largest silver producer being Peru. Peru produced 2908.7 t (102.6 Moz) in 2005, about 15.8% of the annual production of the world. This metal is also obtained during the electrolytic refining of copper. Commercial grade fine silver is at least 99.9% pure silver and purities greater than 99.999% are available. Silver iodide smoke even has the property of causing snowflakes to form in a supercooled cloud[2].

---

[1] D.R. Lide, *CRC Handbook of Chemistry and Physics, 86th edition*, CRC Press (2002-2005).
[2] B. Vonnegut, *J. Applied Phys.*, **18**, 593 (1947).

Phosphorous ligands readily coordinate to silver, even though studies concerning silver-phosphorous ligands have been neglected in the past. Previous studies were mainly conducted in the 1970's and early 1980's, without concerning the possible exploitations of these complexes in catalysis or for other practical applications. The Lewis acid nature of the silver atom allows for the donation of σ-electrons from the phosphorous atom, as well as other elements in group 15, most often nitrogen and arsenic.

1.1.2 LIGANDS

In the oldest "homogeneous" catalyst systems, the enzymes, nitrogen ligands are the predominating donor atoms. They occurred in imidazoles, porphyrins etc. that are involved in many oxidation reactions. Thus, there are numerous derivations of nitrogen ligands used in homogenous catalysis, such as the oxidation of C-H bonds or oxidative coupling reactions of phenols[3]. Nitrogen is found on the periodical table in group 15, the same group as phosphorous.

The most common phosphorous donating ligands are known as phosphines (PR_3) or phosphites ($P\{OR\}_3$) and form a wide variety of complexes, for example the very common triphenylphosphine. The best-known application for a metal complex containing this ligand is as homogenous catalyst for hydrogenation of olefins. This complex, $[RhCl(PPh_3)_3]$, is known as Wilkinson's catalyst[4]. $[RhCl(PPh_3)_3]$ reacts with CO to give $[RhCl(CO)(PPh_3)_2]$, which is isostructural to Vaska's complex, $[IrCl(CO)(PPh_3)_2]$[5], and has the ability to decarbonylate aldehydes. The steric and electronic properties of phosphine ligands can be altered by changing the substituents on the ligand. Electronically, phosphorous ligands can either act as strong σ-donors (eg. t-Bu substituents) or strong π-acceptors (eg. fluoroalkoxide substituents). More bulky substituents on phosphine ligands exhibit stronger π-accepting properties, and when the range is extended to include phosphites, a region is reached where the σ-donating and π-accepting properties of the phosphorous ligand simulates the properties of a CO molecule. Therefore, investigations into the kinetic reactions involving phosphine and

[3] a) P.W.N.M. van Leeuwen, *Homogeneous Catalysis: Understanding the art*, Kluwer Academic Publishers (2004). b) P. Gamez, J.A.P.P. van Dijk, W.L. Driessen, G. Challa, J. Reedijk, *Synth. Catal.*, **344**, 890 (2002).
[4] J.A. Osborn, F.H. Jardine, J.F. Young, G. Wilkinson, *J. Chem. Soc. A*, 1711 (1966).
[5] L. Vaska, J.W. DiLuzio, *J. Am. Chem. Soc.*, **83**, 2784 (1961).

phosphite complexes are necessary to model the reaction of a CO molecule with a silver atom.

1.1.3 CATALYTIC PROCESS

Hydroformylation is the most widely used homogeneous catalytic industrial process for the production of aldehydes[6], and involves the reaction of alkenes with hydrogen and carbon monoxide, in the presence of a catalyst, to yield either linear (normal) or branched (iso) aldehydes. The reaction is illustrated in Scheme 1.1.

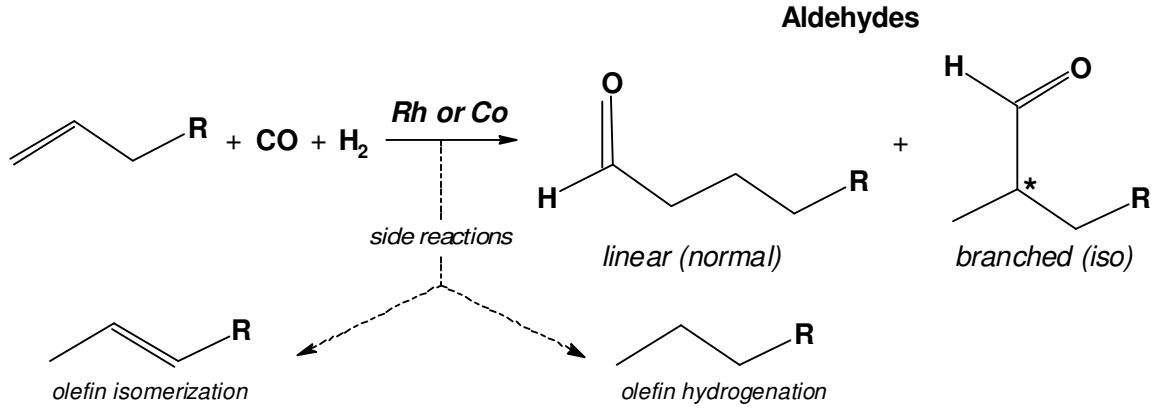

Scheme 1.1 The oxo reaction, or hydroformylation of aldehydes.

The most common catalysts/catalytical precursors for hydroformylation are $[Co_2(CO)_8]$ and $[RhH(CO)_2(PPh_3)_2]$[3.a)]. Both have the ability to coordinate hydrogen and utilize CO as a ligand. The ability to coordinate an olefin is extremely important, as reaction of the CO with the olefin occurs intramolecular, in the form of CO insertion into the metal-alkyl bond, to form a metal complex acyl. The molecule then undergoes oxidative addition with H_2, followed by reductive elimination to liberate the aldehyde and regenerate the catalyst.

1.2 Aim of study

In the periodical table, Ag forms part of the copper triad in group 11, and is located two groups from Rh and Co, which are in group 9. Rh and Co are known hydroformylation catalysts, and Au also exhibits hydroformylation activity. Compared to these metals, Ag

[6] A.M. Trzeciak, J.J. Ziolkowski, *Coord. Chem. Rev.*, **190-192**, 883-900 (1999).

is fairly cheap and easily available. The application of Ag complexes as catalysts would constitute a financial gain for companies, as well as preservation of limited Rh resources.

The goal in designing an effective catalyst system is to optimize the production of the desired products under the mildest conditions. Since higher turnover frequencies, higher linear to branched ratios, and low production of side reaction products are usually required, much effort has been spent to attempt to design catalyst systems with these goals in mind. A catalyst therefore needs to coordinate hydrides, carbonyls and olefins simultaneously, as well as undergo oxidative addition and reductive elimination. Research continues in the design of new ligands and catalyst systems.

Although examples of carbonyl coordinated to silver are known[7], these instances are limited. The silver-carbonyl complexes in literature have electron-accepting counterions, which may be an indication of the electronic influences on the formation of these complexes. Most silver hydrides are only present in silver clusters which are contained in zeolite hosts[8]. Substances containing olefinic bonds readily coordinate to silver, with more than 163 such complexes characterized via X-ray crystallography[9]. Some of these coordinated olefins include ethene[10], benzene and derivatives thereof[11] and nonplanar

[7] a) P.K Hurlburt, O.P. Anderson, S.H. Strauss, *J. Am. Chem. Soc.*, **113**, 6277 (1991). b) P.K. Hurlburt, J.J. Rack, S.F. Dec, O.P. Anderson, S.H. Strauss, *Inorg. Chem.*, **32**, 373 (1993). c) P.K. Hurlburt, J.J. Rack, J.S. Luck, S.F. Dec, J.D. Webb, O.P. Anderson, S.H. Strauss, *J. Am. Chem. Soc.*, **116**, 10003 (1994). d) H.V.R. Dias, W. Jin, *J. Am. Chem. Soc.*, **117**, 11381 (1995).

[8] a) S. Zhao, Z.-P. Liu, Z.-H. Li, W.-N. Wang, K.-N. Fan, *J. Phys. Chem. A*, **110**, 11537 (2006). b) T. Baba, H. Sawada, T. Takahashi, M. Abe, *Appl. Catal., A*, **231**, 55 (2002). c) T. Baba, N. Komatsu, H. Sawada, Y. Yamaguchi, T. Takahashi, H. Sugisawa, Y. Ono, *Langmuir*, **15**, 7894 (1999).

[9] The Cambridge Structural Database Version 1.9, F.H. Allen, *Acta Cryst.*, **B58**, 380 (2002).

[10] a) I. Krossing, A. Reisinger, *Angew. Chem., Int. Ed.*, **42**, 5725 (2003). b) H.V.R. Dias, Z. Wang, W. Jin, *Inorg. Chem.*, **36**, 6205 (1997).

[11] a) R. Uson, A. Laguna, M. Laguna, B.R. Manzano, P.G. Jones, G.M. Sheldrick, *J. Chem. Soc., Dalton Trans.,* 285 (1984). b) L.P. Wu, M. Munakata, T. Kuroda-Sowa, M. Maekawa, Y. Suenaga, Y. Kitamori, *Inorg. Chim. Acta*, **290**, 251 (1999). c) S.H. Strauss, M.D. Noirot, O.P. Anderson, *Inorg. Chem.*, **24**, 4307 (1985). d) M. Munakata, L.P. Wu, T. Kuroda-Sowa, M. Maekawa, Y. Suenaga, G.L. Ning, T.Kojima, *J. Am. Chem. Soc.*, **120**, 8610 (1998). e) C.-W. Tsang, J. Sun, Z. Xie, *J. Organomet. Chem.*, **613**, 99 (2000). f) H. Hatop, H.W. Roesky, T. Labahn, C. Ropken, G.M. Sheldrick, M. Bhattachatjee, *Organometallics*, **17**, 4326 (1998).

aromatic compounds[12]. Exchange between the silver coordinated phosphine and free phosphine is very rapid[13], which may influence the coordination of other ligands to silver.

Based on the above, the following stepwise aims were set for this study:

a) Characterization of tertiary phosphine complexes of Ag(I) of the type $[AgXL_n]$ (L = tertiary phosphine; n = 1-4; X = coordinating or non-coordinating anion) using X-ray crystallography.

b) Investigation of CO coordination to tertiary phosphine complexes of Ag(I) of the type $[AgXL_n]$ using high pressure infrared spectroscopy.

c) Examination of hydroformylation activity of tertiary phosphine complexes of Ag(I) of the type $[AgXL_n]$.

d) Study of the exchange mechanism of L in $[AgXL_4]$ (X = non-coordinating anion).

[12] a) M. Munakata, L.P. Wu, K. Sugimoto, T. Kuroda-Sowa, M. Maekawa, Y. Suenaga, N. Maeno, M. Fujita, *Inorg. Chem.*, **38**, 5674 (1999). b) A. Bailey, T.S. Corbitt, M.J. Hampden-Smith, E.N. Duesler, T.T. Kodas, *Polyhedron*, **12**, 1785 (1993). c) A. Albinati, S.V. Meille, G. Carturan, *J. Organomet. Chem.*, **182**, 269 (1979).

[13] E.L. Muetterties, C.W. Alegranti, *J. Am. Chem. Soc.*, **94**, 6386 (1972).

2 Literature Overview

2.1 Introduction

Silver complexes have been known to act as catalysts for various processes, including carbene-insertion[1], hydrogenation[2], oxidation/reduction reactions[3], imination[4] and hydrogen generation[5], to name a few. A silver atom in a complex can have either positive or negative[6] character, thus creating the possibility of a multitude of reactions. Complexes containing phosphines as ligands have also been known to act as catalysts for a variety of processes[7], with one of the best known applications being hydroformylation with rhodium as metal centre[8]. Hydroformylation of aldehydes is also called the oxo process and involves the reaction of an olefin with carbon monoxide and hydrogen in the presence of a catalyst. A catalyst applied in hydroformylation should therefore exhibit the following properties: the ability to coordinate hydrogen as well as carbon monoxide, ability of forming a metal-alkyl complex and capability to undergo oxidative addition and reductive elimination. Silver readily forms alkyl complexes[9], but literature citations of

---

[1] H.V.R. Dias, R.G. Browning, S.A. Polach, H.V.K. Diyabalanage, C.J. Lovely, *J. Am. Chem. Soc.*, **125**, 9270 (2003).

[2] a) P. Claus, H. Hofmeister, *J. Phys. Chem. B.*, **103**, 2766 (1999). b) W. Grunert, A. Bruckner, H. Hofmeister, P. Claus, *J. Phys. Chem. B*., **108**, 5709 (2004).

[3] a) H. Kestenbaum, A. Lange de Oliveira, W. Schmidt, F. Schuth, W. Ehrfeld, K. Gebauer, H. Lowe, T. Richter, D. Lebiedz, I. Untiedt, H. Zuchner, *Ind. Eng. Chem. Res*., **41**, 710 (2002). b) J.P. Breen, R. Burch, C. Hardacre, C.J. Hill, *J. Phys. Chem. B*., **109**, 4805 (2005). c) E.F. Iliopoulou, E.A. Efthimiadis, I.A. Vasalos, *Ind. Eng. Chem. Res*., **43**, 1388 (2004).

[4] G.Y. Cho, C. Bolm, *Org. Lett*., **7**, 4983 (2005).

[5] N. Kakuta, N. Goto, H. Ohkita, T. Mizushima, *J. Phys. Chem. B*., **103**, 5917 (1999).

[6] a) J. Kleinberg, *Chem. Rev*., **40**, 381 (1947) b) W. Khayata, D. Baylocq, F. Pellerin, N. Rodier, *Acta Cryst.*, **C40**, 765 (1984). c) Y. Yoshida, K. Muroi, A. Otsuka, G. Saito, M. Takahashi, T. Yoko, *Inorg. Chem.*, **43**, 1458 (2004).

[7] a) I.C. Stewart, R.G. Bergman, F.D. Toste, *J. Am. Chem. Soc*., **125**, 8696 (2003). b) E. Vedejs, J.A. MacKay, *Org. Lett*., **3**, 535 (2001). c) N. Mezailles, L. Ricard, F. Gagosz, *Org. Lett*., **7**, 4133 (2005).

[8] B. Cornils, W.A. Herrmann, M. Rasch, *Angew. Chem., Int. Ed.*, **33**, 2144 (1994).

[9] a) B. Donnio, D.W. Bruce, *J. Mater. Chem*., **8**, 1993 (1998). b) H. Nagasawa, M. Maruyama, T. Komatsu, S. Isoda, T. Kobayashi, *Phys. Stat. Sol*., **191**, 67 (2002). c) S. Kuwajima, Y. Okada, Y. Yoshida, K. Abe, N. Tanigaki, T. Yamaguchi, H. Nagasawa, K. Sakurai, K. Yase, *Colloids Surf. A*, **197**, 1 (2002). d) H. Nagasawa, M. Nakamoto, K. Yase, T. Yamaguchi, *Mol. Cryst. Liq. Cryst*., **322**, 179 (1998).

silver complexes containing carbon monoxide are limited[10]. The silver-carbonyl complexes in literature have electron-donating counterions, which may be an indication of the electronic influences on the formation of these complexes. Most silver hydrides are only present in silver clusters which are contained in zeolite hosts[11].

Phosphine ligands readily coordinate to silver, exhibiting a variety of geometries dependent on the ratio of silver to phosphine, as well as the size of the phosphine ligand and the coordination ability of the counterion. Complexes containing a phosphine coordinated to silver are generally stable towards air and light, though some crystals may disintegrate upon exposure to air evaporation of the solvent of crystallization.

2.2 Trivalent Phosphorous-Containing Ligands

2.2.1 INTRODUCTION[12]

Phosphine is the common name for phosphorous hydride (PH_3), also known by the IUPAC name phosphane and, occasionally, phosphamine. It is a colourless, flammable gas that boils at −88 °C at standard pressure. Pure phosphine is odourless, but "technical grade" phosphine has a highly unpleasant odour like garlic or rotting fish, due to the presence of substituted phosphine and diphosphine (P_2H_4). Substituted, or tertiary phosphines, with the structure PR_3, are also known as phosphines, occurring as white powders, crystals or liquids. Other functional groups then substitute the hydrogen atoms of the original phosphine. Examples include triphenylphosphine ($P(C_6H_5)_3$) and BINAP (2,2'-bis(diphenyl-phosphino)-1,1'-binaphthyl), both used as phosphine ligands in metal complexes such as Wilkinson's catalyst. Phosphines coordinate to various metal ions, and therefore have important application in catalysis.

---

[10] a) P.K. Hurlburt, O.P. Anderson, S.H. Strauss, *J. Am. Chem. Soc.*, **113**, 6277 (1991). b) P.K. Hurlburt, J.J. Rack, S.F. Dec, O.P. Anderson, S.H. Strauss, *Inorg. Chem.*, **32**, 373 (1993). c) P.K. Hurlburt, J.J. Rack, J.S. Luck, S.F. Dec, J.D. Webb, O.P. Anderson, S.H. Strauss, *J. Am. Chem. Soc.*, **116**, 10003 (1994). d) H.V.R. Dias, W. Jin, *J. Am. Chem. Soc.*, **117**, 11381 (1995).

[11] a) S. Zhao, Z.-P. Liu, Z.-H. Li, W.-N. Wang, K.-N. Fan, *J. Phys. Chem. A*, **110**, 11537 (2006). b) T. Baba, H. Sawada, T. Takahashi, M. Abe, *Appl. Catal., A*, **231**, 55 (2002). c) T. Baba, N. Komatsu, H. Sawada, Y. Yamaguchi, T. Takahashi, H. Sugisawa, Y. Ono, *Langmuir*, **15**, 7894 (1999).

[12] E. Fluck, *The chemistry of phosphine: Topics in Current Chemistry,* Springer, Berlin, **35**, 64 (1973).

Phosphine (PH_3) may be prepared in a variety of ways[13]. Industrially it can be made by the reaction of white phosphorous with sodium hydroxide, producing sodium hypophosphite and sodium phosphite as a by-product. Alternatively the acid-catalyzed disproportioning of white phosphorous may be used, which yields phosphoric acid and phosphine. The acid route is the preferred method if further reaction of the phosphine to form substituted phosphines is required. This latter step requires purification and application of high pressure. It can also be made by the hydrolysis of a metal phosphide such as aluminium phosphide or calcium phosphide. Pure samples of phosphine, free from P_2H_4, may be prepared using the action of potassium hydroxide on phosphonium iodide (PH_4I).

Metal phosphine complexes are catalysts for reactions such as the Sonogashira coupling, where $Pd(PPh_3)_2$ is used[14]. Most of these phosphines, with the exception of triphenyl phosphine, are made from pressurized, purified phosphine gas as described above.

A large industrial application of phosphine is found in the production of tetrakis(hydroxymethyl) phosphonium salts, made by passing phosphine gas through a solution of formaldehyde and a mineral acid such as hydrochloric acid. These find application as flame retardants for textile ("Proban") and as biocides.

Tertiary phosphines such as triphenylphosphine (PPh_3) undergoes slow oxidation by air to give triphenylphosphine oxide:

$$2PPh_3 + O_2 \rightarrow 2OPPh_3 \quad \textbf{... 2.1}$$

This impurity can be removed by recrystallisation of PPh_3 from either hot ethanol or hot isopropanol[15]. This method capitalizes on the fact that $OPPh_3$ is more polar and hence more soluble in hydroxylic solvents than PPh_3.

The easy oxygenation of PPh_3 is exploited in its use to deoxygenate organic peroxides, which generally occurs with retention of configuration:

$$PPh_3 + RO_2H \rightarrow OPPh_3 + ROH \text{ (R = alkyl)} \quad \textbf{... 2.2}$$

[13] A.D.F. Toy, *The Chemistry of Phosphorous*, Pergamon Press, Oxford, UK (1973).
[14] K. Sonogashira, Y. Tohda, N. Hagihara, *Tetrahedron Lett.*, **16**, 4467 (1975).
[15] D.D. Perrin, W.L.F. Armarego, D.R. Perrin, *Purification of Laboratory Chemicals, 2nd ed.*, Pergamon, New York, 455 (1980).

Triphenylphosphine abstracts sulphur from polysulfide compounds, episulphides, and elemental sulphur, though simple organosulphur compounds such as thiols and thioethers are unreactive. The phosphorous-containing product is Ph_3PS.

PPh_3 is a weak base, but forms stable salts with strong acids such as HBr. The product contains the phosphonium cation $[HPPh_3]^+$.

Trivalent phosphorous compounds, as exemplified by phosphines and phosphites, serve as a important class of ligands in metal complex chemistry[16], as phosphorous ligands are well recognized for their ability to stabilize complexes in a variety of oxidation states and coordination geometries. Various studies have been performed in the past, comparing phosphines and phosphites of different degrees of bulkiness and ratios with regard to silver ions[17], and studying their behaviour with different counterions[18], mostly at low temperatures. Coordinated phosphine chemical shifts are generally downfield from the free ligand and coordinated phosphite, though downfield from coordinated phosphine, is upfield from the free phosphite ligand[17.c].

2.2.2 COMPLEXES WITH DIFFERENT PHOSPHOROUS-CONTAINING LIGANDS

Complexes of $[AgXL_n]$ (L = tertiary phosphine/phosphite; n = 1-4; X = coordinating or non-coordinating anion) have been reported in literature, with L = PPh_3, $P(OEt)_3$ and $P(t\text{-}Bu)_3$ the most common[17]. In a comparative study between complexes with L = $P(p\text{-tol})_3$ and $P(OEt)_3$, it was found that ^{31}P chemical shifts of complexes containing the phosphite were shifted downfield from complexes with the same counterion containing the phosphine.

Reactions of phosphorous ligands are governed by various factors, the most important being steric and electronic. Successive additions of molar equivalents of $[P(OCH_2)_2(\mu_2\text{-}CHO)]$ to $AgBF_4$ resulted in detection at -95°C of $[AgLBF_4]$ species only[17.c]. Ratios of ligand to metal larger than one only gave rise to an additional ^{31}P peak corresponding to

[16] G. Booth, *Adv. Inorg. Chem. Radiochem.*, **6**, 1 (1964).
[17] a) A.F.M.J. van der Ploeg, G. Van Koten, A.L. Spek, *Inorg. Chem.*, **18**, 1052 (1979). b) T.G.M.H. Dikhoff, R.G. Goel, *Inorg. Chim. Acta*, **44**, L72 (1980). c) S.M. Socol, J.G. Verkade, *Inorg. Chem.*, **23**, 3487 (1984). d) S.M. Socol, R.A. Jacobson, J.G. Verkade, *Inorg. Chem.*, **23**, 88 (1984). e) E.L. Meutterties, C.W. Alegranti, *J. Am. Chem. Soc.*, **94**, 6386 (1972).
[18] a) F. Bachechi, A. Burini, R. Galassi, B.R. Pietroni, M. Ricciutelli, *Inorg. Chim. Acta*, **357**, 4349 (2004). b) R.G. Goel, P. Pilon, *Inorg. Chem.*, **17**, 2876 (1978).

the free phosphite, even though the cone angle of this phosphite is relatively small, <101°. The Tolman cone angle[19] is an indication of the approximate amount of space that a ligand consumes about the metal center, in other words an indication of steric bulkiness. A plausible cause is the small OPO and POC bond angles in the ligand[20], resulting in heightened electronegativity of the phosphorous atom by reduction of σ basicity and augmentation of π acidity. The phosphite then acts as a Lewis acid for Ag^+. Sufficient polarization of Ag^+ in this manner could prevent additional ligands from coordinating to the metal. A consideration of cone angles alone leads to the conclusion that $[P(OCH_2CCl_3)_3]$ (115°) should easily form a Ag(I) complex of coordination number greater than 3, since P(O-*i*-Pr)$_3$ (130°), $P(OPh)_3$ (127°) and PPh_3 (145°) all form four-coordinate $[AgL_4^+]$. The low σ basicity of $P(OCH_2CCl_3)_3$ owing to the inductive effects of the halogens appears to be responsible for this.

The isolable [AgLX] complexes where L = P(O-*t*-Bu)$_3$ and P(*t*-Bu)$_3$ and X = CN^-, Cl^- or I^- also afford information regarding the role of ligand electronic effects. Neither phosphine nor phosphite complexes exhibit Ag-P coupling at room temperature, although ligand exchange is slowed down sufficiently to observe coupling at -80°C.[18] A dissociative mechanism may operate here, in which the anion donates strongly enough to permit more facile dissociation of the phosphite than the more strongly basic phosphine. Following dissociation, ligand exchange could be affected by the equilibrium given by Eq. 2.3:

$$[AgLX] + L \leftrightarrow [AgL_2X] \text{ or } [AgL_2]^+ + X^- \quad \textbf{... 2.3}$$

Addition of excess phosphine at -95°C leads to $[AgL_2]^+$ plus free ligand[18.b], whereas addition of the phosphite leads to formation of $[AgL_2X]$ with chloride and iodide as counterions.

2.2.3 Complexes with Different Ratios of Ag : Phosphorous-Containing Ligand and Varied Counterions

Isolable crystalline $[AgXL_n]$ (L = tertiary phosphine/phosphite; n = 1-4; X = coordinating or non-coordinating anion) is obtained by reaction of most silver salts with appropriate

[19] C.A. Tolman, *Chem. Rev.*, **77**, 313 (1977).
[20] L.J. Vande Griend, J.D.G. Verkade, J.F.M. Pennings, H.M. Buck, *J. Am. Chem. Soc.*, **99**, 2459 (1977).

amounts of phosphine or phosphite. Tetrakis [$AgXL_4$] complexes dissolve in non-polar solvents to give essentially the same ^{31}P spectrum[17.e]. At low temperature (below -60°C) the spectra exhibit two doublets, arising from ^{107}Ag-^{31}P and ^{109}Ag-^{31}P spin-spin coupling. Although ^{31}P NMR chemical shifts of the AgL_n^+ species are not diagnostic of the value of n, the multiplets can be assigned through relative peak intensities and the magnitude of the coupling constant. Ratios of $^1J(^{109}Ag$-$^{31}P)/\ ^{107}Ag$-$^{31}P)$ should be close to the $\mu(^{109}Ag$-$^{31}P)/\mu(^{107}Ag$-$^{31}P)$ ratio of 1.149[21]. Complexes containing a silver atom bonded to four phosphine or phosphite ligands only form when the counterion is non-coordinating, as shown by conductance studies. This is confirmed by the invariability of the NMR parameters for phosphine and phosphite complexes with change in counterion. The temperature changes of the ^{31}P NMR spectra are indicative of the phosphorous ligand in AgL_4^+. At temperatures higher than ~-70°C broadening of the ^{31}P multiplets commences, followed by coalescence at -40°C for phosphines and -15°C for phosphites.

For silver bonded to three phosphine ligands, complexes can be neutral, tetrahedral AgL_3X, or ionic trigonal $AgL_3^+X^-$. The neutral form is indicated by conductivity studies, indicated when conductivity is near zero. This form is present for cyanide, cyanate and halide species. Some AgL_3X species show disproportionation in solution, as indicated by the NMR spectrum of $Ag[P(OEt)_3]NO_3$ in Figure 2.1[17.e].

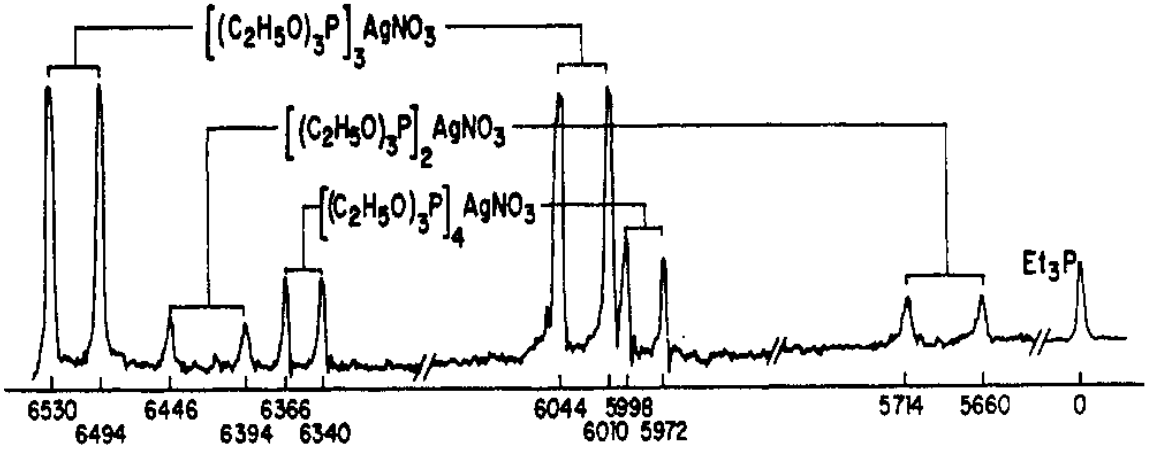

Figure 2.1 ^{31}P 40.5 MHz spectrum for $[Ag\{P(OEt)_3\}_3NO_3]$ at -90°C in 80/20 dichloromethane/toluene[17.e].

[21] P.B. Sogo, C.D. Jeffries, *Phys. Rev.*, **93**, 174 (1954).

However, complexes in which the counterion is tightly bound, for example, cyanide and halide show no NMR evidence of disproportionation. $[AgL_3X]$ complexes are kinetically labile, with phosphorous ligand exchange fast on the NMR time scale at temperatures from -70°C to -50°C. This exchange takes place through a dissociative mechanism as $[AgL_3X]$ complexes are coordinately saturated.

Three possible forms exist for $[AgL_2X]$; neutral trigonal, ionic linear and neutral dimeric. The trigonal form is common for complexes with halide and pseudohalide counterions. When the counterion is bidendate, such as CF_3COO^-, NO_3^-, $B_3H_8^-$ and $S_2PF_2^-$, the complex may accept a tetrahedral, dimeric form.

Complexes of [AgLX] exist as cubane-like structures, $[AgLX]_4$, for counterions of halides, and linear complexes for bulkier counterions. Linear complexes of [AgLX] generally exist when the phosphorous ligand is bulky, as is the case with $P(t\text{-}Bu)_3$, as discussed in section 2.2.2. Most of these complexes are not ionized, as indicated through conductivity studies[18.b], but conductance has been recorded for complexes with counterions of CN^-, SCN^- and NO_3^-, in nitromethane and dichloromethane. This may be due to ionization (Eq 2.4) or disproportionation (Eq 2.5):

$$[AgLX] + n CH_3NO_2 \leftrightarrow [AgL(CH_3NO_2)]^+ + X^- \quad \text{... 2.4}$$

$$2[AgLX] \leftrightarrow [AgL_2]^+ + [AgX_2]^- \quad \text{... 2.5}$$

These ionic species are, however, only formed at low concentration.

2.2.4 PHOSPHOROUS-31 NMR[22]

With a spin quantum number of 1/2, the phosphorous nucleus ^{31}P, the only natural isotope of this element, will give a single spectral line. The chemical shift is highly indicative of the particular phosphorous functional group, and is generally predictable from studying the effects of structural change. NMR particulars are indicated in Table 2.1.

[22] L.D. Quin, A.J. Williams, *Practical Interpretation of P-31 NMR Spectra and Computer-Assisted Structure Verification*, Advanced Chemistry Development, Inc., Toronto (2004).

Table 2.1 NMR particulars for ^{31}P.[23] Common reference compound: H_3PO_4

	^{31}P
Natural abundance (%)	100
Spin (I)	½
Frequency relative to ^{1}H = 100 MHz	40.480742
Receptivity, D^P, relative to ^{1}H = 1.00	0.0665
Receptivity, D^C, relative to ^{31}C = 1.00	391
Magnetogyric ratio, γ (10^7 rad T^{-1} s^{-1})	10.8394
Magnetic moment, μ (μ_N)	1.95999

2.3 Silver Chemistry

2.3.1 INTRODUCTION

Like gold and copper, silver has a single *s* electron outside a filled *d* shell. The most common oxidation state of silver is Ag(I), and the only oxidation state stable to water[24]. The most common coordination states of Ag(I) are 2 and 4, with linear and tetrahedral geometries respectively, but many Ag(I) complexes with coordination numbers of up to 6 have been reported. Due to the small energy difference between the filled *d* orbitals and the unfilled valence shell *s* orbital, extensive hybridization of the d_{z^2} and *s* orbitals is permitted, as shown in Figure 2.2.

[23] D.M. Granty, R.K. Harris, *Encyclopedia of Nuclear Magnetic Resonance*, *vol. 5*, John Wiley & Sons, Chichester, UK (1996).
[24] F.A. Cotton, G. Wilkinson, *Advanced Inorganic Chemistry, 5th ed*, Wiley Interscience, New York (1998).

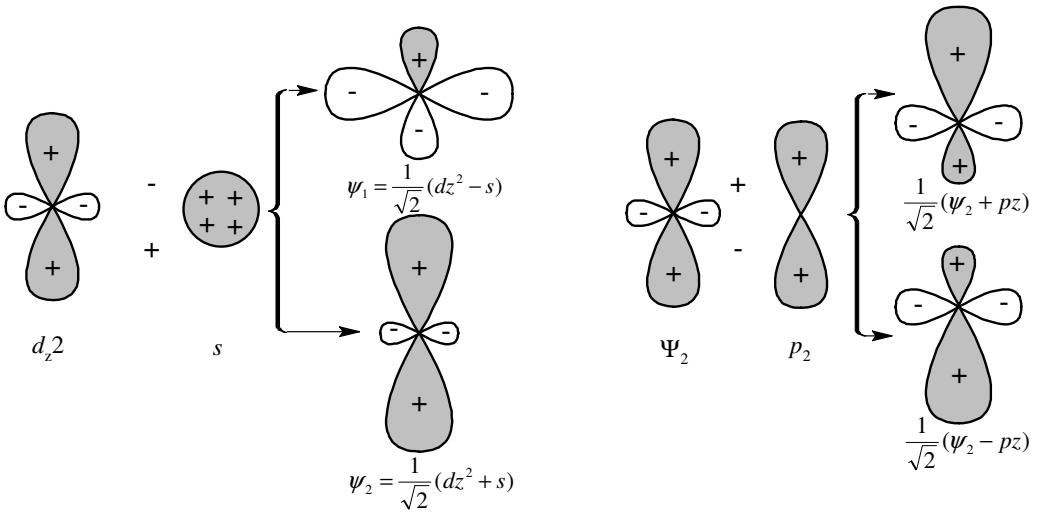

Figure 2.2 The hybrid orbitals of Ag(I) formed from a *dz*2 and an *s* orbital, ψ1 and ψ2, on the left, and the potential hybrids formed from ψ2 and a *p*z orbital, on the right. In each sketch the z axis is vertical and the actual orbital is the figure generated by rotating the sketch about the z axis.

Initially the electrons in the d_{z2} orbitals occupy ψ_1, giving a circular region of relatively high electron density from which ligands are somewhat repelled. The regions above and below this ring has a relatively low electron density that attract ligands. Further mixing of ψ_2 with the p_z orbital produces two hybrid orbitals suitable for forming a pair of linear covalent bonds. Ag(II) are both 4 and 6 coordinated, with planar and distorted octahedral geometries. Ag(III) is similar to Ag(II) with regard to coordination number and geometry.

Au is expected to react in a similar way to Ag and Cu, but differences may be attributed to relativistic effects on 6*s* electrons of Au. Au is also a post-Lanthanide element, which has consequences concerning the radius of the Au atom. As a result of the filled 4*f* orbitals across the lanthanide period, shielding of the outer electrons is reduced, and the atomic radii of the lanthanides are smaller than would normally be expected[25]. This shielding effect is unable to counter decrease in radius due to increasing nuclear charge and is known as lanthanide contraction. Consequently, the radii of the elements following the lanthanides are smaller than would be expected if there were no *f*-transition

[25] P.W. Atkins, L.L. Jones, *Chemistry: Molecules, Matter, and Change, 3rd ed*., W.H. Freeman and Company, New York (1997).

metals and the period 6 elements have only marginally larger atomic radii than the period 5 elements in the same group.

2.3.2 COMPLEXES OF SILVER WITH MONODENDATE LIGANDS

Tertiary phosphine complexes of Ag(I) of the type $[AgXL_n]$ (L = tertiary phosphine; n = 1-4; X = coordinating or non-coordinating anion) were first prepared by 1937[26]. Generally the complexes are synthesized by heating the appropriate amount of phosphine with the silver(I) salt. Silver(I) halides (Cl^-, Br^-, I^-) and pseudo-halides (CN^-, SCN^-) are typically heated in acetonitrile, while silver(I) salts of non-coordinating anions (NO_3^-, ClO_4^-, BF_4^-, PF_6^-) are added to a hot solution of the phosphine in an alcohol. The complexes crystallize out of solution and can be recrystallized from acetone. The crystals show a diversity of structural types, which depend on the stoichiometry of the ligand to silver in the reaction mixture, as well as reaction conditions. Other factors influencing the structure of these complexes include the type of counterion, as well as the solvent.

2.3.2.1 Silver Complexes with AgX:L = 1:1 Stoichiometry

For equimolar stoichiometry both the tetrameric cubane **1** and step **2** structures have been characterised, as illustrated in Figure 2.3.

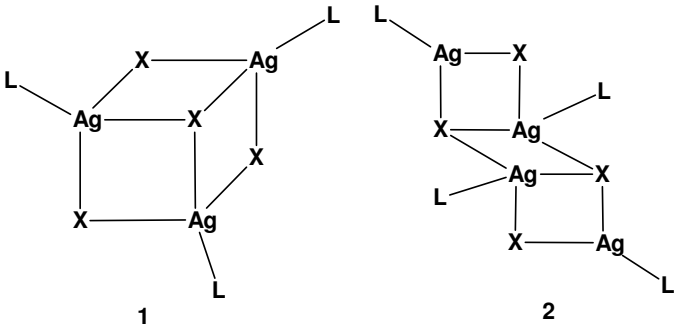

Figure 2.3 Cubane 1 and step 2 structures.

More sterically demanding species relieve strain by forming the step structure **2** rather than the cubane structure **1**, since the three coordinate metal sites and di-bridging halides in the step structure **2** are less crowded. Accordingly, PEt_3 and PPh_2Bu yields tetrameric

[26] F.G. Mann, A.F. Wells, D. Purdue, *J. Chem. Soc.*, 1828 (1937).

cubane clusters $[AgX(PEt_3)]_4$ and $[AgX(PPh_2Bu)]_4$ (X = Cl^-, Br^-, I^-)[27]. The isolation characterization of cubane $[AgI(PPh_3)]_4$[28] from $CHCl_3/Et_2O$ and the step analogue from CH_2Cl_2/Et_2O[29] demonstrates that the nature of the determining factors are not clearly understood. Other factors such as solvent of crystallisation may be important in influencing the formation of either cubane or step structures.

Linear monomeric compounds have been isolated and characterised for adducts of $P(mes)_3$, which is very bulky, and AgX (X = Cl^-, Br^-). The PCy_3[30] and $AsCy_3$[31] adducts of AgX (X = Cl^-, Br^-) show dimerization, with the halides as bridging ligands, while the AgI adduct is a cubane tetramer. Another linear complex is that of $Ag[P(t\text{-}Bu)_3]NO_3$, where two-coordinate silver is also due to the bulky phosphine[32].

2.3.2.2 Silver Complexes with AgX:L = 1:2 Stoichiometry

In general, 1:2 complexes $[AgXL_2]$ have been shown to have dimeric halogen bridges: $[AgXL_2]_2$ (L = PPh_3, X = Cl^- [33], Br^- [34], I^- [29.b]; L = 5-phenyldibezophosphole, X = Cl^- [35]). The dimeric bridging structure and trigonal planar structure are illustrated in Figure 2.4.

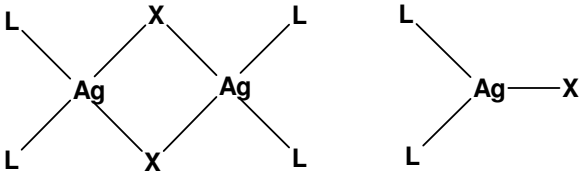

Figure 2.4 Dimeric bridging and trigonal planar structures of $[AgXL_2]$.

$[AgBr(PPh_3)_2]_2{\cdot}CH_3Cl$ is dimeric via bridging bromine[34]. Unsolvated 2:1 PPh_3-AgBr is the first example of a complex with trigonal planar $[AgXL_2]$ coordination[36] and contains

[27] a) M.R. Churchill, J. Donahue, F.J. Rotella, *Inorg. Chem.*, **15**, 2752 (1976). b) M.R. Churchill, B.G. DeBoer, *Inorg. Chem.*, **14**, 2502 (1975). c) R.J. Bowen, D. Kamp, Effendy, P.C. Healy, B.W. Skelton, A.H. White, *Aust. J. Chem.*, **47**, 693 (1994).
[28] a) B.-K. Teo, J.C. Calabrese, *Inorg. Chem.*, **15**, 2467 (1976). b) B.-K. Teo, J.C. Calabrese, *J. Am. Chem. Soc.*, **97**, 1256 (1975).
[29] a) B.-K. Teo, J.C. Calabrese, *Inorg. Chem.*, **15**, 2474 (1976). b) G.A. Bowmaker, Effendy, R.D. Hart, J.D. Kildea, A.H. White, *Aust. J. Chem.*, **50**, 653 (1997).
[30] G.A. Bowmaker, Effendy, P.J. Harvey, P.C. Healy, B.W. Skelton, A.H. White, *J. Chem. Soc., Dalton Trans.*, 2459 (1996).
[31] G.A. Bowmaker, Effendy, P.C. Junk, A.H. White, *J. Chem. Soc., Dalton Trans.*, 2131 (1998).
[32] R.G. Goel, P. Pilon, *Inorg. Chem.*, **17**, 2876 (1978).
[33] A. Cassell, *Acta Cryst.*, **B35**, 17 (1979).
[34] B.-K. Teo, J.C. Calabrese, *J. Chem. Soc., Chem. Commun.*, 185 (1976).
[35] S. Attar, N.W. Alcock, G.A. Bowmaker, J.S. Frye, W.H. Bearden, J.H. Nelson, *Inorg. Chem.*, **30**, 4166 (1991).

the mononuclear species $[AgBr(PPh_3)_2]$. Recrystallization of this complex from $CHCl_3$ results in the formation of solvates $[AgX(PPh_3)_2]_2 \cdot 2CHCl_3$, which contain almost perfect symmetrically hydrogen-bridged dimers. In contrast, the structure of the unsolvated PPh_3-AgCl complex shows the presence of dimers, containing bridging chloride and terminal PPh_3 ligands[33]. This structure also contains unsymmetrical chloride bridging, which may indicate that the complex is an aggregate of two independent $[AgCl(PPh_3)_2]$ units[36]. $[AgX\{P(4\text{-}MeC_6H_4)_3\}_2]$, where X is a halide or CN^-, is thought to exist as a monomer, with trigonal geometries in solution[37]. Complexes with a L:Ag stoichiometry of 2:1, containing bulky phosphine ligands and non-coordinating anions are thought to have linear two coordinate structures. This has been confirmed for $[Ag\{P(2,4,6\text{-}Me_3C_6H_2)_3\}_2]PF_6$[38]. Spectral data and conductance measurements suggested that for $[AgX(P^tBu_3)_2]$ with X = ClO_4^-, BF_4^-, PF_6^- and NO_3^-, the complexes contained the linear $[P\text{-}Ag\text{-}P]^+$ cation[32]. Nonlinear two-coordinate Ag(I) species have also been reported; with a P-Ag-P angle of 166.9° for ionic $[Ag\{P(NMe_2)_3\}_2]BPh_4$[39]. The solid-state CP/MAS ^{31}P NMR data coincided with the solution $\delta(^{31}P)$ and $^1J(^{107}Ag\text{-}^{31}Ag)$ values, indicating the retention of the two-coordinate structure in solution.

2.3.2.3 Silver Complexes with AgX:L = 1:3 Stoichiometry

Three coordinate complexes of type $[Ag(PR_3)_3]^+$ are rare and only observed when steric factors prevent the coordination of two or four ligands. When the ligands of preferred two-coordinate $[Ag(PCy_3)_2]^+$ [40] and $[Ag\{PPh_2(c\text{-}C_5H_9)\}_2]^+$ [41] and the four-coordinate $[Ag(PPh_3)_4]^+$ [42,43] are mixed, the ligands produce steric properties that favour tricoordinate Ag(I) complexes. By utilizing cycloalkyldiphenylphosphines, a series of eighteen salts of formula $[M(PPh_2R)_3]X$ (M = Ag, Au; X = BF_4^-, ClO_4^-; R = *c*-C_5H_9, Cy,

---

[36] G.A. Bowmaker, Effendy, J.V. Hanna, P.C. Healy, B.W. Skelton, A.H. White, *J. Chem. Soc., Dalton Trans.*, 1387 (1993).
[37] E.L. Muetterties, C.W. Alegranti, *J. Am. Chem. Soc.*, **94**, 6386 (1972).
[38] E.C. Alyea, G. Furguson, A. Somogyvari, *Inorg. Chem.*, **21**, 1369 (1982).
[39] S.M. Socol, R.A. Jacobson, J.G. Verkade, *Inorg. Chem.*, **23**, 88 (1984).
[40] a) G.A. Bowmaker, Effendy, P.J. Harvey, P.C. Healy, B.W. Skelton, A.H. White, *J. Chem. Soc., Dalton Trans.*, 2449 (1996). b) M. Camalli, F. Caruso, *Inorg. Chim. Acta*, **144**, 205 (1988).
[41] A. Baiada, F.H. Jardine, R.D. Willet, *Inorg. Chem.*, **29**, 3042 (1990).
[42] a) L.M. Engelhardt, C. Pakawatchai, A.H. White, P.C. Healy, *J. Chem. Soc., Dalton Trans.*, 125 (1985). b) P.F. Barron, J.C. Dyasson, P.C. Healy, L.M. Engelhardt, B.W. Skelton, A.H. White, *J. Chem. Soc., Dalton Trans.*, 1965 (1986).
[43] a) F.A. Cotton, R.L Luck, *Acta Cryst.*, **45C**, 1222 (1989). b) G.A. Bowmaker, P.C. Healy, L.M. Engelhardt, J.D. Kildea, B.W. Skelton, A.H. White, *Aust. J. Chem.*, **43**, 1697 (1990).

c-C_7H_{13}) were isolated and characterized[44]. Forty-nine complexes of the type $[M\{ZPh_m(4\text{-}YC_6H_4)_{3-m}\}_n]X$ (M = Cu, Ag; X = BF_4^-, ClO_4^- ; Z = P, As, Sb; Y = Cl, F, Me, OMe; n = 3, 4; m = 0-2)[45] were prepared and characterized, demonstrating the electronic properties of the ligands. Ligands containing electron-withdrawing aryl groups (Y = F, Cl) behaved in a contrasting way to the electron-rich ligands (Y = Me, OMe), forming $[MXL_3]$ acido complexes with the IR spectra indicating coordinated anions. The formation of the acido complexes are being favoured by the tendency of the electron-poor ligands to accept π-electrons from the metal which reduces the electron density on the Ag(I) ion. The electron-rich ligands only formed $[AgL_3][X]$ type complexes in a few instances.

2.3.2.4 Silver Complexes with AgX:L = 1:4 Stoichiometry

Tetrakisphosphine complexes have been isolated with non-coordinating anions eg. $[Ag(PPh_3)_4]X$ (X = ClO_4^-, BrO_3^- and NO_3^-)[46]. Electron-rich ligands most commonly form $[AgL_4][X]$ type complexes where X is ClO_4^- or BF_4^- [45]. This can be attributed to the large volume occupied by the $5sp^3$ orbitals of silver, enabling accommodation of the lone pair from a fourth tertiary phosphine ligand. Attempts to isolate complexes with a L:Ag = 4:1 stoichiometry with a halide have been problematic due to their instabilities. In general the halide anion binds with the exclusion of a phosphine group to yield $[AgX(PR_3)_3]$ type complexes[37]. However, due to the small size and basicity of $P(c\text{-}NCH_2CH_2)_3$ (*c* = cyclo), complexes of the type $[Ag\{P(c\text{-}NCH_2CH_2)_3\}_4]X$ (X = Cl^- and I^-) have been isolated[39]. The ion is then displaced from the inner sphere. No ligand dissociation was observed for the chloride complex at -95 °C by ^{31}P NMR spectroscopy. For the corresponding iodide complex, however, the equilibrium corresponding to the displacement of the tertiary phosphine by halide was observed. $[AgX\{P(4\text{-}MeC_6H_4)_3\}_n]$ complexes (n = 2-4) have been studied by ^{31}P NMR spectroscopy, where X includes a wide variety of counter-ions[37]. The ligands are labile in all the complexes studied, therefore the first order P-Ag coupling is unresolved above -70 °C. Rapid ligand exchange reactions have been reported for all ^{31}P investigations of ionic Ag(I) monodendate phosphine complexes,

[44] A. Baiada, F.H. Jardine, R.D. Willet, *Inorg. Chem.*, **29**, 4805 (1990).
[45] A. Baiada, F.H. Jardine, R.D. Willett, K. Emerson, *Inorg. Chem.,* **30**, 1365 (1991).
[46] F.A. Cotton, D.M.L. Goodgame, *J. Chem. Soc.*, 5257 (1960).

except for the complexes $[Ag(P^tBu_3)_2]^+$ and $[Ag\{P(2,4,6\text{-}Me_3C_6H_2)_3\}_2]^+$ [32,47]. These ligands are sterically bulky, hindering participation in the associative process involved in the exchange. Well resolved first order P-Ag spin-spin coupling is exhibited by these complexes at ambient temperature.

2.3.3 SILVER NMR

Silver has two NMR active spin ½ nuclei that yield very narrow signals over a wide chemical shift range[48], with high natural abundances of 51.839% for ^{107}Ag and 48.161% for ^{109}Ag. ^{107}Ag and ^{109}Ag both have very low sensitivity, ^{109}Ag being preferred as it has slightly higher sensitivity. In addition, ^{107}Ag has a resonant frequency beyond that of most standard NMR probes. The Larmor frequency for ^{107}Ag is 2.4266 MHz at 14.092 kG and the sensitivity, with respect to proton at constant field, is 6.79×10^{-5}. The corresponding values for ^{109}Ag are 2.7916 MHz and 1.01×10^{-4}.[49] However, it may be that ^{107}Ag yields sharper signals although it is difficult to determine for sure; resolution is not usually the major problem with silver NMR. The relaxation time is very long, $T_1 = 49 \pm 20$ s and $T_2 = 8.2 \pm 2$ s for ^{109}Ag in an 8.3 M aqueous solution[48]. Small amounts of a paramagnetic salt ($MnNO_3$, $Ni(NO_3)_2$, etc.) can be added to the silver salt solution in order to reduce the relaxation time and to broaden the ^{109}Ag resonance line to the point where it can be detected. NMR particulars of silver isotopes are indicated in Table 2.2.

[47] E.C. Alyea, S.A. Dias, S. Stevens, *Inorg. Chim. Acta*, **44**, L203 (1980).
[48] C.W. Burges, R. Koschmieder, W. Sahm, A. Schwenk, *Z. Naturforsch. A*, **28**, 1753 (1973).
[49] A.K. Rahimi, A.I. Popov, *J. Magn. Res.*, **36**, 351 (1979).

Table 2.2 NMR particulars for Ag isotopes[23]. Common reference compound: $AgNO_3/D_2O$.

	^{107}Ag	^{109}Ag
Natural abundance (%)	51.839	48.161
Spin (I)	½	½
Frequency relative to ^{1}H = 100 MHz	4.047878	4.653601
Receptivity, D^P, relative to ^{1}H = 1.00	0.0000350	0.0000495
Receptivity, D^C, relative to ^{31}C = 1.00	0.200	0.282
Magnetogyric ratio, γ (10^7 rad T^{-1} s^{-1})	-1.0889181	-1.2518634
Magnetic moment, μ (μ_N)	-0.19689893	-0.22636279

^{109}Ag chemical shift is concentration dependent[48], and often shifts upfield with increasing concentration of silver salt[50]. It has also been shown that the chemical shift of ^{109}Ag is solvent dependent[49]. In general, the higher the donicity of the solvent, more paramagnetic is the chemical shift of the silver ion, although the relationship is not linear. The chemical shift, however, is also dependent on "hard-soft" interactions. Although acetonitrile has a low donicity of 14.1[51], the ^{109}Ag chemical shift is much more downfield in this solvent than in dimethyl sulfoxide, which has a donicity of 29.8.[51] Acetonitrile forms stable complexes with the silver ion.

2.4 Hydroformylation

2.4.1 INTRODUCTION

Hydroformylation, also known as the oxo reaction, is the most widely used homogeneous catalytic industrial process for the production of aldehydes[52]. It is the reaction of olefins with hydrogen and carbon monoxide, in the presence of a catalyst, to yield either linear (normal) or branched (iso) aldehydes and was discovered in 1937 by Otto Roelen[8]. The best hydroformylation catalysts are generally those that produce the highest ratio of linear to branched products and the fewest side reactions. The side reactions produce olefin isomerization products (internal olefins) and olefin hydrogenation products (hydrocarbons), shown in Scheme 2.1.

[50] A.K. Rahimi, A.I. Popov, *Inorg. Nucl. Chem. Lett.*, **12**, 703 (1976).
[51] V. Gutman, E. Wychera, *Inorg. Nucl. Chem. Lett.*, **2**, 257 (1966).
[52] A.M. Trzeciak, J.J. Ziolkowski, *Coord. Chem. Rev.*, **190-192**, 883-900 (1999).

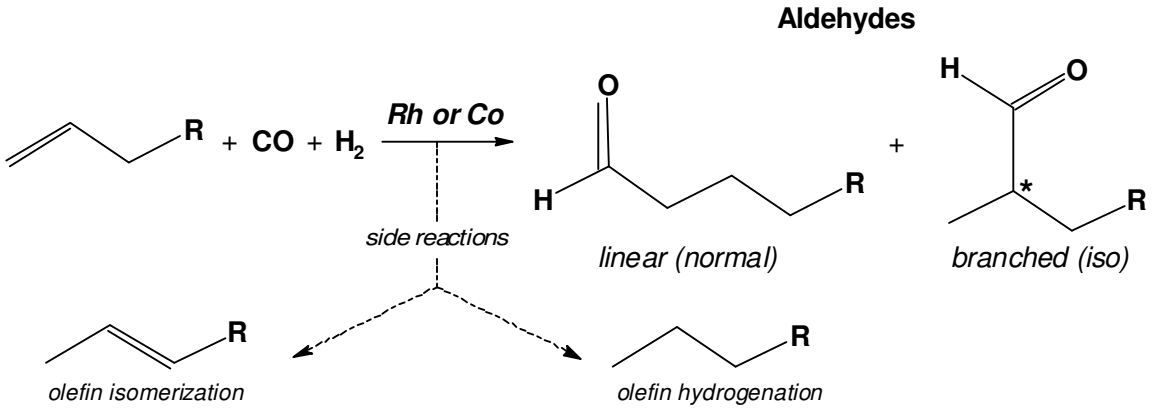

Scheme 2.1 The oxo reaction, or hydroformylation.

After Roelen's discovery, hydroformylation became the dominant homogeneous catalytic process for producing aldehydes. Common commercial catalysts are based on cobalt or rhodium hydride carbonyl complexes, often utilizing phosphite or phosphine ligands to enhance the rate or the linear to branched regioselectivity. Aldehydes are used to produce alcohols and carboxylic acids, which are used in the production of fatty acids[53], plasticizers, detergents, surfactants, lubricants, and solvents[54]. The generally accepted mechanism for the cobalt-catalyzed reaction was provided by Heck and Breslow[55] and is shown in Scheme 2.2.

[53] G.A. Somorjai, *Chemistry in Two Dimensions*, Cornell Univ. Press, Ithaca, New York (1981).
[54] G.W. Parshall, *Homogeneous Catalysis*, Wiley-Interscience, New York (1980).
[55] R.F. Heck, D.S. Breslow, *J. Am. Chem. Soc.*, **83**, 4023 (1961).

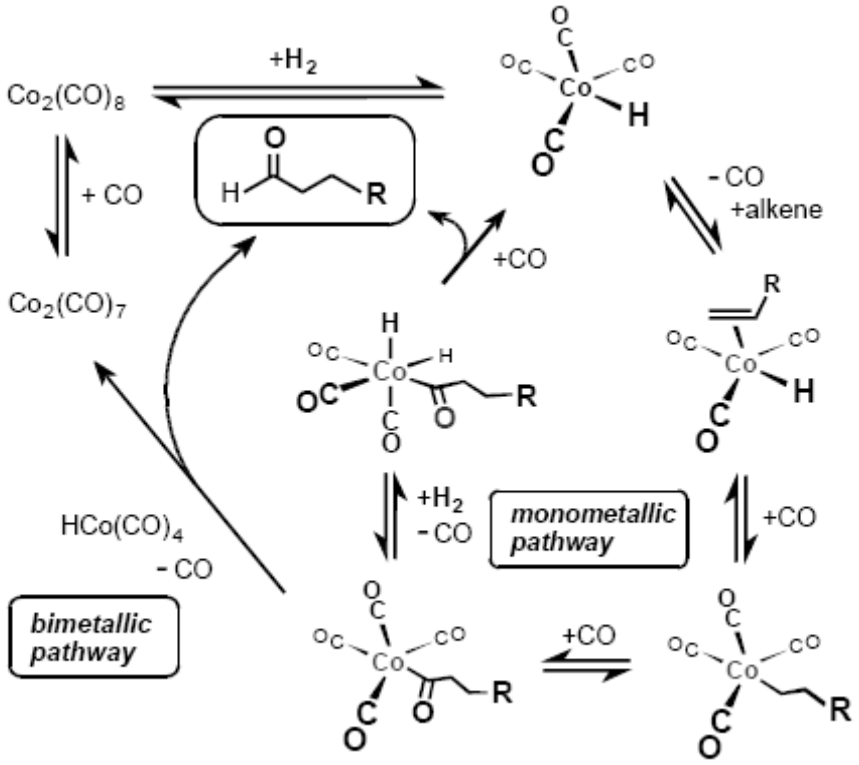

Scheme 2.2 Cobalt-catalyzed hydroformylation mechanism[56].

The basic steps of the catalytic cycle include generation of a cobalt hydride from a mono- or bimetallic cobalt carbonyl complex, olefin coordination to the metal centre via an open coordination site provided by CO ligand dissociation, olefin insertion into the metal-hydrogen bond, CO coordination and insertion into the metal-alkyl bond to form an acyl complex, oxidative addition of hydrogen, and the reductive elimination of the aldehyde product and regeneration of the active catalyst.

Cobalt catalyst systems dominated hydroformylation until the 1970's. In the late 1960's some corporations began using rhodium catalyst systems[57]. These Rh/PPh_3 catalyst systems were highly selective and far more active than their cobalt counterparts, even when used under mild conditions. The generally accepted mechanism for Rh/PPh_3-catalyzed hydroformylation is shown in Scheme 2.3.

[56] P.W.M.N. van Leeuwen, *Homogeneous Catalysis, Understanding the Art*, Kluwer Academic Publishers, Dordrecht (2004).
[57] J.D. Unruh, J.R. Christenson, *J. Mol. Catal.*, **14**, 19-34 (1982).

The mechanism is analogous to the cobalt-catalyzed mechanism described by Scheme 2.2, with PPh_3 ligands replacing the less sterically influential CO ligands.

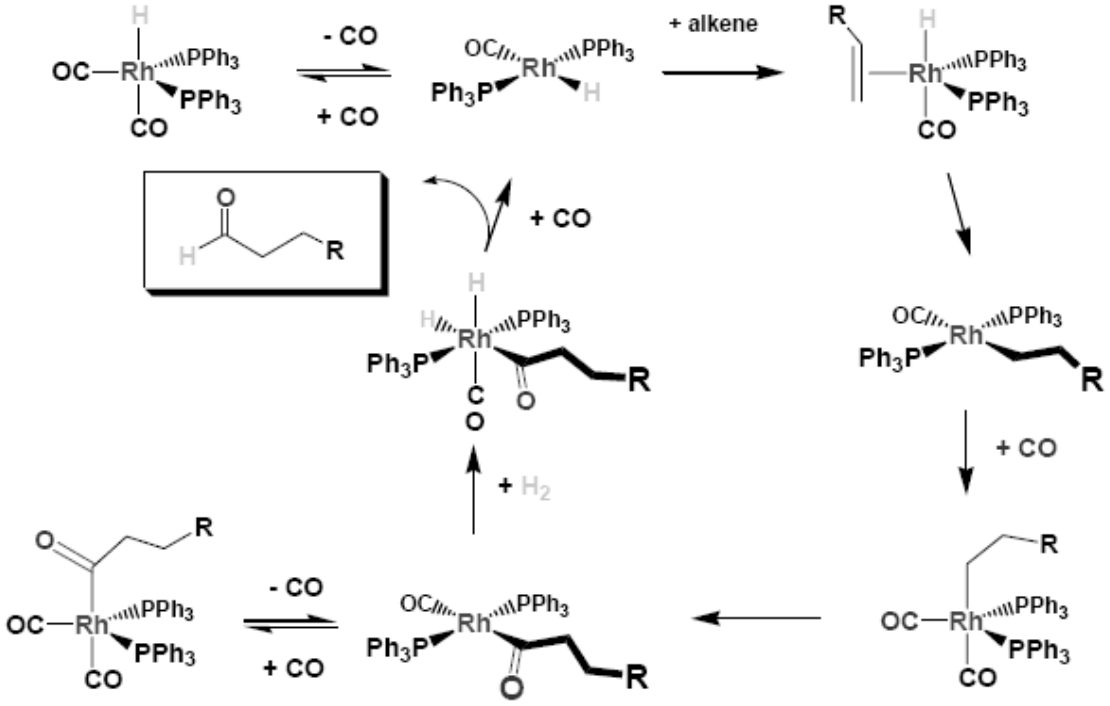

Scheme 2.3 Rh/PPh_3-catalyzed hydroformylation mechanism[56].

Excess PPh_3 stabilizes the Rh complex, minimizing the formation of unsaturated $14e^-$ complexes that promote the fragmentation of PPh_3 which ultimately leads to the formation of phosphide-bridged Rh dimers and clusters, which are poor or inactive hydroformylation catalysts.

The goal in designing an effective catalyst system is to optimize the production of the desired products under the mildest conditions. Since higher turnover frequencies, higher linear to branched ratios, and low production of side reaction products are usually required, much effort has been expended to attempt to design catalyst systems with these goals in mind. Research continues in the design of new ligands and catalyst systems, but is hampered by the necessity of a catalyst to allow coordination of hydrides, carbonyls and olefins, as well as undergoing oxidative addition and reductive elimination.

2.4.2 HYDRIDES

Some silver hydrides exist, most often in zeolite hosts[11.a], and then occurring as silver clusters. Silver hydride species can be formed through the heterolytic dissociation of H-H over Ag_n^+ in Ag-A and Ag-Y zeolite as

$$ZO\text{-}Ag_n^+ + H_2 \rightarrow Ag_n\text{-}H + ZOH \quad \textbf{... 2.6}$$

where ZOH represents the Bronsted acid site. Heterolytic cleavage of a C-H bond of CH_4 proceeding on Ag-Y zeolite can also produce the Ag_n-H species as

$$ZO\text{-}Ag_n^+ + CH_4 \rightarrow Ag_n\text{-}H + ZO^{\delta-}\text{-}CH_3^{\delta+} \quad \textbf{... 2.7}$$

Although the formation of Ag_3–H in zeolites has been established[11.c,58], in the same experiment other unidentified Ag_n–H species have also been observed. The sizes of the clusters are limited by the dimension of the channels in the interior of the zeolite. However, the zeolite structure is not as rigid as it might look, and shape readjustments could take place to accommodate larger guest molecules.

AgH and (H_2)AgH have also been observed via infrared on laser-ablated silver[59]. Some density functional theory (DFT) calculations have been performed on M_mH_n molecules[59.b,60], showing that MH_2^- anions are very stable, but the corresponding neutral MH_2 molecules are higher in energy than M and H_2. Silver hydrides have been observed in clusters with other metals[61], where the unsaturated, neutral $M(\mu\text{-}H)_2M$ moiety (M = Re, Mn) exhibits Lewis basicity towards the silver cation.

2.4.3 CARBONYL REACTIONS

Carbon monoxide bonds to transition metals using synergic pi* back-bonding. The bonding has three components, giving rise to a partial triple bond. A sigma bond arises from overlap of non-bonding electron pair on carbon with a blend of *d*, *s*, and *p*-orbitals

[58] T. Baba, H. Sawada, T. Takahashi, M. Abe, *Appl. Catal. A*, **231**, 55 (2002).
[59] a) L. Andrews, X. Wang, *J. Am. Chem. Soc.*, **125**, 11751 (2003). b) X. Wang, L. Andrews, L. Manceron, C. Marsden, *J. Phys. Chem. A*, **107**, 8492 (2003).
[60] a) C.A. Tsipis, E.E. Karagiannis, P.F. Kladou, A.C. Tsipis, *J. Am. Chem. Soc.*, **126**, 12916 (2004). b) K. Balusubramanian, M.J. Liao, *J. Phys. Chem.*, **92**, 361 (1988). c) K. Balusubramanian, M.J. Liao, *J. Phys. Chem.*, **93**, 89 (1989). d) K. Balasubramanian, *J. Phys. Chem.*, **93**, 6585 (1989). e) R.B. Ross, W.C. Ermler, *J. Phys. Chem.*, **89**, 5202 (1985).
[61] a) T. Beringhelli, G. D'Alfonso, M.G. Garavaglia, M.P.P. Mercandelli, A. Sironi, *Organometallics*, **21**, 2705 (2002). b) R. Carrefio, V. Riera, M.A. Ruiz, C. Bois, Y. Jeannin, *Organometallics*, **11**, 2923 (1992).

on the metal. A pair of π bonds arises from overlap of filled *d*-orbitals on the metal with a pair of π-antibonding orbitals projecting from the carbon of the CO. The π-bonding has the effect of weakening the carbon-oxygen bond compared with free carbon monoxide. Because of the multiple bond character of the M-CO linkage, the distance between the metal and carbon is relatively short, often < 1.8 Å. The interaction between a CO molecule and a metal atom is illustrated in Figure 2.5.

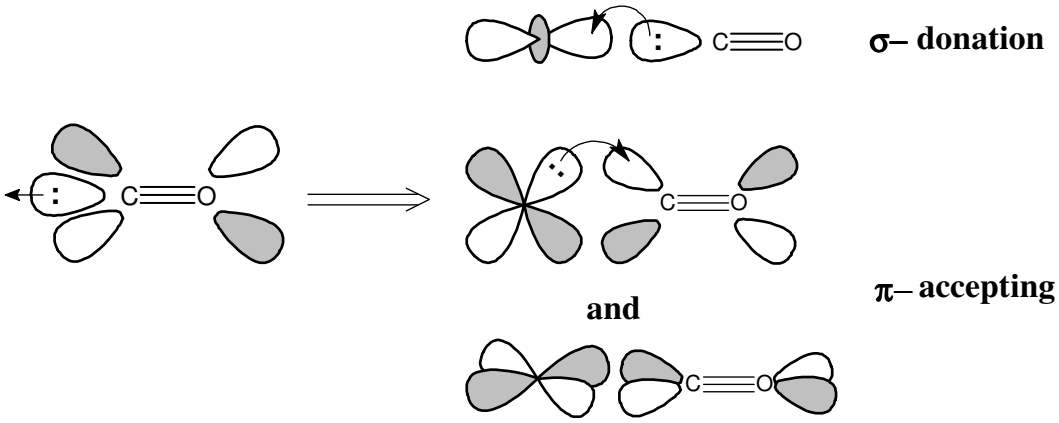

Figure 2.5 Illustration of σ-donation of a CO-molecule and π-backbonding of metal[24].

Metal carbonyl anions have a rich history in chemistry and are important precursors to a tremendous variety of organometallic, inorganic, and organic species. They are also of considerable interest as the first compounds to contain transition metals in formally negative oxidation states[62] and exhibit reactivity patterns that bear striking similarities to those of halides, chalcogenides, and pnictides[63]. Metal carbonyl mono-anions such as $[Co(CO)_4]^-$, $[Mn(CO)_5]^-$, $[V(CO)_6]^-$, etc. are now often considered to be transition metal analogues of classic pseudohalides[64]. Carbonyls can form bi-, tri-, and tetranuclear compounds, often acting as bridging or semi-bridging structures between metal centres. Side-bonding of CO, also analogized by CNR complexes, is illustrated in Figure 2.6.

[62] W. Beck, *Angew. Chem., Int. Ed. Engl.*, **30**, 168 (1991).
[63] J. E. Ellis, *J. Organomet. Chem.*, **86**, 1 (1975).
[64] a) J.E. Ellis, *J. Chem. Educ.*, **53**, 2 (1976). b) A.M. Golub, H. Köhler, V.V. Skopenko, *Chemistry of Pseudohalides*, Elsevier: Amsterdam, Chapter 1 (1986).

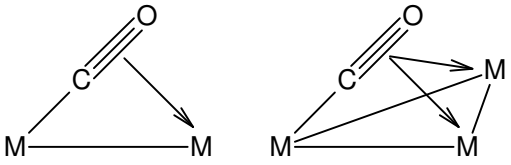

Figure 2.6 CO side-bonding.

Infrared spectroscopy remains the single most powerful technique available for monitoring the reactions of metal carbonyls and for the provisional assignment of structures to new products, because the number, relative intensities, shapes, and energies of the IR-active carbonyl stretching modes, i.e., ν_{CO} absorptions, are extremely sensitive functions of the molecular structure and charge, *Z*, of a carbonyl complex. Carbonyl stretching frequencies for mononuclear metal carbonyls generally range from 2200 to 1500 cm^{-1}. Ion pairing between cations and metal carbonyl anions can cause dramatic changes in the ν_{CO} region, due to strong perturbation of the geometry of the anion. Classically the metal-carbonyl interaction involves synergistic bonding, with carbon monoxide acting as a σ-donor and a π-acceptor for *d*-block metals[65]. This may however not be accurate for all *d*-block metals. While there are many thousands of stable, isolable transition metal carbonyl complexes, there are few or none known for the metals at the extreme fringes of the *d*-block. For example, the group 3 ions Sc^{3+}, Y^{3+}, and La^{3+} have not yielded any isolable carbonyl complexes, presumably because their lack of *d* electrons precludes π-back-bonding and synergistic bonding. Additionally, no isolable carbonyls are known for the group 12 d^{10} ions Zn^{2+} and Cd^{2+}, presumably because their effective nuclear charges are too high to permit effective metal→carbon d→π* π-backbonding.

Very few isolable carbonyl complexes exist for Ag^{+}, despite the fact that silver(I) carbonyl structures have been shown exist more readily in solution. The first, $[Ag(CO)][B(OTeF_5)_4]$, was isolated in 1991[10.a], followed by $[Ag(CO)_2][B(OTeF_5)_4]$ in

[65] a) S. Yamamoto, H. Kashiwagi, *Chem. Phys. Lett.*, **205***,* 306 (1993). b) M.R.A. Blomberg, P.E.M. Siegbahn, T.L. Lee, A.P. Rendel1, J.E.J. Rice, *Chem. Phys.*, **95**, 5898 (1991). c) L.A. Barnes, M. Rosi, C.W.J. Bauschlicher, *Chem. Phys.*, **94**, 2031 (1991). d) S. Smith, I.H. Hillier, W. von Niessen, M.F. Guest, *Chem. Phys.*, **135***,* 357 (1987). e) K. Pierfoot, J. Verhulst, P. Verbeke, L.G. Vanquickenborne, *Inorg. Chem.*, **28**, 3059 (1989). f) R.L. Williamson, M.B. Hall, *Int. J. Quantum Chem.*, **21S**, 503 (1987). g) D.E. Shenvood, M.B. Hall, *Inorg. Chem.*, **19**, 1805 (1980). h) M.B. Hall, R.F. Fenske, *Inorg. Chem.*, **11**, 1620 (1972).

1993[10.b], complexes of $[Ag(CO)]^+$ and $[Ag(CO)_2]^+$ with varied counterions in 1994[10.b] and $[HB(3,5\text{-}(CF_3)_2Pz)_3]Ag(CO)$ in 1995[10.d]. All the counterions in these complexes exhibit electron-withdrawing properties. There has been interest in $Ag(CO)_n^+$ species as catalysts for the carbonylation of alkanes, arenes, olefins, aldehydes, alcohols, and amines[66]. Before 1991, $Ag(CO)_n^+$ species have only been detected in zeolite hosts[67] or in strongly acidic media such as concentrated H_2SO_4 or $BF_3{\cdot}H_2O$ (generally at low temperatures and high pressures)[68]. The weakly coordinating anion $B(OTeF_5)_4^-$ allows the formation of solid state $[Ag(CO)][B(OTeF_5)_4]$ and $[Ag(CO)_2][B(OTeF_5)_4]$. $[Ag(CO)_2][B(OTeF_5)_4]$ decomposes at room temperature, converting to $Ag(CO)OTeF_5$:

$$[Ag(CO)_2][B(OTeF_5)_4] \rightarrow Ag(CO)OTeF_5 + B(OTeF_5)_3 + CO \quad \textbf{... 2.8}$$

Preceding the publication of these structures, the only examples of isolable CO complexes with absent π-backbonding were Au(I) carbonyls[69]. Crystals of $[Ag(CO)_2]^+$ are extremely hygroscopic and thermally labile. Although this was the first structural evidence for a simple two-coordinate $M(CO)_2$ complex of any metal, manometric and spectroscopic data have suggested the existence of solvated $[Ag(CO)_2]^+$ [68] and $[Au(CO)_2]^+$ ions in highly acidic media, $[Au(CO)_2]^+$ ions in the solid state and neutral $M(CO)_2$ species in carbon monoxide matrices[70].

The values of ν_{CO} for $[Ag(CO)]_2[Zn(OTeF_5)_4]$ and $[Ag(CO)]_2[Ti(OTeF_5)_6]$ from IR spectra are 2203 and 2207 cm^{-1} respectively, while ν_{CO} for $[Ag(CO)_2]_2[Zn(OTeF_5)_4]$ and

---

[66] a) Y. Souma, *Jpn. Kokai Tokkyo Koho*, 1 (1989). b) Y. Souma, *Shokubai*, **29**, 317 (1987). c) Y. Souma, H. Sano, *Nippon Kagaku Kaishi*, 263 (1982). d) Y. Souma, *Osaka Kogyo Gijutsu Shikensho Hokoku*, I (1979). e) T. Tsuda, Y. Isegawa, T. Saegusa, *J. Org. Chem.*, **37**, 2670 (1972).

[67] a) J. Baumann, R. Beer, G. Calzaferri, B. Waldeck, *J. Phys. Chem.*, **93**, 2292 (1989). b) H. Beyer, P.A. Jacobs, J.B. Uytterhoeven, *J. Chem. Soc., Faraday Trans. 1*, **72**, 674 (1976). c) Y.Y. Huang, *J. Catal.*, **32**, 482 (1974).

[68] a) W. Backen, A. Ericsson, *Acta Chem. Scand., Ser. A*, **A35**, 1 (1981). b) A. Neppel, J.P. Hickey, I.S. Butler, *J. Raman Spectrosc.*, **8**, 57 (1979). c) Y. Souma, J. Iyoda, H. Sano, *Osaka Kogyo Gijufsu Shikensho Kiho*, **27**, 227 (1976). d) Y. Souma, J. Iyoda, H. Sano, *Inorg. Chem.*, **15**, 968 (1976).

[69] a) H. Willner, J. Schaebs, G. Hwang, F. Mistry, R. Jones, J. Trotter, F.J. Aubke, *J. Am. Chem. Soc.*, **114**, 8972 (1992). b) M. Adelhelm, W. Bacher, E.G. Höhn, E. Jacob, *Chem. Ber.*, **124**, 1559 (1991). c) D.B. Dell' Amico, F. Calderazzo, P. Robino, A.J. Segre, *J. Chem. Soc., Dalton Trans.*, **11**, 3017 (1991). d) H. Willner, F. Aubke, *Inorg. Chem.*, **29**, 2195 (1990).

[70] a) J.H.B. Chenier, C.A. Hampson, J.A. Howard, B. Mile, *J. Phys. Chem.*, **92**, 2745(1988). b) P.H. Kasai, P.M.J. Jones, *J. Am. Chem. Soc.*, **107**, 813 (1985). c) P.H. Kasai, P.M. Jones, *J. Phys. Chem.*, **89**, 1147 (1985). d) D. McIntosh, G.A. Ozin, *Inorg. Chem.*, **16**, 51 (1977). e) D. McIntosh, G.A. Ozin, *J. Am. Chem.* Soc., **98**, 3167 (1976). f) H. Huber, E.P. Kündig, M. Moskovits, G.A. Ozin, *J. Am. Chem.* Soc., **97**, 2097 (1975). g) J.S. Ogden, *J. Chem. Soc., Chem. Commun.*, **16**, 978 (1971).

$[Ag(CO)_2]_2[Ti(OTeF_5)_6]$ are both 2198 cm^{-1}. All of these values are much higher than in free CO (2143 cm^{-1}), an indication of an increase in C-O bond order upon coordination to Ag(I). This also indicates that CO is acting as a Lewis base in this compound. According to theoretic studies, if a Cr(0)-CO bond was stretched ~0.25 Å longer than its equilibrium distance, Cr-C π-bonding would be negligible and CO would act as a σ-only ligand[71]. Significantly, the Ag(I)-CO distances in $[Ag(CO)][B(OTeF_5)_4]$ and $[Ag(CO)_2][B(OTeF_5)_4]$, ~2.1 Å, are ~0.3 Å longer than typical Rh(I)-CO distances, which are ~1.8 Å. The short C-O bond, long Ag-CO bond and unusually high value of ν_{CO} suggest little or no π-backbonding in $[Ag(CO)_n]^+$ complexes. Similar behaviour has been observed for neutral Pt(II) and Pd(II) carbonyls[72].

The structure and properties of the CO molecule have many similarities with the CN molecule. The substance known as cyanide gas exists as HCN, and is extremely toxic. Cyanogen, which is $(CN)_2$, can be prepared by the oxidation of HCN by either O_2 in the presence of a silver catalyst, Cl_2 over activated silica, or NO_2 over calcium oxide-glass[24]. Cyanogen dissociates into CN radicals and can oxidatively add to lower-valent metal atoms giving dicyano complexes. CN^- is a strong nucleophile, with low π-acceptor behaviour with regard to CO, due to the negative charge on the ion. Unidendate CN^- always binds through C, but due to the lone pair of the N-atom, many bidendate structures exist with CN as acting as a bridge.

2.4.4 OXIDATIVE ADDITION

For a substance to react with a metal atom contained in a complex in solution, vacant sites must be available for coordination. In five- or six-coordinated metal complexes, coordination sites may be made available by dissociation of one or more ligands either thermally or photochemically, or by the use of ligands with high trans effects. Steric effects may be important in oxidative addition reactions, as bulky ligands have a greater tendency to dissociate.

In electron-rich complexes the metal atom may have substantial non-bonding electron density located on it and may then be attacked by H^+ or other electrophiles. Coordinately

[71] D.E. Sherwood, Jr., M.B. Hall, *Inorg. Chem.*, **22**, 93 (1983).
[72] F. Calderazzo, *J. Organomet. Chem.*, **400**, 303 (1990).

unsaturated complexes, however, can add neutral or anionic nucleophiles and can therefore exhibit both Lewis acid and Lewis base behaviour. This is an essential property for oxidative addition reactions, with the reverse reaction being reductive elimination. For the addition to proceed, non-bonding electron density must be present on the metal atom, as well as two vacant coordination sites on the complex and a metal with oxidation states separated by two units. Oxidative addition to 16-electron systems produces 18-electron systems. Compounds complying with the 18-electron rule cannot undergo oxidative addition reactions without expulsion of a ligand. Steric properties of ligands influence oxidative addition reactions; bulky ligands such as PEt(*t*-Bu)$_2$ decreases the ease of oxidative addition, while the substitution of an *o*-methoxy group on a phenylphosphine increases the nucleophilicity of the metal by donation.

2.4.5 OLEFIN INTERACTIONS

Unsaturated molecules can form π-complexes with transition metals, with the most widely applied complexes being those with C=C bonds. In coordinated olefins, the axis of the C=C bond is perpendicular to one of the expected bond directions from the metal, although this is not necessarily true for unsymmetrical olefins. As with other π-bonding ligands like CO, there are two components to the total bonding: overlapping of olefin π-electron density with the σ-acceptor orbital of the metal, and a back bond resulting from flow of electron density from filled metal orbitals into antibonding orbitals on the carbon atoms. This is illustrated in Figure 2.7[24].

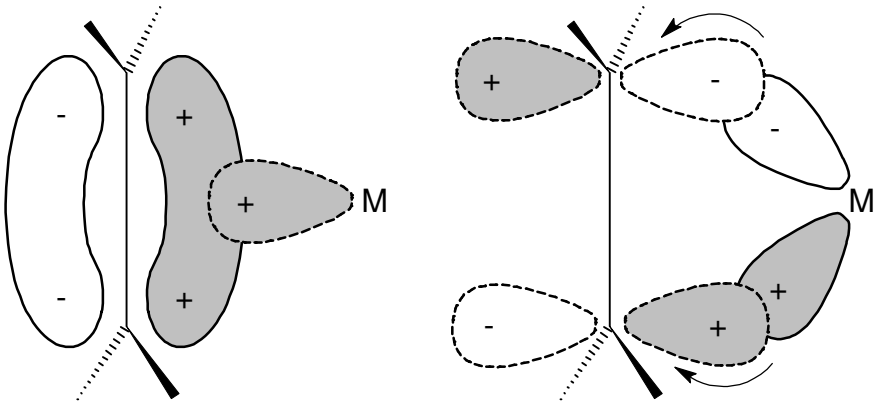

Figure 2.7 The molecular orbital view of olefin-metal bonding. The figure on the left shows the donation of electron density from filled π orbitals to the vacant metal orbital, on the right back-bonding from filled metal orbitals to acceptor π* orbitals are illustrated.

With this model the retention of the double bond character of the olefin upon coordination is implied. The donation of π-bonding electrons to the metal σ orbital and the introduction of electrons into the π-antibonding orbital both weakens the π bonding in the olefin and causes lengthening of the olefin C-C bond. The metal-olefin bonding exhibits dual character: donation of electrons from the initial formation of the C-C π bond, into a metal orbital of suitable symmetry, then donation of electrons from filled metal orbitals of suitable symmetry back into the π-antibonding orbitals of the olefin. These two are synergically related; as one component increases, it tends to promote an increase in the other. The metal-olefin is in essence electroneutral, with donation and back-acceptance approximately balanced.

Although the C-C axis of ethene is perpendicular to the plane of the square coordination for Zeise's salt and other, similar complexes, this is not strongly demanded by the bonding. Another metal orbital, the dπ orbital, is present in the plane and is available for interaction with the olefin pπ* orbital as shown in Figure 2.7. While in-plane bonding is weaker, the difference in stability between the perpendicular and in-plane orientations is not great on a bonding basis, and may be steric in origin.

When two or more conjugated double bonds are engaged in bonding to a metal atom the interactions become more complex, though qualitatively the two types of basic, synergic components are involved.

2.4.6 CARBENES

Complexes formed from reactions of :CR_2 are generally classified as carbenes. Carbene complexes commonly have CO or PR_3 ligands, and although they can be formulated as having a M=C double bond, other canonical forms are also involved, shown in Scheme 2.4.

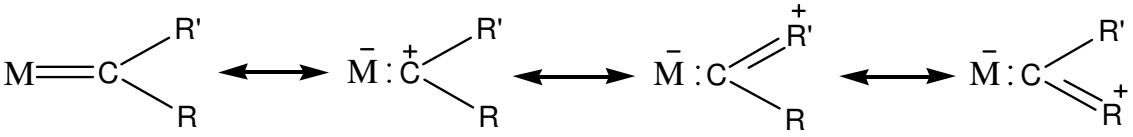

Scheme 2.4 Illustration of different carbene complex geometries.

Many known carbene complexes have OR or NR_2 groups attached to the carbon, and electron flow from lone pairs on O or N leads to a contribution to the C-O or C-N bond through $p\pi \rightarrow p\pi$ bonding. The M-CRR' grouping is always planar, and the M-C distances indicate considerable shortening consistent with multiple bond character. In the case of the C bonded to an OR or NR_2 group, the C-O and C-N distances are also shortened, as expected with π-bonding. In carbene complexes, the C atom bound to the metal is electrophilic and is readily attacked by nucleophilic reagents.

The organometallic and coordination chemistry of N-heterocyclic carbenes (NHCs) has become a well-established area of research[73]. Numerous NHC complexes have been reported, and many of them have been successfully used as catalysts in various reactions over the past decade.

[73] a) J.C. Garrison, W.J. Youngs, *Chem. Rev.*, **105**, 3978 (2005). b) D. Bourissou, O. Guerret, F.P. Gabbai, G. Bertrand, *Chem. Rev.*, **100**, 39 (2000). c) W.A. Herrmann, *Angew. Chem., Int. Ed. Engl.*, **41**, 1290 (2002).

3 Preparation and Characterization of Complexes

3.1 Introduction

The first silver phosphine complex, $[AgPPr_3]SCN$, characterized by X-ray crystallography was reported in 1963[1]. Since then more than a thousand[2] complexes containing silver coordinated to phosphorous donor ligands have been synthesized and characterized. This chapter concerns the preparation of the complexes relevant to this study, and the characterization thereof using infrared spectroscopy and X-ray crystallography.

3.2 Preparation of Complexes

3.2.1 Instruments and Chemicals

All common laboratory reagents used were of analytical reagent grade. AgBr, $AgClO_4$, $AgPF_6$ and P(*p*-tol)$_3$ were all obtained from Sigma Aldrich and used without further purification. Acetone and acetonitrile (reagent grade) were obtained from Merck and used without further purification.

Characteristic stretching frequencies of the complexes were obtained from infrared spectra recorded on a Bruker Tensor 27 spectrometer. The samples were analyzed as KCl disks over the range 4000-400 cm^{-1}, and all spectral scans were collected at room temperature. NMR spectra were recorded at -80 °C in 50% CD_2Cl_2/CH_2Cl_2 on a Bruker Avance II 600 (242.99 MHz for ^{31}P) nuclear magnetic resonance spectrometer. For recording the ^{31}P spectra a capillary tube filled with 80% H_3PO_4 was used for calibration to 0 ppm.

---

[1] C. Panattoni, E. Frasson, *Gazz. Chim. Ital.,* **93**, 601 (1963).
[2] The Cambridge Structural Database Version 1.9, F.H. Allen, *Acta Cryst.*, **B58**, 380 (2002).

3.2.1.1 Preparation of Complex A; $[Ag\{P(p\text{-tol})_3\}_4]PF_6$

(FW = 1470.35 g.mol^{-1})

$AgPF_6$ (0.0861 g, 0.3405 mmol) was heated under reflux with P(*p*-tol)$_3$ (0.4178 g, 1.373 mmol, 4.03 eq) in acetonitrile until dissolved. The product was recrystallized from acetone, giving colourless crystals in a yield of 0.4873 g (96.71 %). ^{31}P NMR (CD_2Cl_2, -80° C, 242.99 MHz): 2.96 (d, $^1J_{^{107}Ag\text{-}^{31}P}$ 224.40 Hz, d, $^1J_{^{109}Ag\text{-}^{31}P}$ 258.54 Hz). IR (KCl): 556.81, 839.67 cm^{-1}.

3.2.1.2 Preparation of Complex B; $[Ag\{P(p\text{-tol})_3\}_3]ClO_4 \cdot CH_3COCH_3$

(FW = 1178.52 g.mol^{-1})

$AgClO_4 \cdot H_2O$ (0.1054 g, 0.4678 mmol) was heated under reflux with P(*p*-tol)$_3$ (0.4129 g, 1.357 mmol, 3.45 eq) in acetonitrile until dissolved. The product was recrystallized from acetone, giving colourless crystals in a yield of 0.4654 g (84.42 %). ^{31}P NMR (CD_2Cl_2, -80° C, 242.99 MHz): 8.59 (d, $^1J_{Ag\text{-}P}$ 340.91 Hz). IR (KCl): 918.95, 1095-1013, 622.40 cm^{-1}.

3.2.1.3 Preparation of Complex C; $[Ag_4\{P(p\text{-tol})_3\}_4Br_4] \cdot CH_3COCH_3$

(FW = 1968.64 g.mol^{-1})

AgBr (0.1913 g, 1.019 mmol) was heated under reflux with P(*p*-tol)$_3$ (0.1570 g, 0.5015 mmol, 0.5 eq) in acetonitrile until dissolved. The product was recrystallized from acetone, giving colourless crystals in a yield of 0.0511 g (20.13 %). The characteristic stretching frequencies of this complex fell outside the range of this spectrometer. ^{31}P NMR (CD_2Cl_2, -80° C, 242.99 MHz): 4.89 (d, $^1J_{^{107}Ag\text{-}^{31}P}$ 439.84 Hz, d, $^1J_{^{109}Ag\text{-}^{31}P}$ 468.39 Hz).

3.2.2 DISCUSSION: SYNTHESIS OF COMPLEXES

Synthesis of the above mentioned complexes were relatively easy; reagents were added together in stoichiometric ratio's in hot solvents and the product readily crystallized from solution. The geometry of the Ag metal and coordination modes depended on the stoichiometry of the reaction, resulting in tetrahedral, trigonal planar and cubane-like structures, respectively. In the synthesis of $[Ag_4\{P(p\text{-tol})_3\}_4Br_4]$ the excess AgBr reagent

did not dissolve and was removed through filtration. The low yield of this polymeric complex can possibly be attributed to monomers still in solution, which could have high energy of crystallization due to steric interactions. These reactions were not light or air sensitive, and the products were stable over a period of months.

3.3 X-Ray Crystallography

3.3.1 INTRODUCTION

X-ray crystallography is a technique in which the diffraction of X-rays through the closely spaced lattice of atoms in a crystal is recorded. The pattern produced is then analyzed to reveal the nature of that lattice. This generally leads to an understanding of the material and molecular structure of a substance. The spacing in the crystal lattice can be determined using Bragg's law. This technique is widely used in chemistry and biochemistry to determine the structures of an immense variety of molecules, including inorganic compounds, DNA, and proteins. X-ray diffraction is commonly carried out using single crystals of a material, but if these are not available, microcrystalline powdered samples may also be used, although this requires different equipment, gives less information, and is much less straightforward.

3.3.2 BRAGG'S LAW[3]

Bragg's law is the result of experiments into the diffraction of X-rays or neutrons off atoms in a crystal at certain angles. When X-rays hit an atom, the electronic cloud re-radiates waves with the same frequency. A similar process occurs upon scattering neutron waves from the nuclei or by a coherent spin interaction with an unpaired electron. These re-emitted wave fields interfere with each other either constructively or destructively, producing a diffraction pattern on a detector or film. The resulting wave interference pattern is the basis of diffraction analysis. The interference is constructive when the phase shift is proportional to 2π, expressed by Bragg's law in Eq. 3.1:

$$n\lambda = 2d \sin\theta \qquad \textbf{... 3.1}$$

[3] W.L. Bragg, *Proceedings of the Cambridge Philosophical Society*, **17**, 43 (1912).

n is an integer, λ the wavelength of x-rays, d is the spacing between the planes in the atomic lattice and θ is the angle between the incident ray and the scattering planes. Bragg's law is illustrated in Figure 3.1.

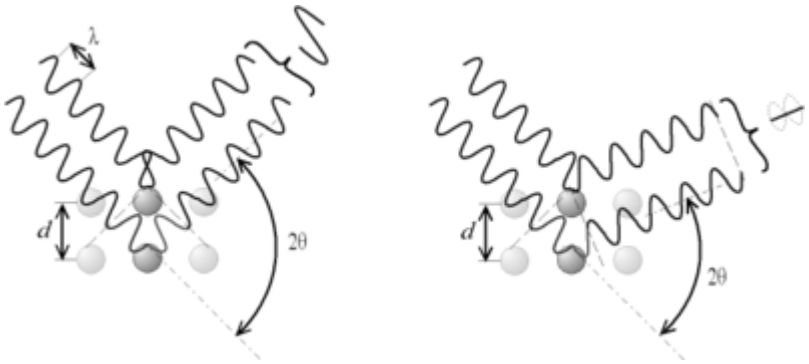

Figure 3.1 Illustration of Bragg's law. According to the 2θ deviation, the phase shift causes constructive (left figure) or destructive (right figure) interferences.

3.3.3 MILLER INDICES[4]

Miller indices are a notation used to describe lattice planes and directions in a crystal. A family of lattice planes is determined by three integers, h, k and l. They are written (hkl) and denote planes orthogonal to a direction (h, k, l) in the basis of the reciprocal lattice vectors. The precise meaning of this notation depends upon a choice of lattice vectors for the crystal.

3.3.4 STRUCTURE FACTOR[5]

The structure factor describes the way in which an incident beam is scattered by the atoms of a crystal unit cell, taking into account the different scattering power of the elements through the term f_i. Due to the periodic arrangement of the atoms, the interference of waves scattered from different atoms may cause a distinct pattern of constructive and destructive interference to form. In the kinematical approximation for diffraction, the intensity of a diffracted beam is given by Eq. 3.2:

$$I(hkl) = |\varphi(hkl)|^2 \propto |F(hkl)|^2 \quad \textbf{... 3.2}$$

φ(hkl) is the wavefunction of a beam scattered to vector (hkl), and $|F(hkl)|^2$ is the structure factor, given by Eq. 3.3:

[4] N.W. Ashcroft, N.D. Mermin, *Solid State Physics*, Harcourt, New York, 1, (1976).
[5] D.E. Sands, *Introduction to Crystallography*, Dover Publications, Minneola, 100 (1969).

$$F(hkl) = \Sigma f_j \exp[2\pi i(hx + ky + lz)] \quad \text{... 3.3}$$

The term $2\pi(hx + ky + lz)$ is the scalar product of the vector (hkl) and the position (x, y, z) of an atom *j* in the unit cell, and f_j is the scattering power of the atom, also called the atomic form factor. The sum is over all atoms in the unit cell. Since the atoms are spatially distributed in the unit cell, there will be a difference in phase when considering the scattered amplitude from two atoms. This phase shift is taken into account by the complex exponential term. The atomic form factor or scattering power, of an element depends on the type of radiation considered. As electrons interact with matter through different processes, for example X-rays, the atomic form factors for the two cases are not the same.

3.3.5 FOURIER TRANSFORMATION[5]

Fourier transform is a linear operator that maps functions to other functions. The Fourier transform decomposes a function into a continuous spectrum of its frequency components, and the inverse transform synthesizes a function from its spectrum of frequency components. A Fourier series often comprises of a sum of sine and cosine terms with appropriate coefficients. The Fourier expansion of the electron density function is given in Eq. 3.4.

$$\rho(xyz) = \Sigma_h \Sigma_k \Sigma_l F(hkl)\exp[-2\pi i(hx + ky + lz)] \quad \text{... 3.4}$$

F(hkl) is the coefficient to be determined and h, k and l are integers over which the series is to be summed.

3.3.6 PATTERSON FUNCTION[5]

Essentially, the Patterson function is the Fourier transform of the intensities rather than the structure factors. To derive the Patterson function, electron density at a point (x, y, z) is multiplied by the electron density at a point (x+u, y+v, z+w). The product is then multiplied by *dxdydz* and integrated over the volume of the unit cell:

$$\iiint \rho(x, y, z)\rho(x + u, y + v, z + w)dxdydz \quad \text{... 3.5}$$

When Eq. 3.4 is substituted for each electron density function, the Patterson function can be defined in Eq. 3.6:

$$P(uvw) = \Sigma\Sigma\Sigma|F(hkl)|^2\cos2\pi(hu + kv + lw) \quad \text{... 3.6}$$

This function will be non-zero at the point (u, v, w) when the points x, y, z exist such that ρ(x, y, z) and ρ(x+u, y+v, z+w) are non-zero. The function will then reach maximum values at the points u, v, w, corresponding to the coordinates of vectors between pairs of atoms, creating a map from which atomic arrangement may be deduced. For each interatomic vector a Patterson peak will exist. A Patterson map of *N* points will have *N(N−1)* peaks, excluding the central peak and any overlap.

3.3.7 THE PHASE PROBLEM

The intensity of X-ray radiation reflected from the hkl plane is proportional to $|F(h, k, l)|^2$, shown in Eq. 3.2. The availability of sets of values of $|F(h, k, l)|^2$, however, does not lead to routine determination of crystal structures, as Eq. 3.4 requires the values of F(h, k, l). This number is complex, as shown in Eq. 3.7,

$$F(hkl) = A(hkl) + iB(hkl) \quad \text{... 3.7}$$

where $i = \sqrt{-1}$. To calculate the crystal structure, the values for A and B must be known. This difficulty is known as the phase problem, but may be solved by different methods known as direct methods or by utilizing the heavy atom method. These methods involve selecting the reflections contributing most to the Fourier transform, calculating the probable relationship among their phases and trying different possible phases to see how well the probability phases are satisfied. Many methods exist and will not be discussed here[5].

3.3.8 DIRECT METHOD - LEAST SQUARE REFINEMENT[6]

A mathematical method that adjusts the parameters of the phases of structure factors, minimizing a function such as $\Sigma(F_0-F_c)^2$. In general, it is used when a measurable physical quantity, Q, has a linear dependence on a set of parameters x, y, z in terms of the known values A, B, C. This method gives estimates of the standard deviations of the atomic parameters, which can be used to calculate the uncertainties in bond lengths and angles.

[6] W. Massa, *Crystal Structure Determination*, Springer-Verlag, Berlin, 115 (2000).

3.3.9 THE PHYSICAL METHOD OF CRYSTAL STRUCTURE DETERMINATION[7]

3.3.9.1 Physical Appearance of the Sample

In the case of single crystal crystallography, all the unit cells of the sample must be identical and aligned in the same orientation (hence called a single crystal). The intensities of X-rays diffracted by a crystal are proportional to its volume, but X-rays are also absorbed by the crystal. This absorption effect increases exponentially with crystal dimensions and affects the measured intensities. The amount of absorption depends on the X-ray wavelength and can be high when heavier elements are present. Errors can also be produced when the crystal is not completely bathed in the incident X-ray beam, usually about 1mm in cross-section. An acceptable crystal is a few tenths of a millimetre, preferably even smaller if the sample contains heavy atoms. This crystal may be glued to a glass rod with amorphous glue, sealed in a thin-walled glass capillary or coated with inert viscous oil and cooled to a low temperature to vitrify the oil to glass. The latter two methods are generally used for air-sensitive samples.

3.3.9.2 Instrumentation

Diffractometers use an electronic device, sensitive to X-rays, as a detector. The most common detector contains a material such as thallium-doped sodium iodide which produces light in the visible region when X-rays fall on it. Various types of diffractometers exist, with different rotation axes for optimum reflection from the crystal. Diffraction of the X-ray from the crystal results in constructive interference according to Bragg's law, detected as spots. The total integrated intensity is measured from these spots and used to calculate I_{hkl}, the electron density distribution, |F(hkl)| and the Patterson function, and therefore the positions of the atoms in the crystal structure.

3.3.10 CRYSTAL STRUCTURE DETERMINATION

3.3.10.1 Experimental

$[Ag\{P(p\text{-tol})_3\}_4]PF_6$, $[Ag\{P(p\text{-tol})_3\}_3]ClO_4 \cdot CH_3COCH_3$ and $[Ag_4\{P(p\text{-tol})_3\}_4Br_4] \cdot CH_3COCH_3$ were characterized using X-ray crystallography. The results are presented

[7] W. Clegg, *Crystal Structure Determination*, Oxford University Press, Oxford, 28 (2003).

below. The initial unit cell and data collection were achieved on a Bruker X8 diffractometer by the APEX2 package[8] utilizing COSMO[9] for optimum collection of more than a hemisphere of reciprocal space. The frames were integrated using a narrow-frame integration algorithm and reduced with the Bruker SAINT-PLUS[10] and XPREP[10] software packages, respectively. Data were corrected for absorption effects using the multi-scan technique SADABS[11]. The structure was solved by direct methods using the programs SIR97[12] and SHELXL[13] and refined using the WINGX software package[14] incorporating SHELXL[13]. The molecular plots were constructed using the DIAMOND program[15] with a 50% thermal envelope probability for non-hydrogen atoms.

Complex A: $[Ag\{P(p\text{-tol})_3\}_4]PF_6$ data collection was done at 100 ± 2 K with an exposure time of 15 seconds/frame, collecting 809 frames with a frame width of 0.3°, covering up to 28.35° and accomplishing 100 % completeness.

Complex B: $[Ag\{P(p\text{-tol})_3\}_3]ClO_4{\cdot}CH_3COCH_3$ data collection was done at 100 ± 2 K with an exposure time of 20 seconds/frame, collecting 633 frames with a frame width of 0.3°, covering up to 28.36° and accomplishing 99.7 % completeness.

Complex C: $[Ag_4\{P(p\text{-tol})_3\}_4Br_4]{\cdot}CH_3COCH_3$ data collection was done at 100 ± 2 K with an exposure time of 20 seconds/frame, collecting 948 frames with a frame width of 0.3°, covering up to 28.31° and accomplishing 99.9 % completeness.

The aromatic and methyl H atoms were placed in geometrically idealized positions (C-H = 0.95 - 0.98 Å) and constrained to ride on their parent atoms with $U_{iso}(H) = 1.5U_{eq}(C)$ and $1.2U_{eq}(C)$ for methyl and aromatic H atoms, respectively (except for the H atoms on the solvent molecule acetone).

A summary of the general crystal data is given in Table 3.1.

[8] Bruker APEX2, Version 1.0-27, Bruker AXS Inc., Madison, Wisconsin, USA (2005).
[9] COSMO, Version 1.48, Bruker AXS Inc., Madison, Wisconsin, USA (2003).
[10] SAINT-PLUS, Version 7.12 (including XPREP), Bruker AXS Inc., Madison, Wisconsin, USA (2004).
[11] SADABS, Version 2004/1, Bruker AXS Inc., Madison, Wisconsin, USA (1998).
[12] A. Altomare, M.C. Burla, M. Camalli, G.L. Cascarano, C. Giacovazzo, A. Guagliardi, A.G.G. Moliterni, G. Polidori, R. Spagna, *J. Appl. Cryst*., **32**, 115 (1999).
[13] G.M. Sheldrick, SHELXL97, University of Göttingen, Germany (1997).
[14] L.J. Farrugia, *J. Appl. Cryst*,. **32**, 837 (1999).
[15] K. Brandenburg, H. Putz, DIAMOND, Release 3.0c. Crystal Impact, GbR, Bonn, Germany (2005).

Table 3.1 Crystal data for structures $[Ag\{P(p\text{-tol})_3\}_4]PF_6$, $[Ag\{P(p\text{-tol})_3\}_3]ClO_4\cdot CH_3COCH_3$ and $[Ag_4\{P(p\text{-tol})_3\}_4Br_4]\cdot CH_3COCH_3$.

Complex identification	**$[Ag\{P(p\text{-tol})_3\}_4]PF_6$**	**$[Ag\{P(p\text{-tol})_3\}_3]ClO_4 \cdot CH_3COCH_3$**	**$[Ag_4\{P(p\text{-tol})_3\}_4Br_4] \cdot CH_3COCH_3$**
Empirical formula	$C_{84}H_{84}AgF_6P_5$	$C_{66}H_{69}AgClO_5P_3$	$C_{84}H_{84}Ag_4Br_4P_4$
Molecular weight	1470.23	1178.44	1968.51
Crystal system	Cubic	Orthorhombic	Trigonal
Space group	$P2_13$ (198)	$Pna2_1$ (33)	$R\bar{3}$ (148)
a (Å)	24.6842(4)	19.8625(8)	16.8810(2)
b (Å)	24.6842(4)	25.3785(9)	16.8810(2)
c (Å)	24.6842(4)	11.6858(5)	51.3161(13)
α / β / γ (°)	90 / 90 / 90	90 / 90 / 90	90 / 90 / 120
Volume (Å^3)	15040.3(4)	5890.6(4)	12664.3(4)
Z	8	4	6
Density$_{cal}$ (g.cm^{-3})	1.299	1.329	1.549
Crystal colour	White	White	White
Crystal size (mm)	0.40 x 0.37 x 0.36	0.31 x 0.26 x 0.24	0.25 x 0.24 x 0.10
Theta ranges (°)	1.17 to 28.35	1.30 to 28.36	1.19 to 28.31
R_{int}	0.031	0.045	0.025
Index ranges	h = −32 to 32	h = −26 to 19	h = −22 to 20
	k = −32 to 32	k = −16 to 33	k = −22 to 20
	l = −30 to 24	l = −11 to 15	l = − 68 to 50
Reflections collected	122435	27027	24282
Independent reflections	12538	7691	7026
Data / parameters	12538 / 588	7691 / 709	7026 / 293
Goodness-of-fit on F^2	1.086	1.048	1.082
R(F^2)	0.0383	0.0388	0.0403
wR(F^2)	0.0908	0.0972	0.1279
Radiation λ (Å) (from Mo Kα)	0.71073	0.71073	0.71073

Supplementary data with complete lists of atomic coordinates, bond distances and angles, anisotropic displacement parameters as well as hydrogen coordinates are given in

Appendix A for $[Ag\{P(p\text{-tol})_3\}_4]PF_6$, Appendix B for $[Ag\{P(p\text{-tol})_3\}_3]ClO_4 \cdot CH_3COCH_3$ and Appendix C for $[Ag_4\{P(p\text{-tol})_3\}_4Br_4]$.

3.3.10.2 Structure of $[Ag\{P(p\text{-tol})_3\}_4]PF_6$

The complex was prepared as reported in section 3.2.1.1. $[Ag\{P(p\text{-tol})_3\}_4]PF_6$ crystallized with a cubic space group $P2_13$ with $Z = 8$. The complex crystallized with two independent tetrahedral silver(I) cations and PF_6^- anions in the asymmetric unit. $[Ag\{P(p\text{-tol})_3\}_4]PF_6$ is shown in Figure 3.2 with 50% probability displacement ellipsoids.

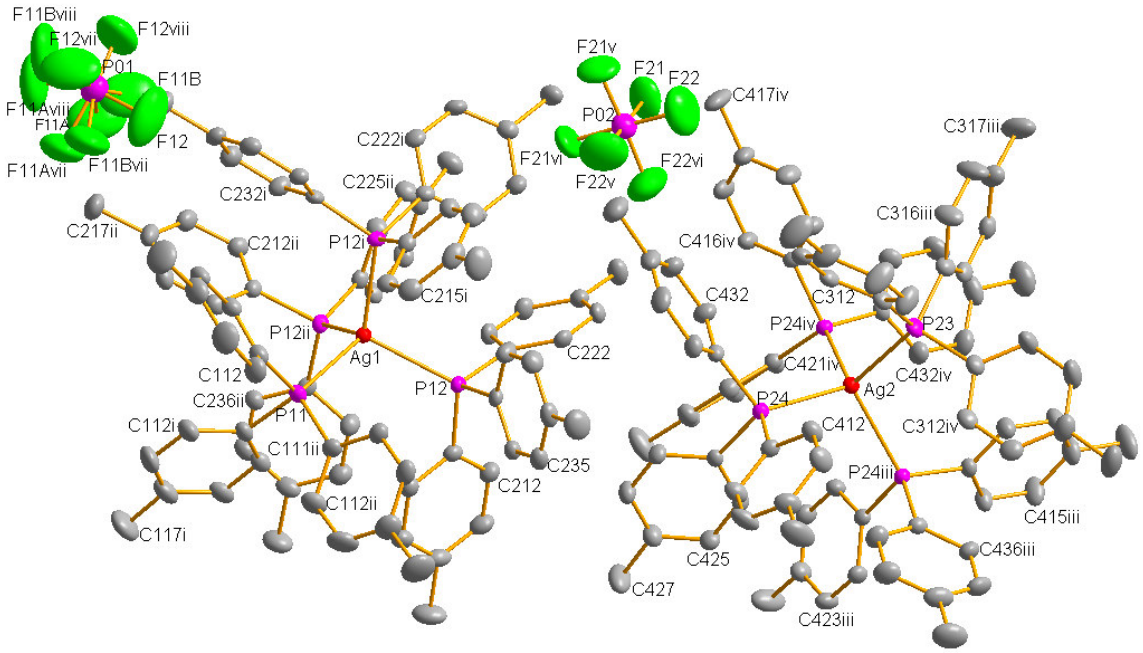

Figure 3.2 DIAMOND view of $[Ag\{P(p\text{-tol})_3\}_4]PF_6$ (50% probability displacement ellipsoids). Hydrogen atoms are omitted for clarity. For the C atoms, the first digit indicates phosphine number, the second digit indicates ring number and the third digit indicates the position of the atom in the ring. Atoms generated by symmetry are indicated by lower case roman numerical labels corresponding to the symmetry codes reported in Table 3.2. Some labels have been omitted for clarity, but all rings are numbered in the same consistent way.

Classical hydrogen bonds exist between phenyl hydrogen atoms and fluoride atoms of the PF_6^- anion, suspending the anion through weak hydrogen interactions of C-H···F. Hydrogen interactions in the structure, illustrated in Figure 3.3, are shown in Table 3.2.

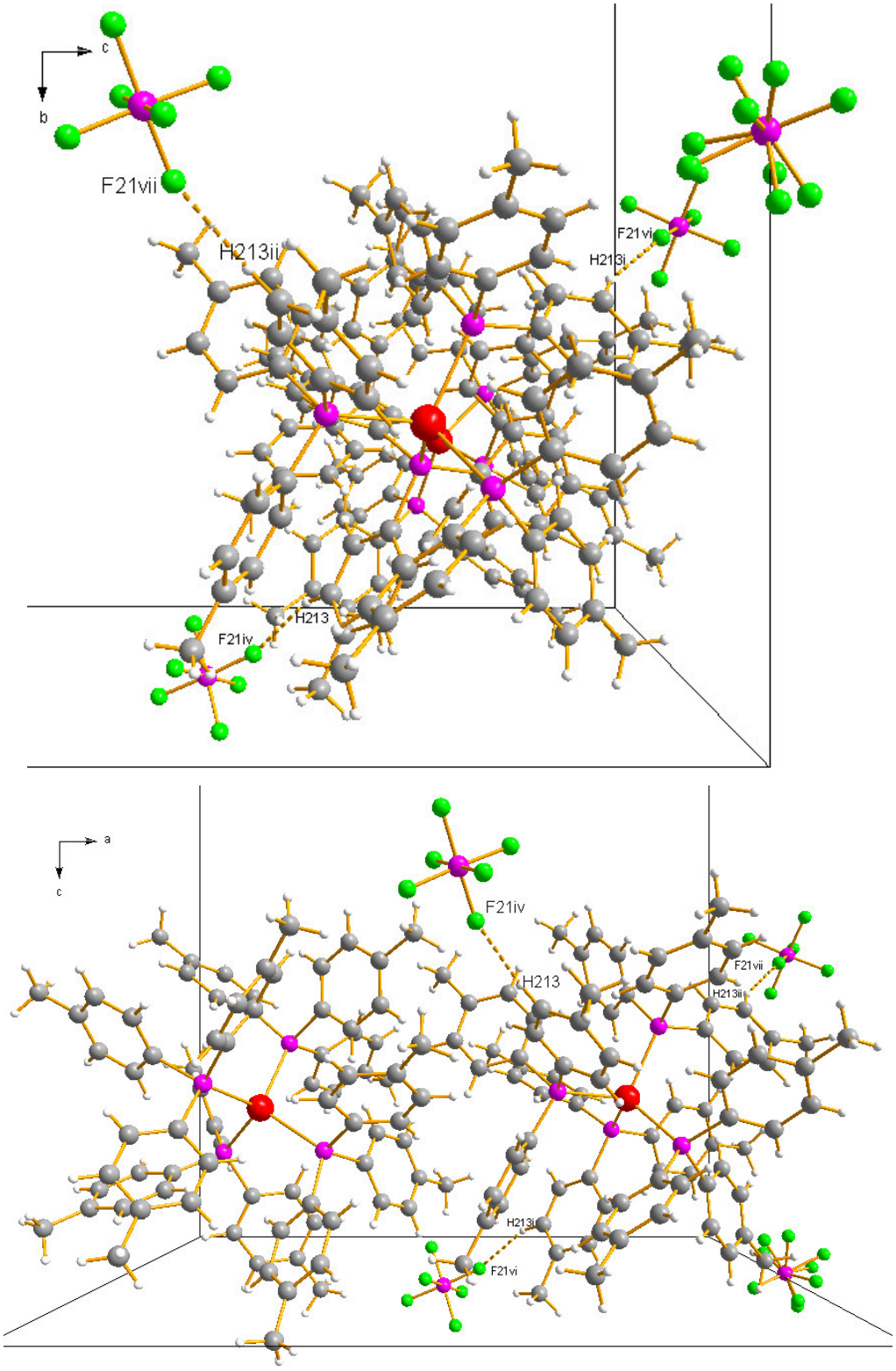

Figure 3.3 Partial unit cell for $[Ag\{P(p\text{-tol})_3\}_4]PF_6$, viewed along a-axis and b-axis, with important intramolecular hydrogen bonding interactions indicated with dashed lines. Symmetry operators are given in Table 3.2.

Table 3.2 Hydrogen bonds for $[Ag\{P(p\text{-tol})_3\}_4]PF_6$ (Å and °). The symmetry operator corresponds to the symmetry operator given in Table 3.3.

D-H...A	d_{D-H} (Å)	$d_{H...A}$(Å)	$d_{D...A}$(Å)	$<_{DHA}$ (°)
C_{213}-H_{213}...F_{21} [ix]	0.95	2.54	3.439(4)	158.8

Symmetry code: (ix) -x + 1, y + ½, -z + 1½

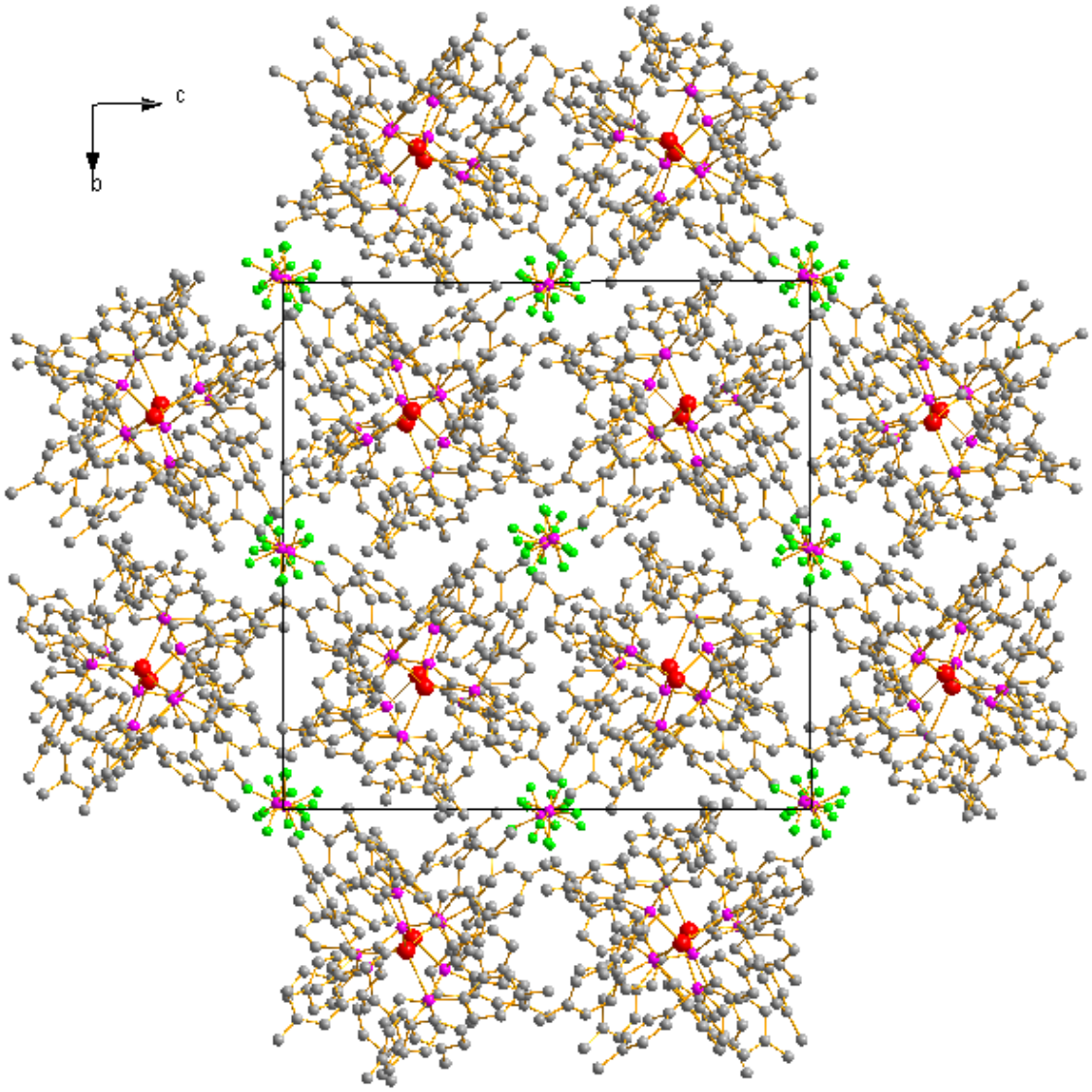

Figure 3.4 View of the unit cell of $[Ag\{P(p\text{-tol})_3\}_4]PF_6$ along the a-axis. The packing is similar to the packing viewed along the b- and c-axes.

$[Ag\{P(p\text{-tol})_3\}_4]^+$ packs symmetrically in the unit cell, surrounded by PF_6^-. This packing is illustrated in Figure 3.4. Selected bond distances and angles, involving silver atoms, are shown in Table 3.3, while selected bond angles of interactions of phosphine in the complex are shown in Table 3.4. The effective cone angles[16] of the phosphorous ligands are shown in Table 3.5.

Table 3.3 Selected bond lengths (Å) and angles (°) involving silver atoms in $[Ag\{P(p\text{-tol})_3\}_4]PF_6$.

Bond	**Bond Lengths (Å)**	**Bond**	**Bond Lengths (Å)**
P_{11}–Ag_1	2.570(1)	P_{23}–Ag_2	2.567(1)
P_{12}–Ag_1	2.5737(7)	P_{24}–Ag_2	2.6142(7)
Angle	**Bond Angles (°)**	**Angle**	**Bond Angles (°)**
P_{11}–Ag_1–P_{12}	109.31(2)	P_{23}–Ag_2–P_{24}	109.50(2)
P_{12}^{i}–Ag_1–P_{12}	109.63(2)	P_{24}^{iii}–Ag_2–P_{24}	109.44(2)
P_{12}^{i}–Ag_1–P_{12}^{ii}	109.63(2)	P_{24}^{iii}–Ag_2–P_{24}^{iv}	109.44(2)
Ag_1–P_{11}–C_{111}	114.9(1)	Ag_2–P_{23}–C_{311}	114.8(1)
Ag_1–P_{12}–C_{211}	112.8(1)	Ag_2–P_{24}–C_{411}	116.5(1)
Ag_1–P_{12}–C_{221}	114.75(9)	Ag_2–P_{24}–C_{421}	113.02(9)
Ag_1–P_{12}–C_{231}	117.05(9)	Ag_2–P_{24}–C_{431}	115.88(9)

Symmetry codes: (i) z, x, y (ii) y, z, x (iii) -z + 1, x + ½, -y + 1½ (iv) y - ½, -z + 1½, -x +1 (v) -y + 1, z - ½, -x + 1½ (vi) -z + 1½, -x + 1, y + ½ (vii) y + ½, -z + 1½, -x + 2 (viii) -z + 2, x - ½, -y + 1½ (ix) -x + 1, y + ½,-z + 1½

Table 3.4 Selected bond angles (°) of interactions in phosphine ligands in the complex $[Ag\{P(p\text{-tol})_3\}_4]PF_6$. Angles are arranged according to connections per phenyl ring.

Angle	**Bond Angle (°)**	**Angle**	**Bond Angle (°)**	**Angle**	**Bond Angle (°)**
P_{11}–C_{111}–C_{112}	123.3(2)	P_{11}–C_{111}–C_{116}	117.7(2)	C_{112}–C_{111}–C_{116}	119.0(3)
P_{12}–C_{211}–C_{212}	123.4(2)	P_{12}–C_{211}–C_{216}	117.8(2)	C_{212}–C_{211}–C_{216}	118.8(3)
P_{12}–C_{221}–C_{222}	124.7(2)	P_{12}–C_{221}–C_{226}	116.4(2)	C_{222}–C_{221}–C_{226}	118.8(3)
P_{12}–C_{231}–C_{232}	119.3(2)	P_{12}–C_{231}–C_{236}	122.5(2)	C_{232}–C_{231}–C_{236}	118.2(3)
P_{23}–C_{311}–C_{312}	117.8(2)	P_{23}–C_{311}–C_{316}	123.4(2)	C_{312}–C_{311}–C_{316}	118.8(3)
P_{24}–C_{411}–C_{412}	119.4(2)	P_{24}–C_{411}–C_{416}	122.1(2)	C_{412}–C_{411}–C_{416}	118.5(3)
P_{24}–C_{421}–C_{422}	125.3(2)	P_{24}–C_{421}–C_{426}	116.8(2)	C_{422}–C_{421}–C_{426}	117.9(3)
P_{24}–C_{431}–C_{432}	118.4(2)	P_{24}–C_{431}–C_{436}	123.4(2)	C_{432}–C_{431}–C_{436}	118.2(3)
P_{11}–C_{111}–C_{114}	177.2(2)	P_{23}–C_{311}–C_{314}	176.8(2)		
P_{12}–C_{211}–C_{214}	176.5(2)	P_{24}–C_{411}–C_{414}	178.5(2)		
P_{12}–C_{221}–C_{224}	175.3(2)	P_{24}–C_{421}–C_{424}	175.3(2)		
P_{12}–C_{231}–C_{234}	177.2(2)	P_{24}–C_{431}–C_{434}	176.7(2)		

[16] C.A. Tolman, *Chem. Rev.*, **77**, 313 (1977).

Table 3.5 Effective cone angles, θ_E, (°) for the P(*p*-tol)$_3$ ligands in [Ag{P(*p*-tol)$_3$}$_4$]PF$_6$.

Ligand	**Effective angle (°)**
P_{11}	143.7
P_{12}	146.6
P_{23}	148.4
P_{24}	142.1

The cone angles of P(*p*-tol)$_3$ in this complex [143.7° to 148.4°] are similar to that of PPh_3, which is 145°[16]. The similarity of the various P-Ag-P angles [from 109.31(2)° to 109.63(2)°] indicates a well-defined tetrahedral geometry around the Ag atom, as the ideal ligand angle of a tetrahedral complex is 109.5°.

The phosphine ligands exhibit a distorted tetrahedral geometry, indicated by the Ag-P-C angles. These angles vary from 112.8(1)° to 117.05(9)°, which is significantly larger than the ideal geometry for tetrahedral complexes. Furthermore, although the ideal angle for P_{11}–C_{111}–C_{112}, P_{11}–C_{111}–C_{116} and C_{112}–C_{111}–C_{116} (as well as similar angles in other ring systems) is 120°, the angles in Table 3.4, varying from 117.7(2)° to 123.3(2)°, suggest a distorted configuration of the complete phenyl rings shifted out of the expected planes. The P(*p*-tol)$_3$ ligand is compressed, as indicated by the Ag-P-C angles [from 112.8(1)° to 117.05(9)°] in Table 3.3, possibly through steric interaction, while the phenyl rings are pushed outwards, away from each other, indicated by the P-C-C angles. This is also predicted by the VSEPR model[17].

The theoretical Ag-P bond length, calculated from the average atomic radii of the atoms, is 2.54 Å[18]. The Ag-P bond lengths in [Ag{P(*p*-tol)$_3$}$_4$]PF$_6$ are considerably longer than this value and vary significantly, from 2.570(1) Å to 2.6142(7) Å, which could be attributed to steric interaction or electronic influences due to packing.

3.3.10.3 Structure of [Ag{P(*p*-tol)$_3$}$_3$]ClO$_4$·CH$_3$COCH$_3$

The complex was prepared as reported in section 3.2.1.2. [Ag{P(*p*-tol)$_3$}$_3$]ClO$_4$·CH$_3$COCH$_3$ crystallized in the orthorhombic space group *Pna*2 with $Z = 4$. Illustrated in

[17] F.A. Cotton, G. Wilkinson, *Advanced Inorganic Chemistry, 5th ed*, Wiley Interscience, New York (1998).
[18] W.L. Jolly, *Modern Inorganic Chemistry, 2nd Ed*., McGraw-Hill, New York (1991).

Figure 3.5 is $[Ag\{P(p\text{-tol})_3\}_3]ClO_4 \cdot CH_3COCH_3$ with 50% probability displacement ellipsoids.

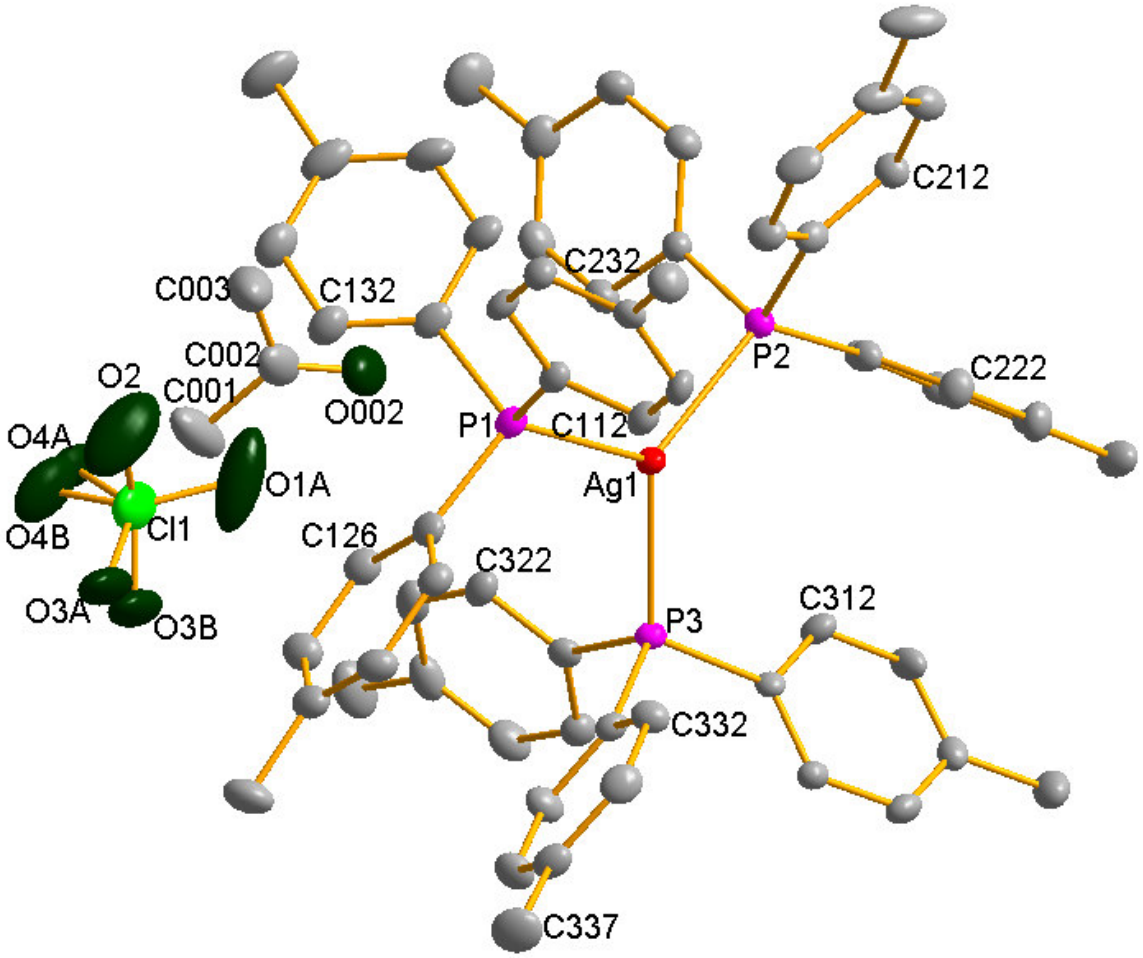

Figure 3.5 DIAMOND view of $[Ag\{P(p\text{-tol})_3\}_3]ClO_4 \cdot CH_3COCH_3$ (50 % probability displacement ellipsoids). Hydrogen atoms are omitted for clarity. For the C atoms, the first digit indicates phosphine number, the second digit indicates ring number and the third digit indicates the position of the atom in the ring. Some labels have been omitted for clarity, but all rings are numbered in the same consistent way. The disorder at the ClO_4^- ion is also shown.

Classical hydrogen bonds exist between phenyl and methyl hydrogen atoms and oxygen atoms of the perchlorate anion, suspending the anion through weak hydrogen interactions. Hydrogen interactions in the molecule are illustrated in Figure 3.6 and are shown in Table 3.6. Intermolecular atoms in this respect represent atoms generated by symmetry operation.

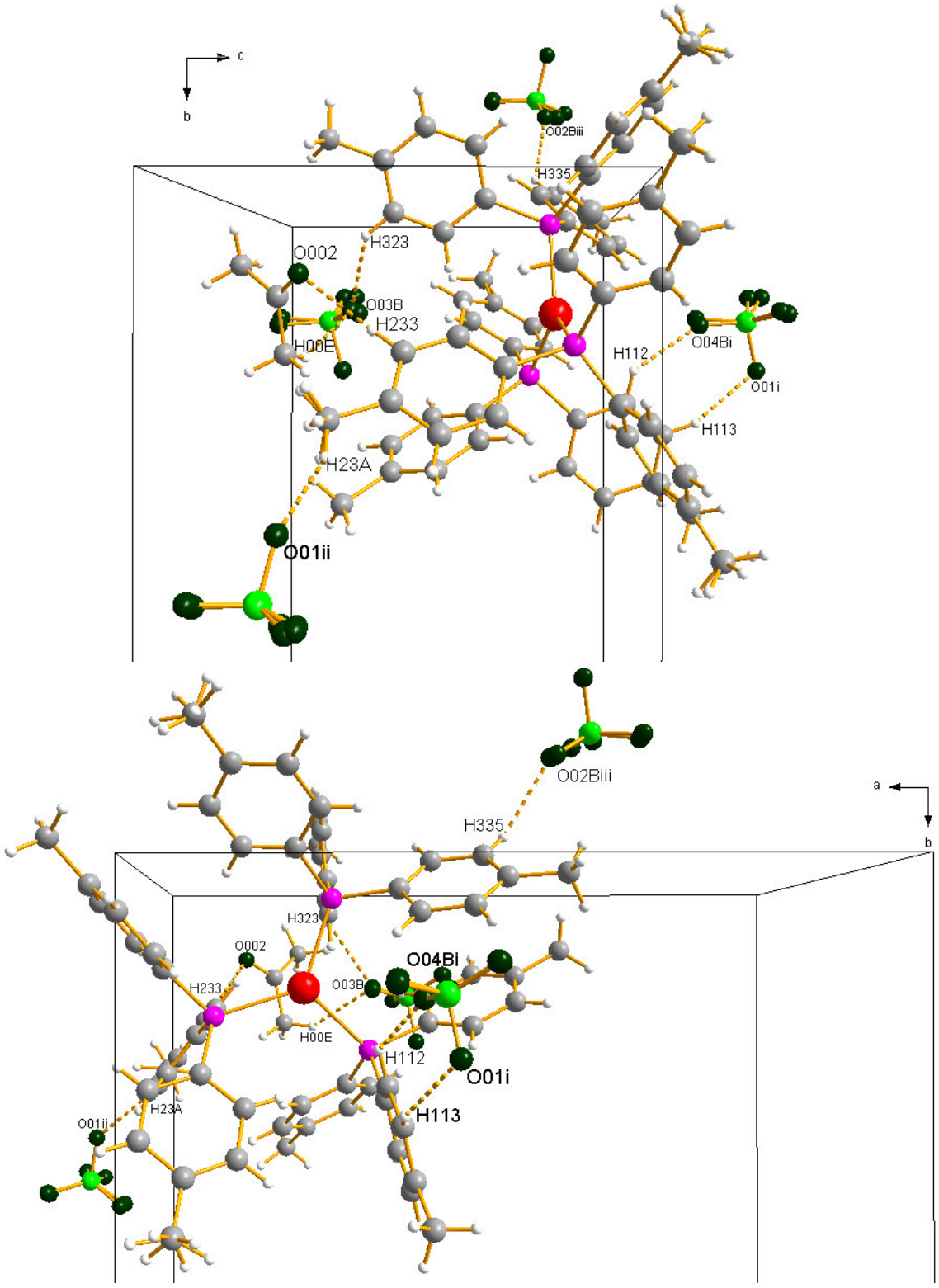

Figure 3.6 Partial unit cell for $[Ag\{P(p\text{-tol})_3\}_3]ClO_4 \cdot CH_3COCH_3$, viewed along a-axis and c-axis, with important intramolecular hydrogen bonding interactions indicated with dashed lines. Symmetry operators are given in Table 3.6.

Table 3.6 Hydrogen bonds for $[Ag\{P(p\text{-tol})_3\}_3]ClO_4 \cdot CH_3COCH_3$ (Å and °). The symmetry operators are specified at the bottom of the table.

D-H...A	$\mathbf{d_{D-H}}$ **(Å)**	$\mathbf{d_{H...A}}$ **(Å)**	$\mathbf{d_{D...A}}$ **(Å)**	$\mathbf{<_{DHA}}$ **(°)**
C_{003}-H_{00E}…O_{03B}	0.98	2.41	3.25(4)	142.8
C_{237}-H_{23A}…O_{01}^{ii}	0.98	2.37	3.277(9)	154.2
C_{112}-H_{112}…O_{04B}^{i}	0.95	2.45	3.077(9)	123.1
C_{113}-H_{113}…O_{01}^{i}	0.95	2.57	3.419(8)	149.6
C_{233}-H_{233}…O_{002}	0.95	2.45	3.397(6)	178.3
C_{323}-H_{323}…O_{3B}	0.95	2.45	3.21(3)	135.7
C_{335}-H_{335}…O_{02B}^{iii}	0.95	2.40	3.16(2)	134.5

Symmetry codes: (i) x + ½, -y + ½, z + 1 (ii) x, y, z + 1 (iii) –x, -y + 1, z + ½

The packing of $[Ag\{P(p\text{-tol})_3\}_3]^+$ in the unit cell, with ClO_4^- and CH_3COCH_3 suspended in the surrounding cavities, is illustrated in Figure 3.7.

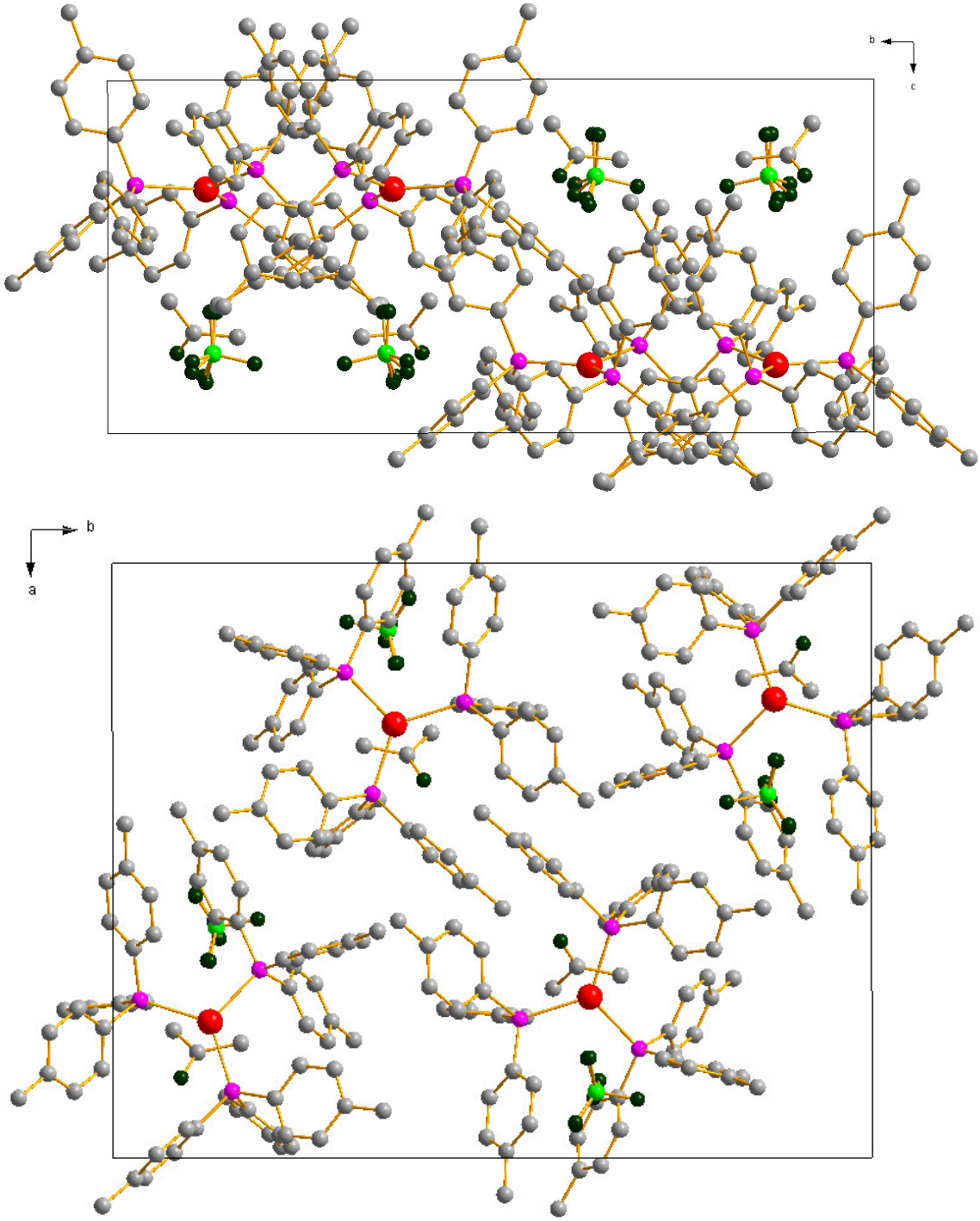

Figure 3.7 View of the unit cell of $[Ag\{P(p\text{-tol})_3\}_3]ClO_4 \cdot CH_3COCH_3$ along the a-axis and c-axis.

Selected bond distances and angles in the complex are shown in Table 3.7, with selected bond angles of interactions of phosphine in the complex shown in Table 3.8.

Table 3.7 Selected interatomic bond lengths (Å) and angles (°) for silver atom connections in [Ag{P(*p*-tol)$_3$}$_3$]ClO$_4$·CH$_3$COCH$_3$.

Bond	**Bond Lengths (Å)**
P_1–Ag_1	2.485(1)
P_2–Ag_1	2.468(1)
P_3–Ag_2	2.461(1)
Angle	**Bond Angles (°)**
P_1–Ag_1–P_2	120.01(4)
P_1–Ag_1–P_3	114.25(4)
P_2–Ag_1–P_3	125.06(3)
Ag_1–P_1–C_{111}	113.5(1)
Ag_1–P_1–C_{121}	114.9(1)
Ag_1–P_1–C_{131}	110.3(1)
Ag_1–P_2–C_{211}	116.8(1)
Ag_1–P_2–C_{221}	118.7(1)
Ag_1–P_2–C_{231}	105.1(1)
Ag_1–P_3–C_{311}	117.1(1)
Ag_1–P_3–C_{321}	112.5(2)
Ag_1–P_3–C_{331}	112.5(1)

Table 3.8 Selected bond angles (°) of interactions in phosphine ligands in the complex in [Ag{P(*p*-tol)$_3$}$_3$] ClO$_4$·CH$_3$COCH$_3$. Angles are arranged according to connections per phenyl ring.

Angle	**Bond Angle (°)**	**Angle**	**Bond Angle (°)**	**Angle**	**Bond Angle (°)**
P_1–C_{111}–C_{112}	118.0(4)	P_1–C_{111}–C_{116}	123.0(3)	C_{112}–C_{111}–C_{116}	119.1(4)
P_1–C_{121}–C_{122}	120.8(3)	P_1–C_{121}–C_{126}	119.9(3)	C_{122}–C_{121}–C_{126}	119.1(4)
P_1–C_{131}–C_{132}	124.9(4)	P_1–C_{131}–C_{136}	116.5(3)	C_{132}–C_{131}–C_{136}	118.5(4)
P_2–C_{211}–C_{212}	123.6(3)	P_2–C_{211}–C_{216}	118.4(3)	C_{212}–C_{211}–C_{216}	117.9(4)
P_2–C_{221}–C_{222}	119.1(3)	P_2–C_{221}–C_{226}	121.9(3)	C_{222}–C_{221}–C_{226}	118.7(4)
P_2–C_{231}–C_{232}	117.9(3)	P_2–C_{231}–C_{236}	123.4(3)	C_{232}–C_{231}–C_{236}	118.7(4)
P_3–C_{311}–C_{312}	117.9(3)	P_3–C_{311}–C_{316}	122.6(3)	C_{312}–C_{311}–C_{316}	119.5(4)
P_3–C_{321}–C_{322}	119.6(4)	P_3–C_{321}–C_{326}	122.0(4)	C_{322}–C_{321}–C_{326}	118.4(4)
P_3–C_{331}–C_{332}	117.9(3)	P_3–C_{331}–C_{336}	122.7(3)	C_{332}–C_{331}–C_{336}	119.5(4)
P_1–C_{111}–C_{114}	177.3(3)	P_2–C_{211}–C_{214}	175.6(3)	P_3–C_{311}–C_{314}	177.4(2)
P_1–C_{121}–C_{124}	176.2(2)	P_2–C_{221}–C_{224}	175.0(2)	P_3–C_{321}–C_{324}	178.4(3)
P_1–C_{131}–C_{134}	174.2(3)	P_2–C_{231}–C_{234}	176.7(3)	P_3–C_{331}–C_{334}	177.5(2)

The effective cone angles of the phosphorous ligands are shown in Table 3.9. The planar geometry of the complex, as well as the displacement of the Ag atom to the amount of 0.1213(3) Å from the plane formed by P_1, P_2 and P_3 is illustrated in Figure 3.8.

Table 3.9 Effective cone angles, θ_E, (°) for the P(*p*-tol)$_3$ ligands in [Ag{P(*p*-tol)$_3$}$_3$]ClO_4·CH_3COCH_3.

Ligand	**Effective angle (°)**
P_1	154.1
P_2	167.6
P_3	160.4

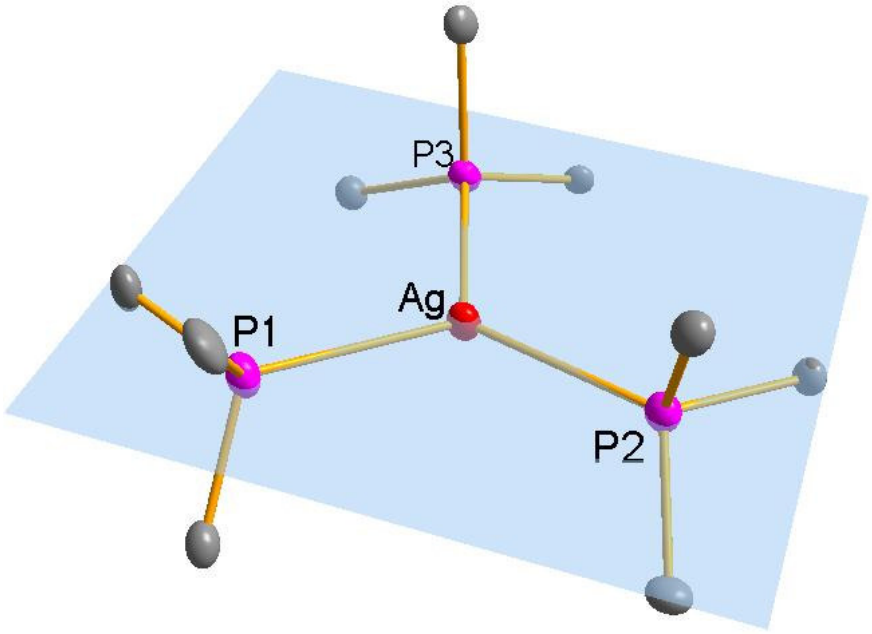

Figure 3.8 DIAMOND illustration of the geometry of [Ag{P(*p*-tol)$_3$}$_3$]ClO_4·CH_3COCH_3.

The cone angles of P(*p*-tol)$_3$ in this complex (154.1° to 167.6°) are not only much larger than those for [Ag{P(*p*-tol)$_3$}$_4$]PF_6, but also larger than that of PPh_3. The absence of a fourth phosphine in [Ag{P(*p*-tol)$_3$}$_3$]ClO_4, unlike the [Ag{P(*p*-tol)$_3$}$_4$]PF_6 complex, allows for the larger volume of those phosphine ligands present. The various P-Ag-P angles [114.25(4)°, 120.01(4)° and 125.06(3)°] indicate a slightly distorted trigonal planar geometry around the Ag atom with the ideal P-Ag-P angle of a trigonal planar complex being 120°. The Ag atom is slightly displaced from the P-P-P plane by a distance of 0.1213(3) Å.

The phosphine ligands exhibit a distorted tetrahedral geometry, indicated by the Ag-P-C angles. These angles vary from 105.1(1)° to 118.7(1)°, which is not only a large range, but also significantly larger than the ideal geometry angles for tetrahedral complexes. This distortion is an indication of strain in the complex, possibly due to steric and packing influences.

The P_{11}–C_{111}–C_{112}, P_{11}–C_{111}–C_{116} and C_{112}–C_{111}–C_{116} angles (as well as similar angles in other ring systems) in Table 3.8, varying from 118.0(4)° to 124.9(4)°, suggest a distortion of the complete phenyl rings out of the expected planes, as the ideal angle is 120°. The Ag-P-C angles [from 110.3(1) to 114.9(1)] in Table 3.7 indicate that the P(*p*-tol)$_3$ ligand is compressed, while the P-C-C angles show that phenyl rings are forced away from each other.

The Ag-P bond lengths in [Ag{P(*p*-tol)$_3$}$_3$]ClO_4·CH_3COCH_3 (2.485(1) Å, 2.468(1) Å and 2.461(1) Å) are shorter than the theoretical Ag-P bond length of 2.54 Å.

3.3.10.4 Structure of [Ag$_4${P(*p*-tol)$_3$}$_4$Br$_4$]·CH_3COCH_3

The complex was prepared as reported in section 3.2.1.3. [Ag$_4${P(*p*-tol)$_3$}$_4$Br$_4$] ·CH_3COCH_3 crystallized with a trigonal space group $R\bar{3}$ with Z = 6. [Ag$_4${P(*p*-tol)$_3$}$_4$Br$_4$]·CH_3COCH_3 is shown in Figure 3.9 with 50% probability displacement ellipsoids. The CH_3COCH_3 molecule was partly generated through symmetry, with C02 and O01 occupying the same site with occupancy numbers of 0.67 and 0.33 respectively.

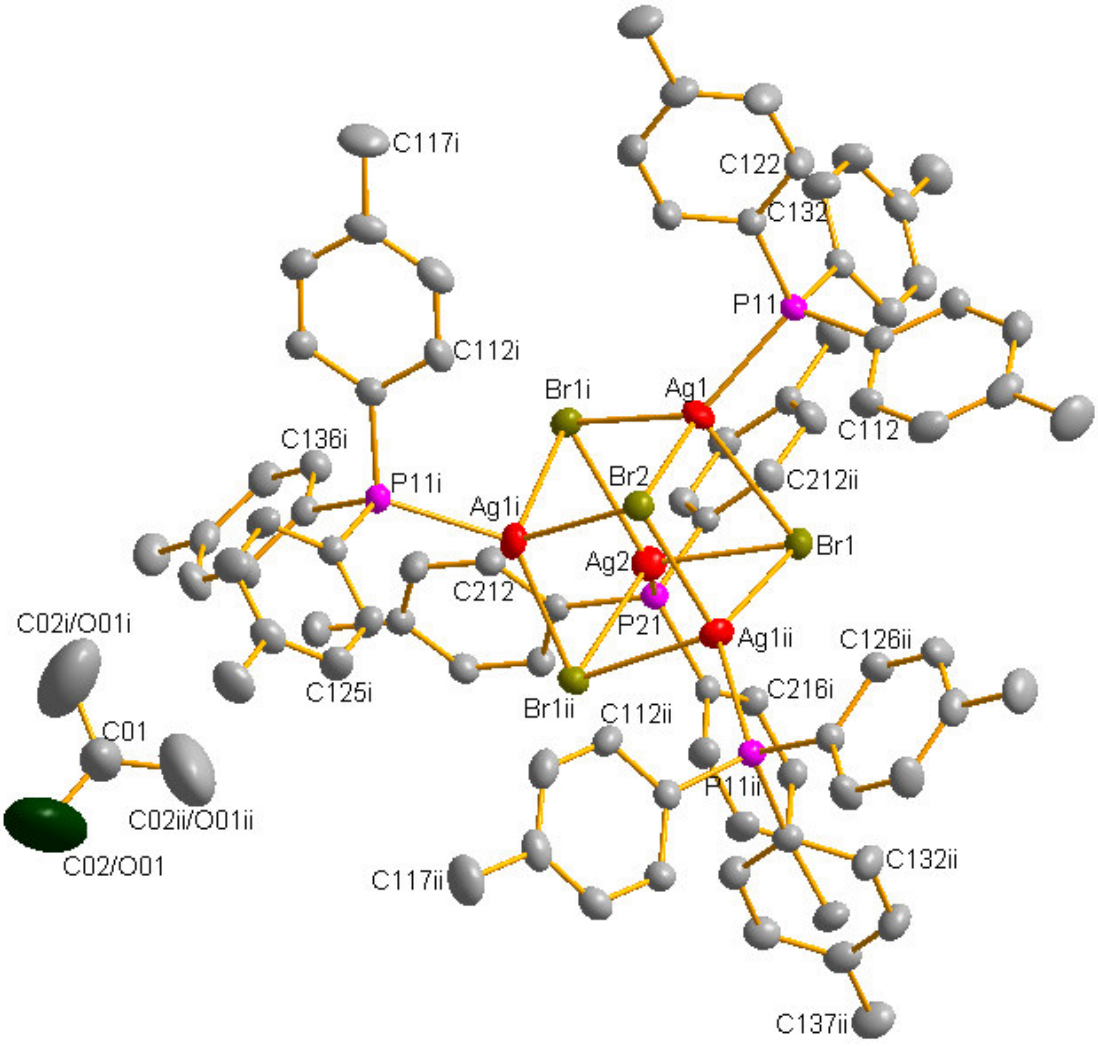

Figure 3.9 DIAMOND view of $[Ag_4\{P(p\text{-tol})_3\}_4Br_4]\cdot CH_3COCH_3$ (50% probability displacement ellipsoids). Hydrogen atoms are omitted for clarity. For the C atoms, the first digit indicates phosphine number, the second digit indicates ring number and the third digit indicates the position of the atom in the ring. Atoms generated by symmetry are indicated by lower case roman numerical labels corresponding to the symmetry codes reported in Table 3.10. Some labels have been omitted for clarity, but all rings are numbered in the same consistent way.

The cubane-like core of the $[Ag_4\{P(p\text{-tol})_3\}_4Br_4]\cdot CH_3COCH_3$ molecule is translated in straight lines along the c-axis, as indicated in Figure 3.10 along with the view along the a-axis. Solvent molecules can be seen suspended in the cavities between molecules.

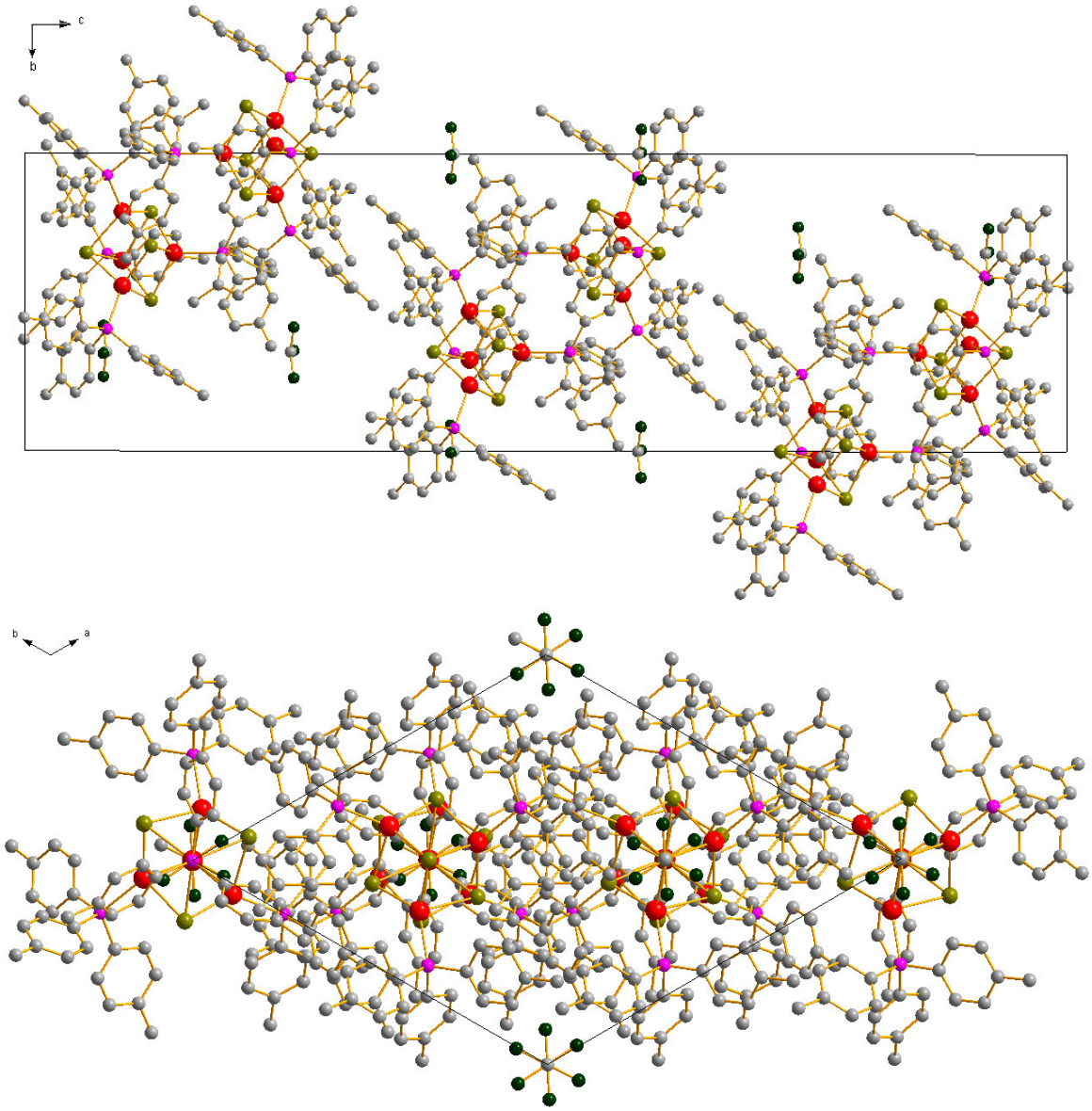

Figure 3.10 View of the unit cell of $[Ag_4\{P(p\text{-tol})_3\}_4Br_4]\cdot CH_3COCH_3$ along the a- and c-axes.

The structure was evaluated for classic hydrogen bonds, but none were located. Selected bond distances and angles of silver atom interactions in the complex are shown in Table 3.10.

Table 3.10 Selected interatomic bond lengths (Å) and angles (°) for silver atom connections in $[Ag_4\{P(p\text{-}tol)_3\}_4Br_4]\cdot CH_3COCH_3$.

Bond	**Bond Lengths (Å)**	**Bond**	**Bond Lengths (Å)**
P_{11}–Ag_1	2.400(1)	P_{21}–Ag_2	2.408(2)
Br_1–Ag_1	2.8335(5)	Br_1–Ag_2	2.7483(6)
Br_1^{i}–Ag_1	2.6516(7)	Br_1^{i}–Ag_2	2.7493(4)
Br_2–Ag_1	2.7742(6)	Br_1^{ii}–Ag_2	2.7499(6)
Angle	**Bond Angles (°)**	**Angle**	**Bond Angles (°)**
Br_1–Ag_1–P_{11}	103.05(3)	Br_1–Ag_2–P_{21}	113.98(1)
Br_1^{i}–Ag_1–P_{11}	132.31(4)	Br_1^{i}–Ag_2–P_{21}	113.98(1)
Br_2–Ag_1–P_{11}	119.59(3)	Br_1^{ii}–Ag_2–P_{21}	113.98(1)
Br_1–Ag_1–Br_1^{i}	104.32(2)	Br_1–Ag_2– Br_1^{i}	104.64(2)
Br_1–Ag_1–Br_2	92.71(2)	Br_1–Ag_2– Br_1^{ii}	104.62(2)
Br_1^{i}–Ag_1–Br_2	96.82(1)	Br_1^{i}–Ag_2– Br_1^{ii}	104.60(1)
Ag_1–P_{11}–C_{111}	113.1(2)	Ag_2–P_{21}–C_{211}	114.1(1)
Ag_1–P_{11}–C_{121}	114.2(1)	Ag_2–P_{21}–C_{211}^{i}	114.1(1)
Ag_1–P_{11}–C_{131}	114.8(2)	Ag_2–P_{21}–C_{211}^{ii}	114.2(1)

Symmetry codes: (i) 1 - x + y, -x + 1, z (ii) -y + 1, x - y, z

Selected bond angles of interactions in the phosphine in the complex are shown inTable 3.11, and the effective cone angles of the phosphorous ligands in Table 3.12.

Table 3.11 Selected bond angles (°) of interactions in phosphine ligands in the complex in $[Ag_4\{P(p\text{-}tol)_3\}_4Br_4]\cdot CH_3COCH_3$. Angles are arranged according to connections per phenyl ring.

Angle	Bond Angle (°)	Angle	Bond Angle (°)	Angle	Bond Angle (°)
$P_{11}–C_{111}–C_{112}$	118.3(3)	$P_1–C_{111}–C_{116}$	123.3(4)	$C_{112}–C_{111}–C_{116}$	118.4(4)
$P_{11}–C_{121}–C_{122}$	123.3(3)	$P_1–C_{121}–C_{126}$	118.7(4)	$C_{122}–C_{121}–C_{126}$	118.1(5)
$P_{11}–C_{131}–C_{132}$	122.4(3)	$P_1–C_{131}–C_{136}$	118.6(3)	$C_{132}–C_{131}–C_{136}$	118.7(4)
$P_{21}–C_{211}–C_{212}$	118.6(4)	$P_2–C_{211}–C_{216}$	122.9(4)	$C_{212}–C_{211}–C_{216}$	118.5(4)
$P_1–C_{111}–C_{114}$	176.9(3)				
$P_1–C_{121}–C_{124}$	177.5(3)				
$P_1–C_{131}–C_{134}$	174.4(2)				
$P_2–C_{211}–C_{214}$	177.9(3)				

Table 3.12 Effective cone angles, θ_E, (°) for the $P(p\text{-tol})_3$ ligands in $[Ag_4\{P(p\text{-tol})_3\}_4Br_4]\cdot CH_3COCH_3$.

Ligand	Effective angle (°)
P_{11}	155.2
P_{21}	161.8

$[Ag_4\{P(p\text{-tol})_3\}_4Br_4]\cdot CH_3COCH_3$ consists of an extremely distorted tetrameric cubane-like core consisting of four Ag atoms and four Br atoms, while four $P(p\text{-tol})_3$ ligands complexes the peripheral part of the cluster. The distortion is shown by the P-Ag-Br and Br-Ag-Br angles, which vary from 92.72(2) Å to 132.31(4) Å, while a true cubane-like geometry would have exhibited Br-Ag-Br angles of 90°.

The cone angles of $P(p\text{-tol})_3$ in this complex (155.2° and 161.8°) are larger than that of PPh_3. This could be ascribed to steric attributes of the cubane-like core structure. The phosphine ligands exhibit a distorted tetrahedral geometry, indicated by the Ag-P-C angles. These angles vary from 113.1(2) ° to 114.8(2) °, which is larger than the ideal geometry for tetrahedral complexes (109.5 °).

Two tetrahedra are defined in the cubane-like core of the complex, one with Br-atoms as corners and another with Ag-atoms as corners. These tetrahedra are shown in Figure 3.11.

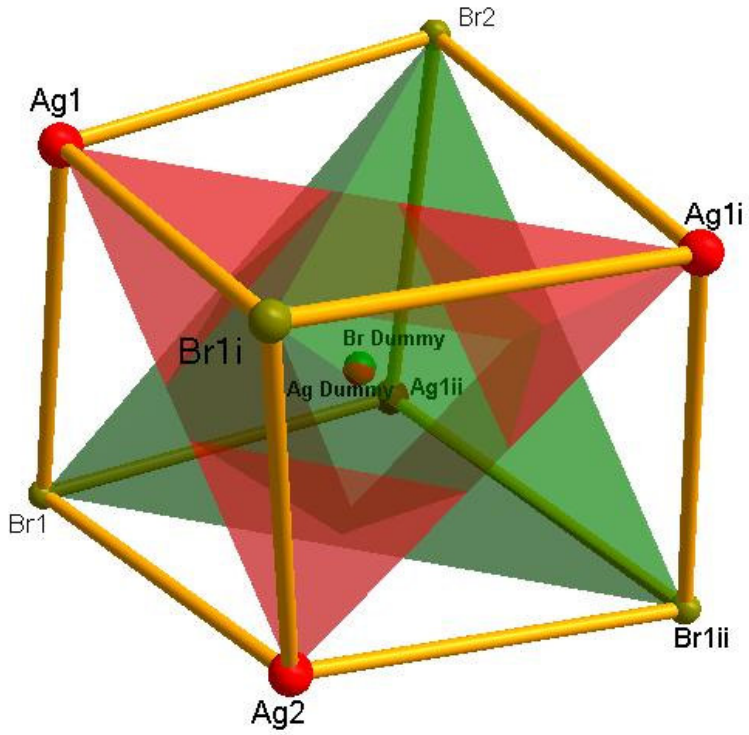

Figure 3.11 View of constructed tetrahedra in the cubane-like core of $[Ag_4\{P(p\text{-tol})_3\}_4Br_4]\cdot CH_3COCH_3$ with a) Br-atoms as corners (green), and b) Ag-atoms as corners (red).

Br-Br distances as well as Ag-Ag distances are shown in Table 3.13.

Table 3.13 Br-Br and Ag-Ag distances (Å). Symmetry operators agree with those shown in Table 3.10 and are shown at the bottom of the table.

Atoms	**Br distances (Å)**	**Atoms**	**Ag distances (Å)**
Br_1- Br_1^{i}	4.3510(7)	Ag_1- Ag_1^{i}	3.7023(7)
Br_1- Br_1^{ii}	4.3510(9)	Ag_1- Ag_1^{ii}	3.7023(4)
Br_1- Br_2	4.0580(7)	Ag_1- Ag_2	3.3158(6)
Br_1^{i}- Br_1^{ii}	4.3510(6)	Ag_1^{i}- Ag_1^{ii}	3.7023(7)
Br_1^{i}- Br_2	4.0587(7)	Ag_1^{i}- Ag_2	3.3168(6)
Br_1^{ii}- Br_2	4.0591(7)	Ag_1^{ii}- Ag_2	3.3161(6)

Symmetry codes: (i) 1 - x + y, -x + 1, z (ii) -y + 1, x - y, z

The theoretical distances for Br-Br and Ag-Ag covalent bonds are 2.48 Å and 2.88 Å respectively. The large difference between these theoretical distances and the distances in Table 3.13 illustrate the absence of direct interactions between alike atoms in this complex. Also, Ag-Ag distances should be larger than Br-Br, but the opposite is true. The elongation of distances also adds to distortion of the complex.

A dummy atom was defined at the centre of each tetrahedron. The dummy atoms for the Br-tetrahedron and Ag-tetrahedron have the same coordinates of (0.6667, 0.3332, 0.1057). The relevant distances and angles between the corner atoms and the dummy atoms are shown in Table 3.14. Atoms situated on the corners of the tetrahedral are labelled CA and the dummy atom D.

Table 3.14 Relevant bond distances (Å) and angles (°) for constructed tetrahedra in $[Ag_4\{P(p\text{-}tol)_3\}_4Br_4]\cdot CH_3COCH_3$. Symmetry elements agree with those shown in Table 3.10.

Tetrahedron bonds	**Br distances (Å)**	**Ag distances (Å)**	**Tetrahedron angles**	**Br angles (°)**	**Ag angles (°)**
CA_1-D	2.6315(6)	2.2294(4)	CA_1–D–CA_1^{i}	111.52(2)	112.26(1)
CA_1^{i}-D	2.6318(4)	2.2295(3)	CA_1–D–CA_1^{ii}	111.52(2)	112.26(1)
CA_1^{ii}-D	2.6319(5)	2.2298(5)	CA_1–D–CA_2	107.332(9)	106.502(9)
CA_2-D	2.4031(7)	1.9016(6)	CA_1^{i}–D–CA_1^{ii}	111.52(2)	112.26(1)
			CA_1^{i}–D–CA_2	107.349(9)	106.536(9)
			CA_1^{ii}–D–CA_2	107.360(9)	106.513(9)

Symmetry codes: (i) 1 - x + y + 1, -x + 1, z (ii) -y + 1, x - y, z

The short CA_2-D distances, as well as the differences in angles of the tetrahedra, demonstrate the distortion of the complex to dodecahedral-like[19] geometry. This distortion is illustrated in Figure 3.12.

[19] J. Leipoldt, S.S. Basson, A. Roodt, *Adv. Inorg. Chem.*, **40**, 240 (1994).

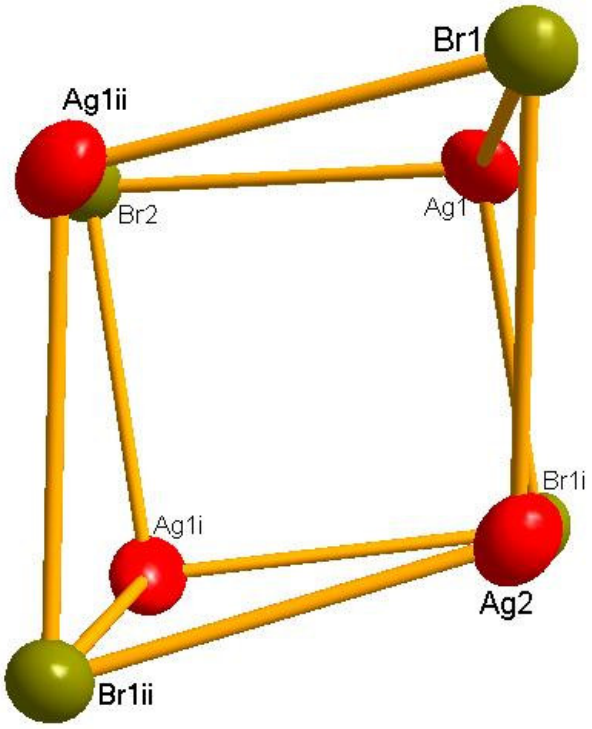

Figure 3.12 Distortion of the $[Ag_4\{P(p\text{-tol})_3\}_4Br_4]$ metal-halide core showing dodecahedral[19] character.

The geometry of $[Ag_4\{P(p\text{-tol})_3\}_4Br_4]\cdot CH_3COCH_3$, which has a cubic core, is comparable in geometry to a ML_8 complex. A cubic molecule can generally adopt three geometries; square antiprism, dodecahedron and bicapped trigonal prism[19]. Calculations to minimize repulsion between ligands have shown that repulsion energy coefficients for these three forms are about the same, but that the square antiprism should be the most stable configuration for a ML_8 polyhedron. There are, however, no large energy barriers between any two of these forms, allowing facile interconversions. The shape of this molecule may therefore differ in solution. The ideal dodecahedron, resulting from two interpenetrating bisphenoids, has two sets of symmetry equivalent D-C bonds, in this case D-Ag and D-Br. The deviation of $[Ag_4\{P(p\text{-tol})_3\}_4Br_4]\cdot CH_3COCH_3$ from this rule is an indication that the complex is not a true dodecahedron, but only shows similarities to dodecahedral geometry. For a true dodecahedron, a quasi-$\bar{4}$-axis would exist, through a corner atom, for example Ag, the centre of the molecule and bisecting a line between two atoms of the same type on the opposite side of the molecule. In this molecule, however, the distortion is so large that the axis goes through an atom of another corner atom of a different type, Br.

The angles in Table 3.10 suggest a distorted configuration of the complete phenyl rings out of the expected planes, as the ideal angle is 120°. The Ag-P-C angles (113.1(2)° to 114.8(2)°, ideally 109.5°) suggest that the P(*p*-tol)$_3$ ligand is slightly compressed, possibly through steric interaction, as predicted by the VSEPR model[17], while the P-C-C angles (118.3(3)° to 123.3(3)°, ideally 109°) indicate that the phenyl rings are forced outwards, away from each other. The sideways displacement of the phosphorus atom allows the symmetry with regard to the core to be disrupted.

The bond lengths of Ag-P in [Ag$_4${P(*p*-tol)$_3$}$_4$Br$_4$]·CH$_3$COCH$_3$ (2.400(1) Å and 2.408(2) Å) are shorter than the theoretical Ag-P bond length of 2.54 Å, while the Ag-Br bond lengths (from 2.6516(7) Å to 2.8335(5) Å) are significantly longer than the theoretical Ag-Br bond length of 2.58 Å. This contributes to the distortion of the structure, and could be attributed to steric strain as well as packing influences.

3.3.10.5 Discussion

In this section, compounds A, B and C are compared to complexes containing monodendate phosphine ligands, most often PPh$_3$, as silver(I) complexes containing P(*p*-tol)$_3$ as ligand are extremely rare.

Some structurally characterized complexes were found in literature of the type [AgL$_4$]X (L = PPh$_3$, X = SbF_6^- [20], PF_6^- [21], SiF_6^- [22] ClO_4^- [23], NO_3^- [24], BPh_4^- [25]), many of which crystallized with a $R\bar{3}$ spacegroup. P-Ag-P angles confirmed the tetrahedral geometry of this type of complex, the theoretical value being 109.5°. The Ag-P distances in these complexes vary between 2.601(1) Å[25] and 2.674(1) Å[21.a] and are generally longer than the Ag-P distances of 2.567(1) Å to 2.6142(7) Å in [Ag{P(*p*-tol)$_3$}$_4$]PF$_6$. This disparity may by attributed to differences in packing effects of different anions.

---

[20] Z. Ma, Y. Lin, Z.-N. Chen, *Jiegou Huaxue (Chin.) (Chinese J. Struct. Chem.)*, **23**, 1277 (2004).
[21] a) F.A. Cotton, R.L. Luck, *Acta Cryst., **C**45*, 1222 (1989). b) G.A. Bowmaker, P.C. Healy, L.M. Engelhardt, J.D. Kildea, B.W. Skelton, A.H. White, *Aust. J. Chem.*, **43**, 1697 (1990).
[22] G.A. Bowmaker, Effendy, R.D. Hart, J.D. Kildea, E.N. de Silva, B.W. Skelton, A.H. White, *Aust. J. Chem.*, **50**, 539 (1997).
[23] L.M. Engelhardt, C. Pakawatchai, A.H. White, P.C. Healy, *J. Chem. Soc., Dalton Trans.,* 125 (1985).
[24] P.F. Barron, J.C. Dyason, P.C. Healy, L.M. Engelhardt, B.W. Skelton, A.H. White, *J. Chem. Soc., Dalton Trans.*, 1965 (1986).
[25] D.D. Ellis, A.L. Spek, *Acta Cryst.,* **C56**, e547 (2000).

Structurally characterized complexes of $[ML_4]PF_6$ (L = monodendate phosphine, M = Au(I) [26], Pt(II) [27], Ir(I) [28], Cu(I) [21.b]) are few, and only the Cu(I) complex[29] contains PPh_3 as ligand. These complexes are compared in Table 3.15.

Table 3.15 A comparison of selected geometrical parameters for $[ML_4]PF_6$

Bond distances	**Ag(I) (Å, °)**	**Au(I)[26] (Å, °)**	**Pt(II)[27] (Å, °)**	**Ir(I)[28] (Å, °)**	**Cu(I)[29] (Å, °)**
$M-P_1$	2.570(1)	2.449(1)	2.313(4)	2.282(5)	2.465(2)
$M-P_2$	2.5737(7)	2.449(1)	2.305(4)	2.289(5)	2.567(7)
$M-P_3$	2.5737(7)	2.449(1)	2.311(4)	2.290(4)	2.567(7)
$M-P_4$	2.5737(7)	2.449(1)	2.311(4)	2.290(5)	2.567(7)
Bond angles					
P_1-M-P_2	109.31(2)	105.24(4)	91.1(1)	149.3(1)	109.88(7)
P_1-M-P_3	109.31(2)	105.24(4)	173.6(1)	93.2(2)	109.88(7)
P_1-M-P_4	109.31(2)	105.24(4)	89.7(1)	93.2(2)	109.88(7)
P_2-M-P_3	109.63(2)	118.32(4)	90.0(1)	94.7(2)	109.06(5)
P_2-M-P_4	109.63(2)	118.32(4)	167.0(1)	94.7(2)	109.06(5)
P_3-M-P_4	109.63(2)	118.32(4)	90.7(1)	150.3(1)	109.06(5)

The M-P distances vary between 2.311(4) Å for the Pt(II) complex[27] (theoretical distance 2.48 Å) and 2.449(1) Å for the Au(I) complex[26] (theoretical distance 2.54 Å). In these instances the bond distances are shorter than the theoretical values, which could be due to *trans* influence in the case of the Pt(II) complex (distorted planar geometry) and steric effects in the Au(I) complex. Some M-P bonds are subject to considerable variation in length, where the bond exists between a 'soft' ligand and a low-valent metal ion. For methyldiphenylphosphine there appears no great difficulty in attaining nearly regular tetrahedral coordination, whereas more bulky ligands such as triphenylphosphine force elongation of the M-P bonds due to steric factors.

Instances of structurally characterized complexes of the type $[AgL_3]X$ (L = monodendate phosphine, X = NO_3^- [24,30], BF_4^- [31]) in literature are rare. These complexes have distorted trigonal planar geometries (ideal angle 120°), as exemplified by the P-Ag-P angles for the BF_4^- complex (117.4(1) ° as defined by symmetry operations). The NO_3^- complex[30.a] was

[26] R.C. Elder, E.H.K. Zeiher, M. Onady, R.R. Whittle, *Chem. Commun.*, 900 (1981).
[27] Q.-B. Bao, S.J. Geib, A.L. Rheingold, T.B. Brill, *Inorg. Chem.*, **26**, 3453 (1987).
[28] O. Blum, J.C. Calabrese, F. Frolow, D. Milstein, *Inorg. Chim. Acta*, **174**, 149 (1990).
[29] G.A. Bowmaker, P.C. Healy, L.M. Engelhardt, J.D. Kildea, B.W. Skelton, A.H. White, *Aust. J. Chem.,* **43**, 1697 (1990).
[30] E.R.T. Tiekink, *J. Coord. Chem.*, **28**, 223 (1993).
[31] A. Baiada, F.H. Jardine, R.D. Willett, *Inorg.Chem.*, **29**, 4805 (1990).

even more distorted with P-Ag-P angles of 112.07(4)°, 116.44(5)° and 118.37(5)°. The distortion further manifests itself in the displacement of the Ag atom from the P-P-P plane, with the largest displacement occurring in the NO_3^- complex with a value of 0.5436(4) Å[30.a]. The Ag-P bond distances for $[AgL_3]X$ complexes vary between 2.525(1) Å[30.b] and 2.630(2) Å[30.a], which are significantly longer than the distances in $[Ag\{P(p\text{-}tol)_3\}_3]ClO_4 \cdot CH_3COCH_3$ (from 2.461(1) Å to 2.485(1) Å). A possible explanation could be the coordination effect of the different anions, and therefore the distortion of the complex from the idealized geometry.

$[ML_3]ClO_4$ type complexes (L = monodendate phosphine, M = Hg(II)[32], Au(I)[33], Rh(I)[34], Cu(I)[35]) also generally exhibit a slightly distorted trigonal planar geometry. These complexes are compared in Table 3.16.

Table 3.16 A comparison of selected geometrical parameters for $[ML_3]ClO_4$.

Bond distances	**Ag(I) (Å, °)**	**Hg(II)[32] (Å, °)**	**Au(I)[33] (Å, °)**	**Rh(I)[34] (Å, °)**	**Cu(I)[35] (Å, °)**
d(M-Plane)	0.1213(3)	0.3171(7)	0.09(2)		0.227(3)
$M\text{-}P_1$	2.485(1)	2.500(3)	2.421(3)	2.24	2.302(3)
$M\text{-}P_2$	2.468(1)	2.503(3)	2.421(3)	2.21	2.302(3)
$M\text{-}P_3$	2.461(1)	2.534(3)	2.421(3)	2.56	2.302(3)
Bond angles					
$P_1\text{-}M\text{-}P_3$	114.25(4)	113.1(1)	119.9(3)	97.7(2)	119.1(1)
$P_1\text{-}M\text{-}P_2$	120.01(4)	115.5(1)	119.9(3)	102.4(4)	119.1(1)
$P_2\text{-}M\text{-}P_3$	125.06(3)	126.7(1)	119.9(3)	159.3(2)	119.1(1)

Distances of M-P for Hg(II) vary between 2.500(3) Å and 2.534(3) Å (theoretical value 2.65 Å), between 2.21(2) Å and 2.24(2) Å for Rh(I) (theoretical value 2.49 Å), Au-P distances are 2.421(3) Å (theoretical 2.54 Å) and Cu-P distances are 2.302(3) Å (theoretical value 2.38 Å). These M-P distances are generally shorter than the theoretical values, which could be due to the steric bulkiness of the phosphine ligand. The Au(I) atom is only slightly displaced out of the P-P-P plane with a distance of 0.09(2) Å, while the Hg(II) atom is displaced by 0.3171(7) Å and Cu(I) by 0.227(3) Å.

[32] T. Allman, R.G. Goel, A.L. Beauchamp, *Acta Cryst.,* **C44**, 1557 (1988).
[33] J.A. Muir, S.I. Cuadrado, M.M. Muir, *Acta Cryst.,* **C48**, 915 (1992).
[34] Y.W. Yared, S.L. Miles, R. Bau, C.A. Reed, *J. Am. Chem. Soc.*, **99**, 7076 (1977).
[35] A. Baiada, F.H. Jardine, R.D. Willett, K. Emerson, *Inorg. Chem*., **30**, 1365 (1991).

The largest distortion from the ideal trigonal geometry, with P-M-P angles of 120°, was found in the Rh(I), which has P-M-P angles of 97.7(2) °, 102.4(2) ° and 159.3(2) °. The P-M-P angles for Hg(II) are 113.1(1) °, 115.5(1) ° and 126.7(1) °, angles for Au(I) are 119.9(3) ° (defined by symmetry) and 119.1(1) ° for Cu(I) (defined by symmetry).

Complexes of the type $[L_4Ag_4X_4]$ (L = PPh_3, X = Br^- [36], Cl^- [37], I^- [38]) exhibit distortions similar to $[Ag_4\{P(p\text{-tol})_3\}_4Br_4]$. These complexes share the characteristic distortion from the ideal cubic T_d geometry to a variation of space groups, often with threefold symmetry. The distortion can be attributed to intramolecular nonbonding repulsions of the types (Ph)H ··· H(Ph) and (Ph)H ··· X, or weak Van der Waals interaction. For L = I^-, a step structure (Section 2.3.3.1) was also present, possibly for accommodation of the larger halogen atom.

Few complexes have been found in literature of the type $[L_4M_4Br_4]$ (L = monodendate phosphine, M = Cu(I) [39], Ag(I) [40]). Interestingly, these cubane-like clusters exhibit similar distortion to $[Ag_4\{P(p\text{-tol})_3\}_4Br_4]$, in spite of containing other metal centres. This confirmed the indication that the distortion could be caused by van der Waals interactions. When a range of phosphines were investigated for these complexes, the interactions eventually become large enough to distort the cubane-like structure to a step structure to accommodate very bulky ligands.

3.3.11 CONCLUSION

$[Ag\{P(p\text{-tol})_3\}_4]PF_6$, $[Ag\{P(p\text{-tol})_3\}_3]ClO_4\cdot CH_3COCH_3$ and $[Ag_4\{P(p\text{-tol})_3\}_4Br_4]\cdot CH_3COCH_3$ are comparable to similar complexes containing transition metals, other phosphine ligands or different counterions, as described in Section 3.3.10.5. Occurrences of similar structures in literature, however, were limited, indicating a field open to study. These similar complexes often share characteristics with, varying only on minor aspects

[36] B.-K. Teo, J.C. Calabrese, *Chem. Commun.,* 185 (1976).
[37] B.-K. Teo, J.C. Calabrese, *Inorg. Chem.*, **15**, 2467 (1976).
[38] B.-K.Teo, J.C.Calabrese, *J. Am. Chem. Soc.*, **97**, 1256 (1975).
[39] a) R.G. Goel, A.L. Beauchamp, *Inorg. Chem.*, **22**, 395 (1983). b) P.F. Barron, J.C. Dyason, L.M. Engelhardt, P.C. Healy, A.H. White, *Inorg.Chem.*, **23**, 3766 (1984). c) M.R. Churchill, B.G. DeBoer, S.J. Mendak, *Inorg. Chem.*, **14**, 2041 (1975). d) H.-G. Zheng, Q.-H. Jin, X.-Q. Xin, K.-B. Yu, *Jiegou Huaxue (Chin.) (Chinese J. Struct.Chem.)*, **20**, 124 (2001). e) R.D. Pike, W.H. Starnes, Jnr, G.B. Carpenter *Acta Cryst..,* **C55**, 162 (1999).
[40] a) R.J. Bowen, D. Camp, Effendy, P.C. Healy, B.W. Skelton, A.H. White, *Aust. J. Chem.*, **47**, 693 (1994). b) M.R. Churchill, J. Donahue, F.J. Rotella, *Inorg. Chem.*, **15**, 2752 (1976).

such as bond angles. Metal-phosphine bond lengths tend to be shorter than theoretical distances, possibly due to steric bulk of the phosphine ligand.

Silver(I) complexes of the type $[AgL_nX]$, as described in this section, are easily prepared by reacting stoichiometric ratios of silver salt and phosphine ligand under reflux. The complexes readily crystallize from solution and are stable in air and light.

Complexes of the type $[ML_4]PF_6$ (L = monodendate phosphine, M = Au(I)[26], Pt(II) [27], Ir(I) [28], Cu(I)[29]) tend towards tetrahedral geometry, although P-M-P angles varying between 89.7(1) ° and 173.6(1) ° for Pt(II) and 93.2(2) ° and 150.3(1) ° for Ir(I) indicate large distortions towards square planar geometry from the ideal P-M-P angles of 109.5° for tetrahedral geometry.

Displacement of the metal centre from the P-P-P plane in $[ML_3]ClO_4$ (L = monodendate phosphine, M = Hg(II)[32], Au(I) [33], Rh(I) [34], Cu(I) [35]) complexes are small, and these complexes assume a trigonal planar geometry, except in the case of Rh(I)[34]. In the complex with Rh(I) as metal centre, the angles are 97.7(2) °, 102.4(4) ° and 159.3(2) °, which is significantly different from the ideal angles of 120° in the trigonal planar geometry. No interactions exist between the metal centre and the perchlorate anion though, and the stereochemistry seems to result from an electronically dictated distortion away from trigonal planarity towards a T shape to allow diamagnetism.

Complexes of $[L_4Ag_4X_4]$ (L = PPh_3, X = halide) have been found in literature, most often with a cubane-like structure but also with a step structure for complexes containing the larger I-atom. The only similar complexes with different metal centres referenced to literature contained Cu(I). The same phenomenon was seen in these complexes, that the complex containing a large halide, like I^-, exhibited step and cubane-like bimorphic geometries. The cubane-like core of $[L_4M_4X_4]$ complexes are often distorted, with corner angles differing from the ideal cubane-like angles of 90°. This distortion could be attributed to van der Waals interactions.

Ag-P bond lengths tend to increase when Ag(I) is coordinated to a larger amount of phosphine ligands, probably due to steric interactions. Ag-P bond distances for $[Ag_4\{P(p\text{-tol})_3\}_4Br_4]\cdot CH_3COCH_3$ are 2.400(1) Å and 2.408(2) Å, increases to between 2.461(1) Å and 2.485(1) Å for $[Ag\{P(p\text{-tol})_3\}_3]ClO_4\cdot CH_3COCH_3$ and varies between 2.567(1) Å and 2.6142(7) Å for $[Ag\{P(p\text{-tol})_3\}_4]PF_6$. In this order, the number of

phosphine ligands coordinated to Ag(I) increases from one, to three, to four. Packing of $[Ag\{P(p\text{-tol})_3\}_3]ClO_4\cdot CH_3COCH_3$ and $[Ag\{P(p\text{-tol})_3\}_4]PF_6$ in the crystal structure is influenced by hydrogen interactions with anion atoms, and the due suspension of the anion in the cavities formed by packing of the bulky cation. No usual hydrogen interactions are present in $[Ag_4\{P(p\text{-tol})_3\}_4Br_4]\cdot CH_3COCH_3$.

The solid state coordination chemistry of Ag(I) shows a vast array of different modes, which will be expanded on in future investigations. This study nicely illustrated three different types, which could be obtained by spontaneous supermolecular assembly. The behavior of Ag/PX_3 complexes in solution are however not yet explored, due to, amongst others, rapid and complex kinetics, and will be expanded on in the next chapter.

4 Solution Studies

4.1 Introduction

Since a homogenous catalyst is most often applied in solution, investigation of the properties of a potential catalyst in solution state is important. The electronic contribution of PR_3 ligands decrease for more bulky R-groups, for example the range from R = Cy to C_6F_5 shown in literature[1], followed by $P(OR)_3$ groups. Some $P(OR)_3$ groups even mimic the electronic properties of CO, making the study of these complexes important in the search for CO-containing silver(I) complexes.

The study of the influences of the PR_3 group on the kinetics of a $[AgL_nX]$ complex (L = tertiary phosphine; n = 1 - 4; X = coordinating or non-coordinating anion) is important, as these groups could have an effect on the reaction of the molecule with other ligands, most importantly the coordination with CO, hydrogen and olefins. The coordination of these ligands to a metal centre is important in the use of such complexes as hydroformylation catalysts. In this study, the coordination of CO to different $[AgL_nX]$ complexes, as well as the exchange between free and coordinated PPh_3 in the complex $[Ag(PPh_3)_4]PF_6$ was investigated. The exchange of the coordinated phosphine with the free phosphine might prevent other ligands, such as olefins, from reacting, especially if the exchange takes place through an associative mechanism.

Since the complexes studied cannot be detected through ultraviolet/visible spectroscopy, the samples were investigated using infrared and nuclear magnetic resonance spectroscopy.

[1] A. Roodt, S. Otto, G. Steyl, *Coord. Chem. Rev.*, **245**, 121 (2003).

4.2 Infrared spectroscopy

4.2.1 INTRODUCTION

Infrared spectroscopy plays a vital role in science for the determination of sample composition. Many compounds cannot be investigated by NMR due to various factors which include solubility and sensitivity problems, and samples are often insensitive to light in the frequency region employed in UV/Vis spectroscopy. X-ray crystallography is a useful method for determination of structure composition, but often a product is not crystalline, the structure of the compound in the solid state does not correspond to the structure of the complex in solution, or problems occur with the collection of data. Infrared spectroscopy, however, can be used for both quantitative and qualitative analysis, in both solid and liquid state. Often this is the only method available for determination of coordination in a sample, as well as being a simple method for monitoring reaction of a complex with a ligand. A widely used application is the determination of coordination of a CO ligand to a complex.

4.2.2 PRINCIPLES OF INFRARED SPECTROSCOPY[2]

The energy of a molecule can be separated into three components, associated with the rotation of the molecule as a whole, the vibrations of the component atoms and the motion of the electrons in the molecule. The velocity of the electrons is much greater then the vibrational velocity of nuclei, which is then greater than the velocity of molecular rotation. When placed in an electromagnetic field, for example light, energy is transferred from the field to the molecule when Bohr's frequency condition is satisfied according to Eq. 4.1[2].

$$\Delta E = h\nu \qquad \text{... 4.1}$$

ΔE is the difference in energy between the ground and excited states, h is Planck's constant and ν is the frequency of the light. A molecule excited to a higher state absorbs radiation, and emits radiation of the same frequency when it reverts back to the ground state.

[2] K. Nakamoto, *Infrared Spectra of Inorganic and Coordination Compounds, 2nd ed.,* Wiley-Interscience, New York (1970).

Rotational energy levels are relatively close to each other; therefore transitions between the levels occur at low frequencies in the range between 1 cm^{-1} and 10^2 cm^{-1}. The separation of vibrational energy levels is greater, with transitions occurring at higher frequencies than rotational transitions. As a result, pure vibrational spectra are observed in the range between 10^2 cm^{-1} and 10^4 cm^{-1}. Electronic energy levels are usually far apart, consequently electronic spectra are observed in the range between 10^4 cm^{-1} and 10^2 cm^{-1}. Therefore pure rotational, vibrational, and electronic spectra fall in the microwave and far-infrared, infrared, and visible and ultraviolet regions, respectively. Infrared spectra originates in transitions between two vibrational levels of the molecule in the electronic ground state and are usually observed as absorption spectra in the infrared region, while the electronic polarizations caused by ultraviolet or visible light create Raman spectra.

Vibrations of the nuclei in a molecule can be represented by a number of normal vibrations. Every nucleus is expressed in terms of rectangular coordinate systems with the origin of each system at the equilibrium position of each nucleus. The frequency of normal vibrations is described by Eq. 4.2[2].

$$\nu_i = \frac{1}{2\pi}\sqrt{\lambda_i} \qquad \textbf{... 4.2}$$

λ_i is the wavelength of the vibration frequency. For a general N-atom molecule, the number of normal vibrations equals 3N – 6, since six coordinates are required to describe the translational and rotational motion of the molecule as a whole. Linear molecules have 3N – 5 normal vibrations as no rotational freedom exists around the molecular axis. For any given molecule, however, a selection rule applies limiting the vibrations that appear in the infrared and Raman spectra. This selection rule is determined by the symmetry of the molecule, which will not be discussed in this study.

4.2.3 EXPERIMENTAL

All chemicals were of analytical grade and all measurements were carried out in air. Complex preparation and characterization are outlined in sections 3.2.1 and 3.3.10. The attempted interaction of silver(I) complexes with CO-gas was monitored on a Tensor 27 Bruker infrared spectrometer equipped with OPUS 5.5 software[3] and an autoclave.

The autoclave consists of a stainless steel chamber that is closed with a flange cover. The cover is provided with a mechanical stirrer. The six rotor blades of the stirrer force the solution from the bottom of the vessel through the infrared windows and loop back into the chamber. The whole system (including the infrared windows) can be brought under pressure and heated by means of electrical heaters. The autoclave is equipped with a temperature controller and a pressure device, and the pressure was provided by CO-gas, through the connection of a gas cylinder to the autoclave system. The system was flushed with CO-gas three times before the onset of each set of measurements to ensure a homogenous CO-atmosphere. The windows are made of ZnS, with 0.1 mm optical path length.

A typical experiment consisted of the following: $[Ag\{P(p\text{-tol})_3\}_4]PF_6$ (0.331 g, 0.225 mmol), $[Ag\{P(p\text{-tol})_3\}_3]ClO_4 \cdot CH_3COCH_3$ (0.243 g, 0.206 mmol) and $[Ag_4\{P(p\text{-tol})_3\}_4Br_4]$ (0.223 g, 0.226 mmol) were dissolved in dichloromethane (15 ml) and pressurized with CO-gas from 0 bar to 55 bar in increments of 5 bar. After each increase in pressure the solution was stirred to ensure a homogenous environment. The experiment was repeated using only solvent, to be used as control spectra. The spectra were collected in the range 2300 cm^{-1} to 1700 cm^{-1}.

To investigate the effect of CO on a Ag^+ cation i.e. in the absence of PR_3 ligands, the above experimental procedure was repeated using $AgSO_3CF_3$ (0.053 g, 0.208 mmol).

[3] OPUS 5.5, Bruker Optik GmbH (2005).

4.2.4 RESULTS AND DISCUSSION

A typical spectrum resulting from this experiment is shown in Figure 4.1.

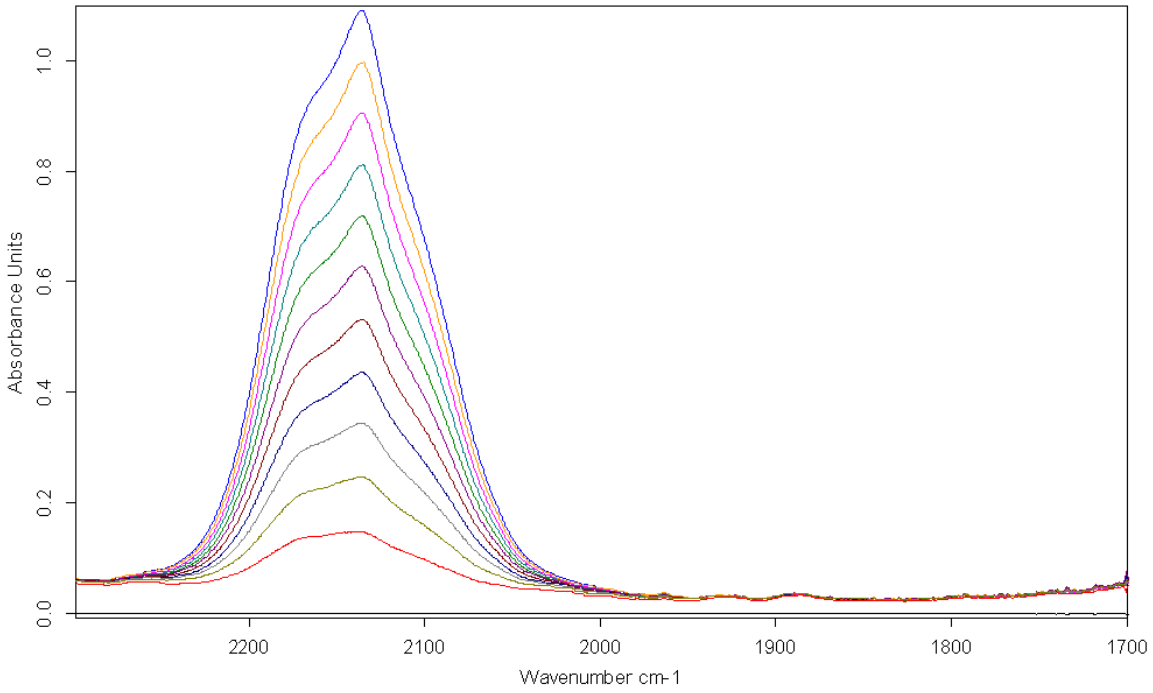

Figure 4.1 Infrared spectrum of $[Ag_4\{P(p\text{-tol})_3\}_4Br_4]$ pressured with CO-gas, with applied pressure varied from 5 bar to 55 bar in 5 bar intervals. As the pressure increases, the intensity of the peak indicating CO shows an increase.

The expected peak at 2200 cm^{-1}, resulting from CO absorption by the Ag metal, could not be detected from the IR-spectra. This could be seen more prominently after the subtraction of the control spectra, which looks similar to the spectrum in Figure 4.1. Subtraction of the control spectra from the spectra observed from the Ag(I) complexes yielded a flat line. Similarly, no evidence was found of coordination of the "naked" Ag^+ cation of $AgSO_3CF_3$ to CO. The clear, broad peak at 2136 cm^{-1} in Figure 4.1 indicates the presence of CO in solution. The aversion of the complexes to react with CO is unexpected, as CO acts as a Lewis base, which should be an ideal reagent with a Ag^+ cation. The inability of the CO-molecule to react with complexes of $[Ag\{P(p\text{-tol})_3\}_n]X$ (n = 1, 3, 4, X = Br^-, ClO_4^-, PF_6^-) may be overcome by applying an electrophilic ligand as stabilizer, which would enhance the π-donating properties of the silver atom. Examples

in literature where successful coordination was achieved are $[B(OTeF_5)_4]$[4] and $[HB(3,5\text{-}(CF_3)_2Pz)_3]$[5], with boron and nitrogen having Lewis base properties and being good σ-donors and poor π-acceptors. In $[HB(3,5\text{-}(CF_3)_2Pz)_3]$ the electron-donating properties are enhanced by the presence of both boron and nitrogen.

4.3 Nuclear Magnetic Resonance Spectroscopy

4.3.1 Introduction

NMR is a widely used spectroscopic method today, for purposes ranging from geological measurements via medical imaging to biomolecular dynamics. NMR has a long history and already in 1936 Görter described an apparatus that, in theory, could detect the magnetic resonance of protons[6]. In 1946 two groups independent of each other performed both solid-state and liquid-state NMR experiments[7]. Already early in NMR history biological studies were performed: as early as in 1954 DNA was studied and 1957 a 40 MHz ^{1}H-spectrum of ribonuclease was obtained[8]. Today the magnetic fields are significantly higher and 800-900 MHz magnets are not uncommon. The methods used to study biological molecules have an increasing complexity and have developed from continuous wave 1D methods to Fourier transformed pulsed heteronuclear multidimensional experiments.

In this study, magnetic spin transfer methods were employed to investigate the exchange of coordinated phosphine in $[Ag(PPh_3)_4]PF_6$ with free phosphine. The rate of this exchange is important in catalysis, as it may influence the interaction of the complex with other reagents such as CO, hydrogen and olefins. The exchange between free and coordinated phosphine is very fast, as will be shown later, implying that low temperatures are required, and that magnetic spin transfer methods will be more efficient than line broadening experiments.

---

[4] a) P.K Hurlburt, O.P. Anderson, S.H. Strauss, *J. Am. Chem. Soc.*, **113**, 6277 (1991). b) P.K. Hurlburt, J.J. Rack, S.F. Dec, O.P. Anderson, S.H. Strauss, *Inorg. Chem.*, **32**, 373 (1993).
[5] H.V.R. Dias, W. Jin, *J. Am. Chem. Soc.*, **117**, 11381 (1995).
[6] C.J. Görter, *Phys. Rev.*, **3**, 503 (1936).
[7] F. Bloch, *Phys. Rev.*, **70**, 460 (1946). b) F. Bloch, W.W. Hansen, M. Packard, *Phys. Rev.*, **70**, 474 (1946). c) E.M. Purcell, H.C. Torrey, R.V. Pound, *Phys. Rev.*, **69**, 37 (1946).
[8] B. Jacobson, W. Anderson, J. Arnold, *Nature*, **173**, 772 (1954). b) M. Saunders, A. Wishnia, J. Kirkwood, *J. Am. Chem. Soc.*, **76**, 3289 (1957).

4.3.2 PRINCIPLES OF NUCLEAR MAGNETIC RESONANCE SPECTROSCOPY

4.3.2.1 The Properties of the Nucleus of an Atom[9]

Nuclei of certain natural isotopes of the majority of the elements possess intrinsic angular momentum or spin, J, the total magnitude equalling $\hbar\sqrt{I(I+1)}$. The largest measurable component of this angular moment is $I\hbar$ (I = nuclear spin quantum number, $\hbar$ = h/2π; the reduced Planck's constant). I has integral or half-integral values (0, ½, 1, 1½, …) depending on the isotope. Several discrete values of angular momentum may be observable since I is quantized, their magnitudes given by $\hbar m$ (m = I, I-1, I-2, …, -I). Thus, there are 2I+1 equally spaced spin states of a nucleus with angular momentum quantum number I.

A nucleus with spin also has an associated magnetic moment μ, which has components associated with the spin states through $m\mu/I$. Therefore, μ also has 2I+1 components. In the absence of an external magnetic field the spin states all possess the same potential energy, but they take different energy values if a magnetic field is applied.

The magnetic moment and angular momentum behave as parallel and non-parallel vectors. The magnetogyric ratio between them, γ, is defined by Eq. 4.3:

$$\gamma = \frac{2\pi}{h}\frac{\mu}{I} \qquad \text{... 4.3}$$

γ has a characteristic value for each magnetically active nucleus and is positive for parallel and negative for anti-parallel vectors.

If I > ½, the nucleus possesses an additional electric quadrupole moment, Q. The distribution of charge in the nucleus is then non-spherical and can interact with electric field gradients arising from the electric charge distribution in the molecule. This interaction provides a means by which the nucleus can exchange energy with the molecule in which it is situated and can greatly affect certain NMR spectra.

[9] J.W. Akitt, B.E. Mann, *NMR and Chemistry: An introduction to modern NMR spectroscopy, 4th ed.*, Stanley Thornes (Publishers) Ltd., Cheltenham, (2000).

4.3.2.2 The Nucleus in a Magnetic Field

A nucleus placed in a magnetic field $\mathbf{B}_0$ can take up $2I+1$ orientations in the field, each at a angle θ to the field direction and associated with a different potential energy, shown by Eq. 4.4:

$$E = -\mu_z \mathbf{B}_0 \quad \text{... 4.4}$$

μ_z is the component of μ in the field direction. The energy separation between the levels of the various spin states is constant and given by Eq. 4.5:

$$\Delta E = \frac{\mu B_0}{I} = -\frac{m\gamma h}{2\pi} B_0 \quad \text{... 4.5}$$

The value of m changes sign as it is altered from I to $-I$ and accordingly the contribution of the total magnetic moment to total nuclear energy can be either positive or negative, the energy increasing when m is positive.

The presence of a series of states of differing energy in an atomic system allows interaction to take place with electromagnetic radiation of the correct frequency, causing transition between the energy states. This frequency, obtained from the Bohr relation and written in terms of the magnetogyric ratio, is given in Eq. 4.6:

$$\nu = \gamma B_0/2\pi \quad \text{... 4.6}$$

Thus the nucleus can interact with radiation whose frequency depends on the applied magnetic field and the nature of the nucleus.

The nuclear moments in a sample may be polarized with or against the magnetic field, lying at an angle θ to it. The total angular momentum is $\sqrt{I(I+1)}$ and the angle θ is given by Eq. 4.7:

$$\cos\theta = \frac{m}{\sqrt{I(I+1)}} \quad \text{... 4.7}$$

The magnet axis becomes inclined to the field axis and rotates or precesses around it, describing a conical surface around the field axis, illustrated in Figure 4.2.

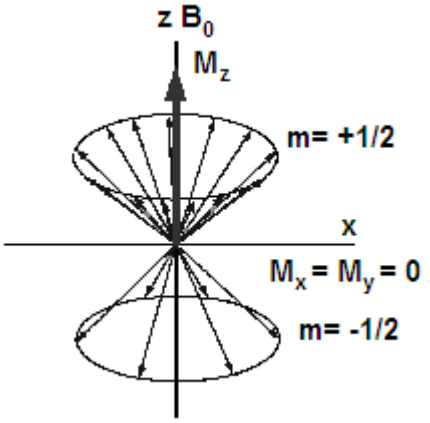

Figure 4.2 Precession of nuclei in a sample, the nuclear vectors spread evenly over a conical surface[9].

The half-apex angle is equal to θ and the angular velocity around the cone is $\gamma\mathbf{B}_0$. The frequency of complete rotation is $\gamma\mathbf{B}_0/2\pi$ and is known as the Larmor frequency. For nuclei with $I = ½$ two such precession cones exist, one for $m = ½$ and another for $m = -½$, pointing in opposite directions. However, only the precession cone of the excess low-energy nuclei is usually considered, spread evenly over a conical surface and rotating with the same angular velocity around the magnetic field axis $\mathbf{B}_0$, which is made the z axis. The excess low-energy nuclear spins all have components along the z axis pointing in the same direction, resulting in a net magnetization $\mathbf{M}_z$ along the z axis. Components in the x and y directions average to zero, therefore $\mathbf{M}_x = \mathbf{M}_y = 0$.

When a magnetic field, $\mathbf{B}_1$, with frequency equal to $\gamma\mathbf{B}_0/2\pi$, is applied in the xy plane, energy is absorbed resulting in the excitation of spins to the high-energy state. The vector $\mathbf{B}_1$ rotates at the same angular velocity as the nuclei and is therefore stationary relative to them. This induces transitions from the one energy level to the other, resulting in the rotation of the net nuclear magnetization, $\mathbf{M}$, around $\mathbf{B}_1$. A resultant magnetization $\mathbf{M}_{xy}$ then exists transverse to the main field, rotating at the nuclear precession frequency. The magnetization of the system is then no longer static, with $\mathbf{M}_{xy}$ inducing a radiofrequency current in the coils placed around the sample which can be detected.

After the system has been disturbed from the equilibrium state, and the disturbing influence removed, the system returns to the original equilibrium condition. This relaxation to equilibrium is characterized by a time T. When relaxation is fast, T is small,

and vice versa. When a system is disturbed through application of a magnetic field, two relaxation processes may be present, with different relaxation times, T_1 and T_2.

4.3.2.3 Characteristics of T_1

The maximum NMR signal is obtained after a 90° $\mathbf{B}_1$ pulse. The same is obtained after a 270° pulse, except that the spins have been inverted relative to the 90° pulse and the output is 180° out of phase with that after the shorter pulse. If the 90° pulse results in a positive absorption peak from the FID, then the 270° pulse will create a negative peak. When a 180° pulse is used instead, no $\mathbf{M}_{xy}$ is created, but the low energy spins are turned into the high-energy state, $-\mathbf{M}_y$. These spins will relax to their normal state with characteristic time T_1 and the magnetization will change from $-\mathbf{M}_z$ through zero to $+\mathbf{M}_z$. If, at a time τ after the 180° pulse, a second pulse of 90° is applied, a magnetization $\mathbf{M}_{xy}$ is created equal to in magnitude to $\mathbf{M}_z$ at that instant. The spectrum that results from processing the FID will be negative if $\mathbf{M}_z$ is still negative at that time and positive if $\mathbf{M}_z$ has passed through zero. A series of spectra are obtained in this way for a number of different values of τ, allowing the extraction of a value for T_1. The equations governing the transverse and longitudinal magnetization $\mathbf{M}_{xy}$ and $\mathbf{M}_z$ is given by Eq. 4.8:

$$(M_z)_t = (M_z)_\infty[1 - 2\exp(t/T_1)] \quad \textbf{... 4.8}$$

Sufficient time must elapse between each 180°/90° pair of pulses to allow $\mathbf{M}_z$ to relax fully to its equilibrium value. Usually the delay time of five to ten times T_1 is used.

4.3.2.4 Characteristics of T_2

When a 90° pulse is used, the magnetization in the z $\mathbf{B}_0$ direction is zero, returning to normal in a time T_1. A transverse magnetization has however been created in the xy plane, rotating at the nuclear Larmor frequency. This magnetization decays to zero, but as the frequency of each spin is slightly different, the magnetization fans out, loses coherence and therefore decreases. Eventually the spins take all directions in the xy plane and $\mathbf{M}_{xy}$ is zero. The time of this process is T_2, also called transverse relaxation, or spin-spin relaxation in solid materials. The T_2 process involves no energy change, and is usually encountered in the linewidth of a signal. The linewidth at half-height, $W_{½}$, is given by Eq. 4.9:

$$W_{½} = 1/\pi T_2 \quad \text{... 4.9}$$

This is true for a singlet in a homogeneous magnetic field, but in practice inhomogeneity in the magnetic field and unresolved coupling often contributes to the linewidth. Nevertheless, T_2 can be measured from the linewidth or from the rate of decay of the FID when there is only a single resonance.

4.3.3 MAGNETISATION TRANSFER

4.3.3.1 Introduction[9]

The difficulty of lineshape analysis is that the only information available is the rate of leaving each site. No information is directly available on the destination. In the case of multisite exchange problems, the destination is often far from obvious. There is a number of different magnetization transfer experiments used to examine such situations and they involve disturbing the Boltzmann population distribution in one or more sites. The simplest experiment is saturation transfer.

4.3.3.2 Spin Saturation Transfer

In this type of experiment, the decoupler is turned on to one site for several seconds. Then the decoupler is turned off and a general 90° pulse is applied to examine the effect. A second reference spectrum is taken where the decoupler is set on a region of the region where there is no signal. A difference spectrum is taken to show what changes have been induced in the spectrum as a result of the radiation. For exchange between two sites, A and B, before the decoupler was turned on, the spin system was at equilibrium with equilibrium magnetization, $\mathbf{M}_z(0)$, at both sites. The decoupler, applied to site A, destroys the magnetization and $\mathbf{M}_z^A = 0$. If there is interaction between sites A and B, nuclei from site A move to site B and vice versa. Nuclei from site A have no effect on site B, having no magnetization, but magnetization of nuclei moving from site B is destroyed. The magnetization of site B decreases as a result. The time dependence of the magnetization at site B, $\mathbf{M}_z^B(t)$, is given by Eq. 4.10:

$$\frac{dM_z^B(t)}{dt} = \frac{M_z^B(0) - M_z^B(t)}{T_1^B} - k_B M_z^B(t) \quad \text{... 2.10}$$

k_B is the rate of exchange. The first term produces the T_1 recovery of the magnetization in site B and the second term is due to the loss of magnetization from site B by exchange. When t = ∞, the exchange is at equilibrium and the magnetization does not change, then $\frac{dM_z^B(t)}{dt} = 0$. k_B can then be calculated by Eq. 4.11:

$$k_B = \frac{1}{T_1^B} \frac{M_x^B(0) - M_z^B(\infty)}{M_z^B(\infty)} \quad \text{... 4.11}$$

For $k_B >> 1/T_1^B$, $\mathbf{M}_z^B(\infty) \sim 0$, and for $k_B << 1/T_1^B$, $\mathbf{M}_z^B(\infty) \sim \mathbf{M}_z^B(0)$. Therefore, if $k_B >> 1/T_1^B$, magnetization transfer causes the signal due to B to vanish as well as the signal due to A. When $k_B << 1/T_1^B$, the signal due to exchange from site B is unaffected by magnetization transfer.

4.3.4 EXPERIMENTAL

4.3.4.1 Magnetisation Transfer

Solutions of $AgPF_6$ (0.3 ml) was added to solutions of PPh_3 (0.4 ml) in varied concentrations, in 50% CD_2CL_2/CH_2Cl_2. These concentrations are shown in Table 4.1.

Table 4.1 Experimental concentration values for $AgPF_6$ and PPh_3 solutions

[PPh_3] (mM)	**[$AgPF_6$] (mM)**
20.0	0.541
10.0	0.427
5.0	0.462

These samples were investigated at -80 °C using magnetic spin transfer spectroscopy, recorded on a Varian Unity Inova 500 (202.302 MHz for ^{31}P) spectrometer. A normal spectrum was first collected to establish the frequency of the saturation signal, as shown in Figure 4.3. The sample was then saturated at the set frequency and the spectra recorded at different time intervals, d_2. The relaxation time, d_1, was 30 s and d_2 was arrayed from 3 x 10^{-5} to 30 s.

4.3.4.2 Results

The initial normal spectrum at -80°C of a sample containing containing [PPh_3] = 20.0 mM and [$AgPF_6$] = 0.541 mM is shown in Figure 4.3.

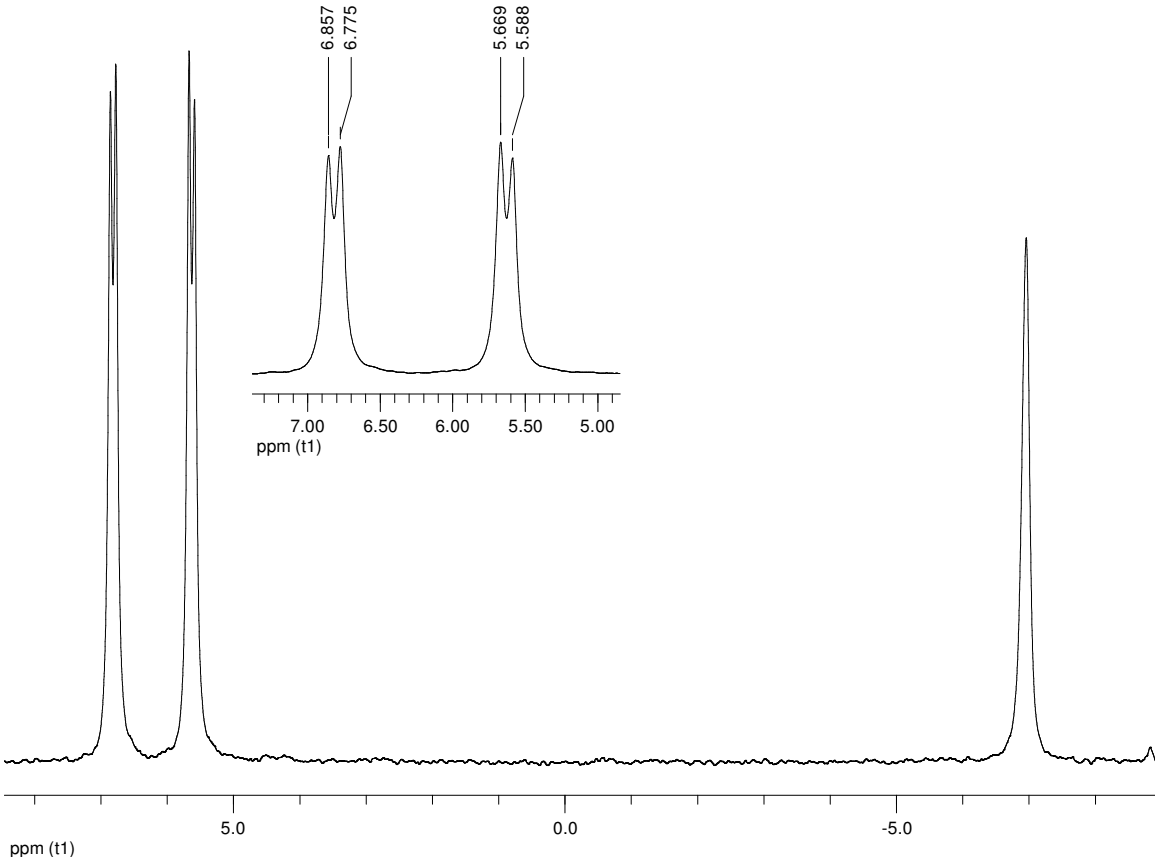

Figure 4.3 Spectrum of sample of [PPh_3] = 5.01 mM and [$AgPF_6$] = 0.462 mM at -80°C before saturation.

NMR spectra observed at different time intervals for magnetic transfer experiments are shown in Figure 4.4 – Figure 4.6. Different vertical scales were employed for free and coordinated phosphine sites for improved clarity.

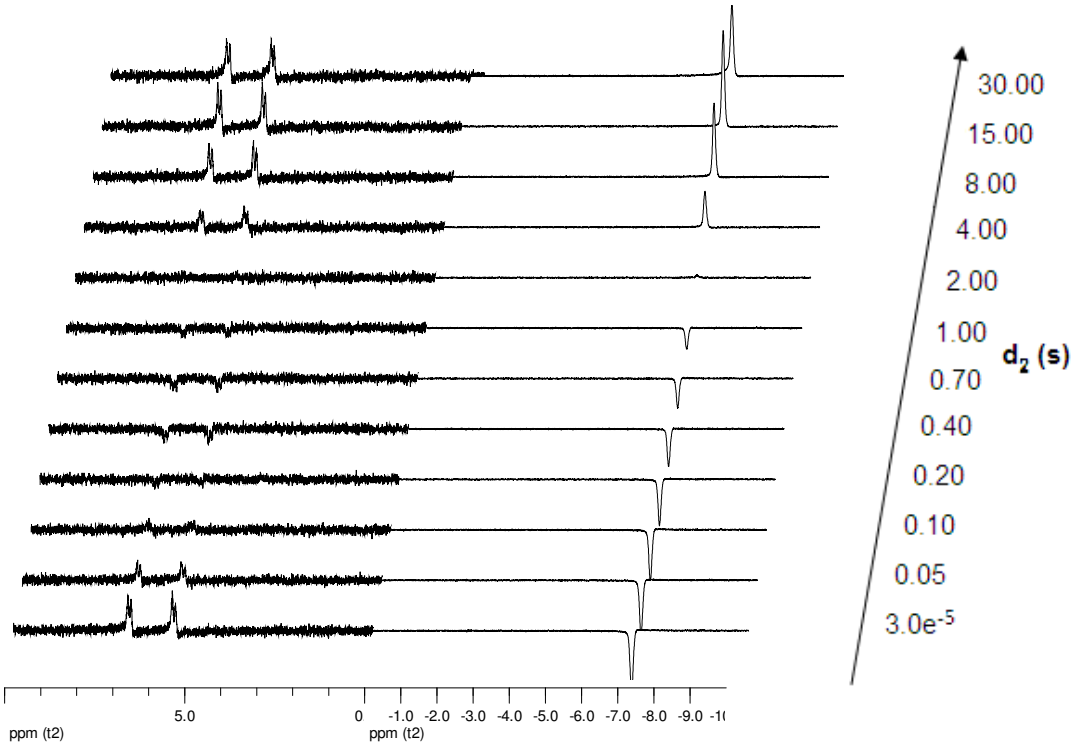

Figure 4.4 NMR stacked plot of spectra for solution containing [PPh_3] = 20.0 mM and [$AgPF_6$] = 0.541 mM at -80°C.

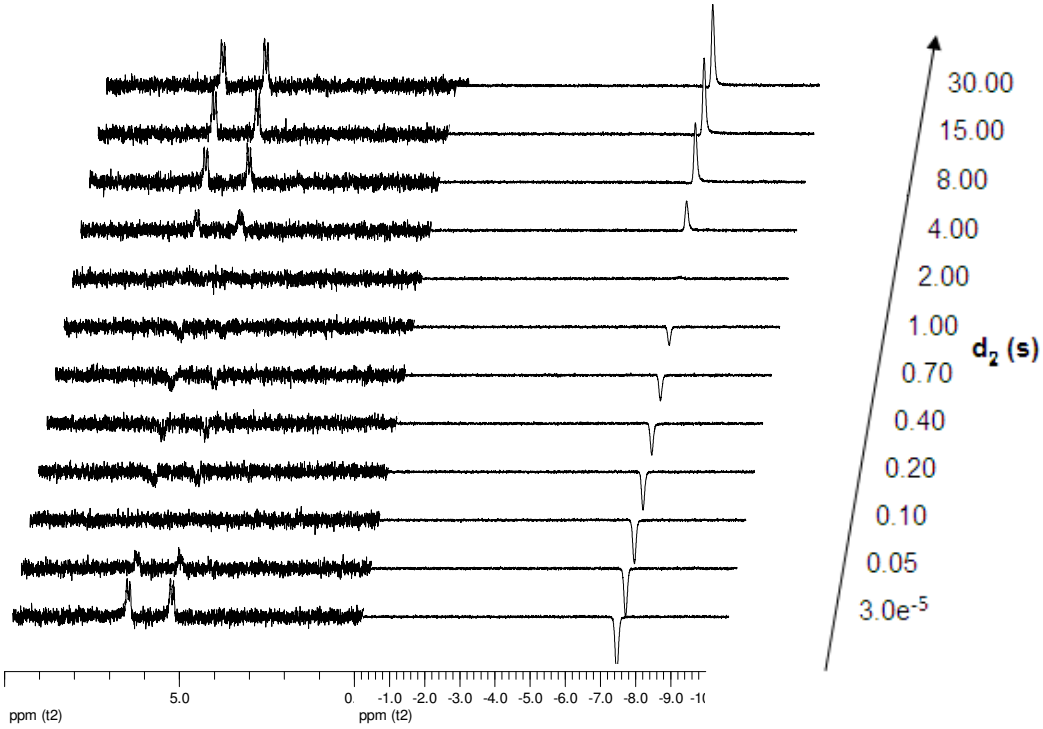

Figure 4.5 NMR stacked plot of spectra for solution containing [PPh_3] = 10.0 mM and [$AgPF_6$] = 0.427 mM at -80°C.

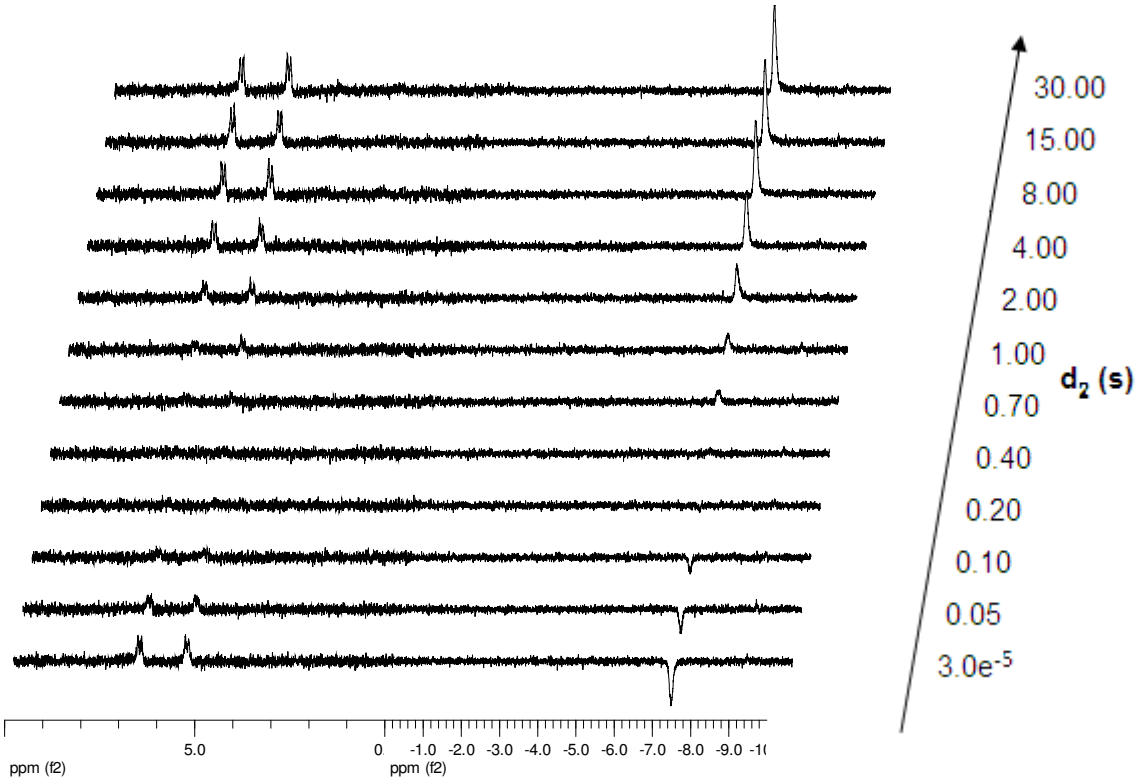

Figure 4.6 NMR stacked plot of spectra for solutions containing [PPh_3] = 5.0 mM and [$AgPF_6$] = 0.462 mM at -80°C.

Observed and calculated intensity values for the samples are illustrated in Figure 4.7 - Figure 4.9, where the data has been fitted by the cifit program[10].

[10]A.D. Bain, J.A. Cramer, *J. Magn. Reson.*, **118A**, 21 (1996).

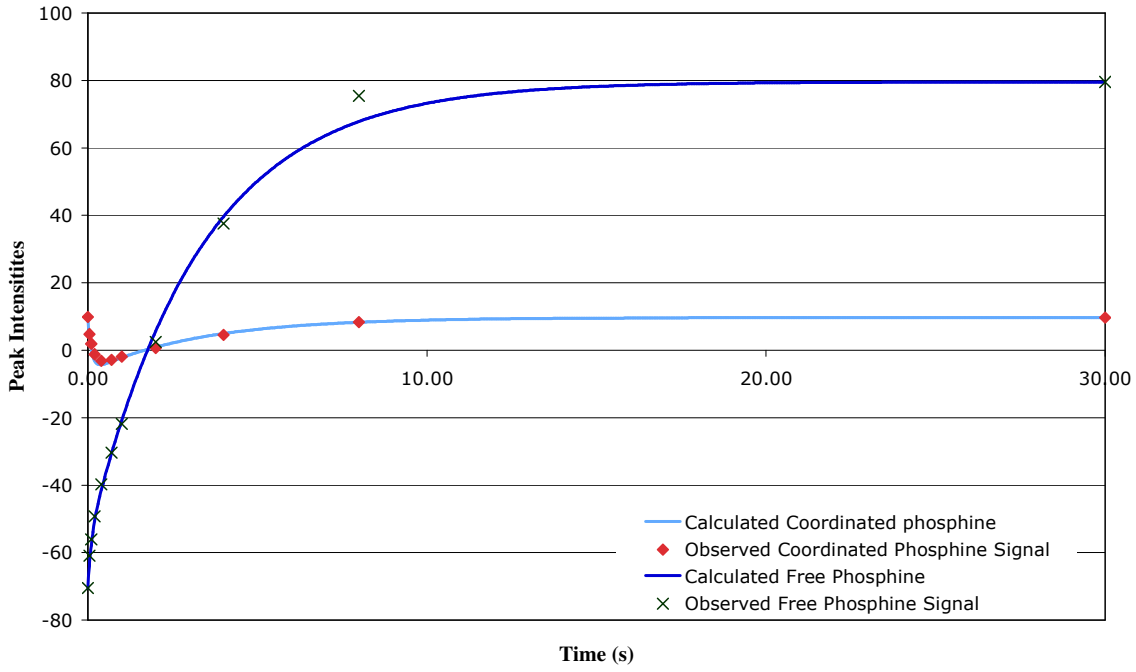

Figure 4.7 Peak intensities vs. time for solution containing [PPh_3] = 20.0 mM and [$AgPF_6$] = 0.541 mM at -80°C.

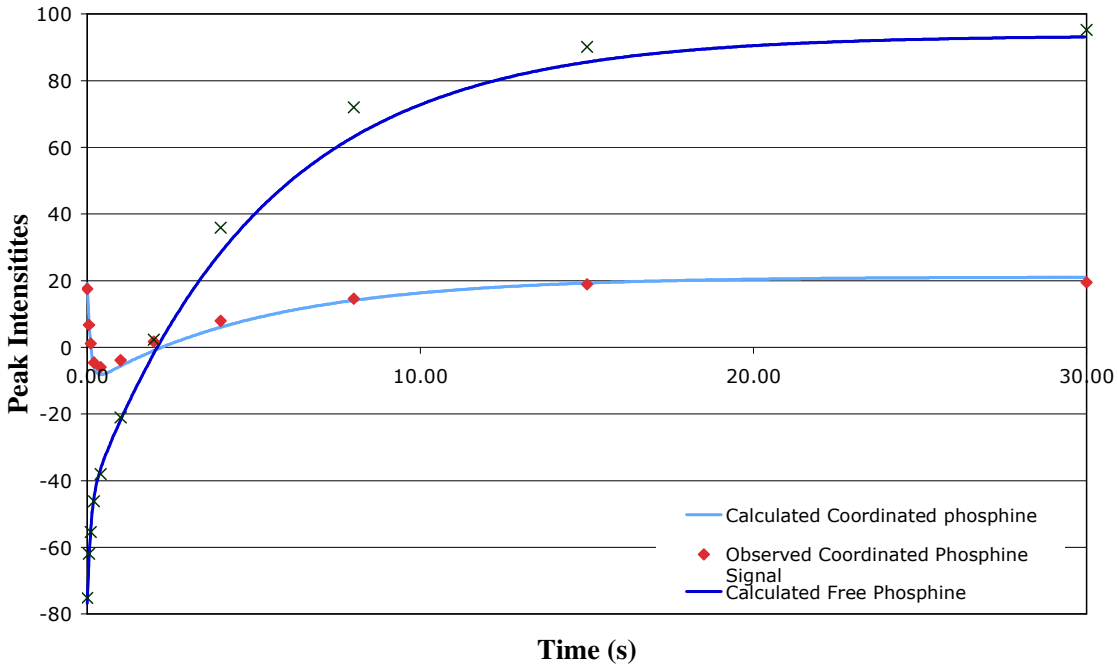

Figure 4.8 Peak intensities vs. time for solution containing [PPh_3] = 10.0 mM and [$AgPF_6$] = 0.427 mM at -80°C.

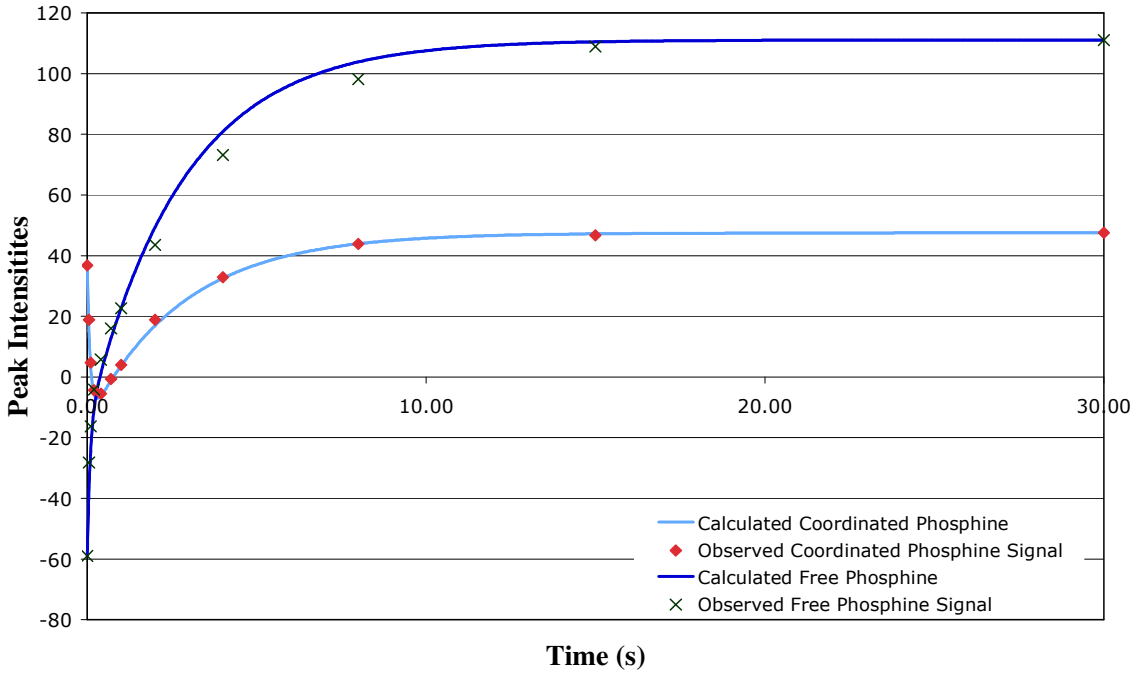

Figure 4.9 Peak intensities vs. time for solution at -80°C containing [PPh_3] = 5.0 mM and [$AgPF_6$] = 0.462 mM.

The rates of exchange between free and coordinated phosphine, as calculated by the cifit program[10], as well as values for T_1 for the free and coordinated phosphine, are tabulated in Table 4.2. The values of k_{obs} for solutions containing varied concentrations of PPh_3 do not differ significantly. The effect of [PPh_3] on the rate of exchange is illustrated by Figure 4.10.

Table 4.2 Calculated values for the first order rate constant k_{obs} and T_1, the relaxation time of the applied signal.

$[PPh_3]_{Total}$ (mM)	$[PPh_3]_{Free}$ (mM)	$[AgPF_6]$ (mM)	k_{obs} (s^{-1}) [a]	$\sigma(k_{obs})$ (s^{-1})	$T_{1,Free}$ (s) [a]	$T_{1,Coord}$ (s)
20.0	17.8	0.541	7.17	1.60	8.29 [a]	0.587
10.0	8.9	0.427	7.61	1.44	4.81	0.870
5.0	3.2	0.462	6.64	1.34	4.50	0.633

a) No e.s.d.'s were obtained from the fitting program, but are estimated to be ca. 10%.

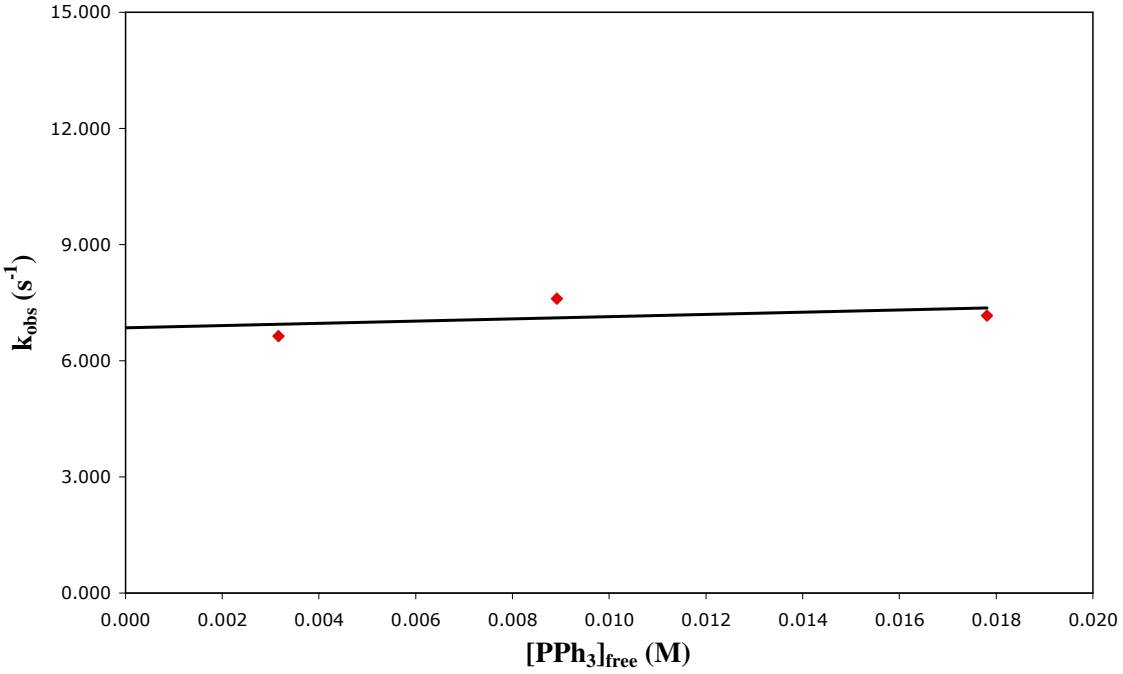

Figure 4.10 Rate of exchange vs. $[PPh_3]_{Free}$

The fitted line in Figure 4.10 is described by Eq. 4.12, the well-known expression for a straight line.

$$y = mx + c \quad \text{... 4.12}$$

where m = 29±60 $mM^{-1}.s^{-1}$ (which = 0 within e.s.d.) and c = 6.9±0.7 s^{-1}. As the standard deviations are very large, these values are only estimations.

4.3.5 DISCUSSION

The exchange process studied is represented in Eq. 4.13.

$$[Ag(PX_3)_n]^+ + PX_3^* \leftrightarrow [Ag(PX_3^*)]^+ + PX_3 \quad \text{... 4.13}$$

where n is uncertain in solution.

The rate of exchange of free phosphine with coordinated phosphine is fast, in the range of ca. 7 s^{-1} at -80 °C. The rate of exchange between coordinated and free phosphine in the complex $[Ag(PPh_3)_4]PF_6$ has been found to be independent of the concentration of phosphine, indicating a possible dissociative mechanism. For this process, the rate law is given by Eq. 4.14.

$$Rate = k_1[PX_3][Ag^+]_r - k_{-1}[Ag^+]_p \quad \text{... 4.14}$$

where k_1 and k_{-1} are the forward and reverse rate constants respectively, and r and p denote the concentrations of the reactant and product species respectively. For Eq. 4.14 the first order rate constant is given by Eq. 4.15.

$$k_{obs} = k_1[PX_3] + k_{-1} \quad \text{... 4.15}$$

The k_1 and k_{-1} values were obtained from Figure 4.10 and Eq. 4.15. These values are k_1 = 29±60 $mM^{-1}.s^{-1}$ and k_{-1} =6.9±0.7 s^{-1}.

Due to the complexity of the experiments, as well as a shortage of NMR time only this preliminary study was possible. However, further studies, confirming the results, should be conducted to study the exchange process in detail, including electronic end steric factors which influences the reaction.

4.4 Conclusion

No evidence was obtained for substantial coordination of CO to Ag(I) complexes of the type $[AgL_nX]$ (L = tertiary phosphine; n = 1 - 4; X = coordinating or non-coordinating anion). PPh_3 ligands are strong σ-donors, but weaker π-acceptors than CO and thus compete more effectively for π-electron density. The presence of the bulky phosphine ligand could therefore inhibit the coordination of the CO molecule to the silver complex. Another explanation is the high electron density surrounding the silver atom, with possible less effective spacially orientated d-orbitals which might result in less effective overlap with π^*-orbitals of CO, resulting in less stable Ag(CO) moieties. prevents π-back bonding from the silver atom to the CO molecule.

The exchange between free and coordinated phosphine in the complex $[Ag(PPh_3)_n]PF_6$ is rapid, which are k_1 = 29±60 $mM^{-1}.s^{-1}$ and k_{-1} = 6.9±0.7 s^{-1}, and could inhibit the coordination of other ligands to the metal centre. Without coordination of a CO ligand and hydrogen, hydroformylation of an alkene to an aldehyde will not occur. The investigation of phosphine exchange in Ag(I) complexes through magnetisation transfer at low temperatures cannot be compared to other metal-phosphine exchange systems, as no such instances are available in literature.

Ag(I) complexes of this type therefore seem to be not viable hydroformylation catalysts, and since these metal centres undergo the basic coordination reactions (olefin, CO and hydrogen formation), other inherent properties such as the large energy barrier to undergo oxidative addition (to be examined by computational methods in future) might prevent it being hydroformylation active.

5 Study Evaluation

5.1 Success of the study

Three tertiary phosphine complexes of Ag(I) of the type $[AgXL_n]$ (X = Br, ClO_4^-, PF_6^-, L = P(*p*-tol)$_3$, n = 1, 3, 4) were synthesized and successfully characterized by X-ray crystallography, infrared and ^{31}P NMR. These complexes were compared to similar complexes containing transition metals, other phosphine ligands or different counterions. Occurrences of similar structures in literature were limited, indicating a field open to study. The solid state coordination chemistry of Ag(I) shows a vast array of different modes, which will be expanded on in future investigations. This study nicely illustrated three different types, which could be obtained by spontaneous supermolecular assembly.

High-pressure infrared studies were conducted to investigate the coordination of CO to these complexes, which proved to be difficult. No evidence could be obtained through high-pressure infrared of coordination of CO to Ag(I) complexes. The aversion of the silver metal centre to coordinate the CO molecule could be attributed to the coordination of bulky phosphine ligands, which could prevent the coordination of CO ligand to the metal centre, as well as the absence of a strong electron-accepting ligand, for example boron- or nitrogen-containing ligands. Another explanation is the high electron density surrounding the silver atom, which prevents π-back bonding from the silver atom to the CO molecule. The presence of weakly coordinating solvents such as toluene, nitromethane, diethyl ether and dichloromethane could also have an influence, as postulated for the complex $[Ag(CO)]B(OTeF_5)_4$[1]. Based on this study, these solvents, although only weakly coordinating, apparently complex more strongly to Ag^+ than CO. Tertiary phosphine complexes of Ag(I) of the type $[AgXL_n]$ therefore do not exhibit the properties necessary to act as hydroformylation catalysts.

[1] P.K Hurlburt, O.P. Anderson, S.H. Strauss, *J. Am. Chem. Soc.*, **113**, 6277 (1991).

Magnetization transfer experiments were conducted at -80°C to investigate the rate of exchange between silver-coordinated phosphine and free phosphine. This rate was established to be very rapid, even at low temperature, and the observed first order rate law is given by $k_1[PX_3] + k_{-1}$, where k_1 and k_{-1} are the forward and reverse rate constants respectively, and r and p denote the concentrations of the reactant and product species. The rate constant of the exchange is described with the equation

$$k_{obs} = k_1[PX_3] + k_{-1}$$

where $k_1 = 29\pm60\ mM^{-1}.s^{-1}$ and $k_{-1} = 6.9\pm0.7\ s^{-1}$. The exchange rate between free and coordinated phosphine in Ag(I) complexes should be explored further.

This study was complicated by technical difficulties involving the high-pressure infrared, as well as the low temperature NMR equipment.

5.2 Future Studies

The following stepwise aims have been set for possible future research:

a) Exploration of coordination chemistry of Ag(I) complexes of the type $[AgXL_n]$ (X = coordinating or non-coordinating anion, n = 1-4) with L = P(*p*-tol)$_3$, to investigate different coordination modes of such complexes. The solution state characteristics of these complexes also offer a vast field for investigation, as very little is known of such properties.

b) Synthesis and characterization of Ag(I) complexes with electron-withdrawing ligands. These ligands should contain atoms such as nitrogen or boron, as exemplified in literature[1,2]. Such ligands may alleviate the problem of electron density surrounding the Ag(I) atom, enabling the coordination of Ag(I) with other ligands, such as CO, hydrogen and olefins, which proved problematic in the complexes discussed in this study.

c) Evaluation of above-mentioned Ag(I) complexes for hydroformylation activity. Complexes of Ag(I) able to coordinate to an array of ligands, such as CO, H and

[2] a) P.K. Hurlburt, J.J. Rack, S.F. Dec, O.P. Anderson, S.H. Strauss, *Inorg. Chem.*, **32**, 373 (1993). b) H.V.R. Dias, W. Jin, *J. Am. Chem. Soc.*, **117**, 11381 (1995).

alkenes, could act as hydroformylation catalysts, as a more cost-effective alternative to rhodium catalysts.

d) Evaluation of phosphine ligand exchange in tertiary phosphine complexes of Ag(I) of the type $[AgXL_n]$ (L = tertiary phosphine; n = 1-4; X = coordinating or non-coordinating anion) using magnetic spin transfer methods. Only one example of such exchange rate investigations exist in literature[3], and was not conducted through magnetization transfer methods.

[3] E.L. Muetterties, C.W. Alegranti, *J. Am. Chem. Soc.*, **94**, 6386 (1972).

A Appendix - [Ag{P(*p*-tol)$_3$}]PF$_6$

Table A.1 Atomic coordinates (x 10^4) and equivalent isotropic displacement parameters (Å^2 x 10^3) for [Ag{P(p-tol)$_3$}$_4$]PF$_6$. U(eq) is defined as one third of the trace of the orthogonalized Uij tensor.

Atom	x	y	z	U(eq)
Ag(1)	7321(1)	7321(1)	7321(1)	16(1)
Ag(2)	2552(1)	7552(1)	7448(1)	18(1)
P(01)	10047(1)	5047(1)	9953(1)	48(1)
P(02)	4875(1)	5125(1)	10125(1)	42(1)
P(11)	7923(1)	7923(1)	7923(1)	20(1)
P(12)	6375(1)	7752(1)	7240(1)	18(1)
P(23)	1951(1)	6951(1)	8049(1)	23(1)
P(24)	3412(1)	7846(1)	7991(1)	17(1)
F(11A)	10014(7)	5327(5)	9360(4)	134(4)
F(11B)	9719(7)	5089(5)	9448(4)	134(4)
F(12)	9513(2)	5287(3)	10141(2)	147(2)
F(21)	4689(1)	4848(2)	9587(1)	78(1)
F(22)	4317(2)	4946(2)	10381(2)	110(2)
C(111)	8321(1)	7559(1)	8428(1)	24(1)
C(112)	8339(1)	7705(2)	8972(1)	35(1)
C(113)	8645(2)	7404(2)	9333(2)	46(1)
C(114)	8950(2)	6964(2)	9163(2)	40(1)
C(115)	8931(1)	6824(1)	8620(2)	30(1)
C(116)	8612(1)	7110(1)	8258(1)	26(1)
C(117)	9306(2)	6650(2)	9545(2)	59(1)
C(211)	6392(1)	8425(1)	6937(1)	21(1)
C(212)	6028(1)	8597(1)	6542(1)	26(1)
C(213)	6079(2)	9109(1)	6311(1)	32(1)
C(214)	6485(2)	9459(1)	6469(2)	33(1)
C(215)	6839(1)	9288(1)	6870(1)	31(1)
C(216)	6794(1)	8778(1)	7105(1)	25(1)
C(217)	6540(2)	10013(2)	6222(2)	49(1)

C(221)	5910(1)	7393(1)	6792(1)	20(1)
C(222)	5380(1)	7257(1)	6923(1)	24(1)
C(223)	5061(1)	6990(1)	6546(1)	26(1)
C(224)	5250(1)	6861(1)	6031(1)	25(1)
C(225)	5782(1)	6991(1)	5914(1)	28(1)
C(226)	6109(1)	7252(1)	6289(1)	26(1)
C(227)	4894(1)	6585(2)	5624(2)	35(1)
C(231)	5999(1)	7853(1)	7865(1)	20(1)
C(232)	5917(1)	7415(1)	8212(1)	28(1)
C(233)	5651(1)	7483(2)	8701(1)	32(1)
C(234)	5460(1)	7987(2)	8857(1)	29(1)
C(235)	5538(1)	8422(1)	8512(1)	28(1)
C(236)	5805(1)	8357(1)	8023(1)	23(1)
C(237)	5178(2)	8063(2)	9393(2)	45(1)
C(311)	2281(1)	6693(1)	8655(1)	24(1)
C(312)	2810(1)	6511(1)	8608(1)	25(1)
C(313)	3086(1)	6311(1)	9054(1)	28(1)
C(314)	2842(2)	6285(2)	9559(2)	38(1)
C(315)	2316(2)	6477(2)	9605(2)	48(1)
C(316)	2035(2)	6682(2)	9159(1)	39(1)
C(317)	3142(2)	6063(2)	10034(2)	58(1)
C(411)	3294(1)	8195(1)	8633(1)	21(1)
C(412)	2890(1)	8013(1)	8976(1)	28(1)
C(413)	2788(2)	8273(2)	9461(1)	34(1)
C(414)	3086(2)	8719(1)	9617(1)	33(1)
C(415)	3497(2)	8897(1)	9281(1)	36(1)
C(416)	3602(1)	8638(1)	8794(1)	27(1)
C(417)	2971(2)	9000(2)	10149(2)	51(1)
C(421)	3834(1)	8329(1)	7624(1)	19(1)
C(422)	4395(1)	8323(1)	7608(1)	24(1)
C(423)	4672(1)	8712(1)	7319(1)	30(1)
C(424)	4404(1)	9124(1)	7049(1)	29(1)
C(425)	3844(1)	9133(1)	7068(1)	27(1)
C(426)	3566(1)	8740(1)	7346(1)	24(1)
C(427)	4704(2)	9562(2)	6741(2)	53(1)
C(431)	3879(1)	7304(1)	8175(1)	20(1)
C(432)	4008(1)	6920(1)	7787(1)	30(1)

C(433)	4349(2)	6492(1)	7907(2)	36(1)
C(434)	4559(1)	6428(1)	8423(2)	37(1)
C(435)	4432(1)	6808(2)	8806(2)	36(1)
C(436)	4094(1)	7244(1)	8688(1)	28(1)
C(437)	4923(2)	5955(2)	8555(2)	54(1)

Table A.2 Bond lengths (Å) and angles (°) for $[Ag\{P(p\text{-}tol)_3\}_4]PF_6$. Symmetry operations appear at the end of the table.

Atoms	Distance (Å)
Ag(1)-P(11)	2.570(1)
Ag(1)-P(12)	2.5737(7)
Ag(1)-P(12)$^{\#3}$	2.5737(7)
Ag(1)-P(12)$^{\#4}$	2.5737(7)
Ag(2)-P(24)	2.6142(7)
Ag(2)-P(23)	2.567(1)
Ag(2)-P(24)$^{\#5}$	2.6142(7)
Ag(2)-P(24)$^{\#6}$	2.6142(7)
P(01)-F(11A)	1.622(10)
P(01)-F(11A)$^{\#7}$	1.622(10)
P(01)-F(11A)$^{\#8}$	1.622(10)
P(01)-F(11B)	1.49(1)
P(01)-F(11B)$^{\#7}$	1.49(1)
P(01)-F(11B)$^{\#8}$	1.49(1)
P(01)-F(12)	1.518(4)
P(01)-F(12)$^{\#7}$	1.518(4)
P(01)-F(12)$^{\#8}$	1.518(4)
P(02)-F(21)	1.562(3)
P(02)-F(21)$^{\#1}$	1.562(3)
P(02)-F(21)$^{\#2}$	1.562(3)
P(02)-F(22)	1.579(4)
P(02)-F(22)$^{\#1}$	1.579(4)
P(02)-F(22)$^{\#2}$	1.579(4)
P(11)-C(111)	1.826(3)
P(11)-C(111)$^{\#3}$	1.826(3)
P(11)-C(111)$^{\#4}$	1.826(3)

P(12)-C(211)	1.824(3)
P(12)-C(221)	1.824(3)
P(12)-C(231)	1.818(3)
P(23)-C(311)	1.818(3)
P(23)-C(311)$^{\#5}$	1.818(3)
P(23)-C(311)$^{\#6}$	1.818(3)
P(24)-C(411)	1.828(3)
P(24)-C(421)	1.823(3)
P(24)-C(431)	1.823(3)
F(11B)-F(12)$^{\#8}$	1.603(13)
F(11B)$^{\#7}$-F(12)	1.603(14)
C(111)-C(116)	1.384(5)
C(111)-C(112)	1.390(4)
C(112)-C(113)	1.385(5)
C(112)-H(112)	0.9500
C(113)-C(114)	1.386(6)
C(113)-H(113)	0.9500
C(114)-C(115)	1.385(5)
C(114)-C(117)	1.503(5)
C(115)-C(116)	1.386(4)
C(115)-H(115)	0.9500
C(116)-H(116)	0.9500
C(117)-H(11A)	0.9800
C(117)-H(11B)	0.9800
C(117)-H(11C)	0.9800
C(211)-C(216)	1.385(4)
C(211)-C(212)	1.390(4)
C(212)-C(213)	1.393(5)
C(212)-H(212)	0.9500
C(213)-C(214)	1.382(5)
C(213)-H(213)	0.9500
C(214)-C(215)	1.387(5)
C(214)-C(217)	1.504(5)
C(215)-C(216)	1.389(5)
C(215)-H(215)	0.9500
C(216)-H(216)	0.9500
C(217)-H(21A)	0.9800

C(217)-H(21B)	0.9800
C(217)-H(21C)	0.9800
C(221)-C(226)	1.380(4)
C(221)-C(222)	1.388(4)
C(222)-C(223)	1.386(4)
C(222)-H(222)	0.9500
C(223)-C(224)	1.393(5)
C(223)-H(223)	0.9500
C(224)-C(225)	1.383(5)
C(224)-C(227)	1.498(5)
C(225)-C(226)	1.385(5)
C(225)-H(225)	0.9500
C(226)-H(226)	0.9500
C(227)-H(22A)	0.9800
C(227)-H(22B)	0.9800
C(227)-H(22C)	0.9800
C(231)-C(236)	1.389(4)
C(231)-C(232)	1.393(4)
C(232)-C(233)	1.382(4)
C(232)-H(232)	0.9500
C(233)-C(234)	1.386(5)
C(233)-H(233)	0.9500
C(234)-C(235)	1.384(5)
C(234)-C(237)	1.506(5)
C(235)-C(236)	1.384(4)
C(235)-H(235)	0.9500
C(236)-H(236)	0.9500
C(237)-H(23A)	0.9800
C(237)-H(23B)	0.9800
C(237)-H(23C)	0.9800
C(311)-C(316)	1.384(4)
C(311)-C(312)	1.387(5)
C(312)-C(313)	1.385(5)
C(312)-H(312)	0.9500
C(313)-C(314)	1.385(5)
C(313)-H(313)	0.9500
C(314)-C(315)	1.387(6)

C(314)-C(317)	1.492(5)
C(315)-C(316)	1.397(5)
C(315)-H(315)	0.9500
C(316)-H(316)	0.9500
C(317)-H(31A)	0.9800
C(317)-H(31B)	0.9800
C(317)-H(31C)	0.9800
C(411)-C(412)	1.382(4)
C(411)-C(416)	1.389(4)
C(412)-C(413)	1.383(5)
C(412)-H(412)	0.9500
C(413)-C(414)	1.379(5)
C(413)-H(413)	0.9500
C(414)-C(415)	1.383(5)
C(414)-C(417)	1.511(5)
C(415)-C(416)	1.386(5)
C(415)-H(415)	0.9500
C(416)-H(416)	0.9500
C(417)-H(41A)	0.9800
C(417)-H(41B)	0.9800
C(417)-H(41C)	0.9800
C(421)-C(422)	1.387(4)
C(421)-C(426)	1.391(4)
C(422)-C(423)	1.378(4)
C(422)-H(422)	0.9500
C(423)-C(424)	1.383(5)
C(423)-H(423)	0.9500
C(424)-C(425)	1.385(5)
C(424)-C(427)	1.514(5)
C(425)-C(426)	1.372(4)
C(425)-H(425)	0.9500
C(426)-H(426)	0.9500
C(427)-H(42A)	0.9800
C(427)-H(42B)	0.9800
C(427)-H(42C)	0.9800
C(431)-C(436)	1.382(4)
C(431)-C(432)	1.383(4)

C(432)-C(433)	1.383(5)
C(432)-H(432)	0.9500
C(433)-C(434)	1.383(5)
C(433)-H(433)	0.9500
C(434)-C(435)	1.368(6)
C(434)-C(437)	1.509(5)
C(435)-C(436)	1.393(5)
C(435)-H(435)	0.9500
C(436)-H(436)	0.9500
C(437)-H(43A)	0.9800
C(437)-H(43B)	0.9800
C(437)-H(43C)	0.9800

Atoms	Angle (°)
Ag(1)-P(11)-C(111)	114.95(10)
Ag(1)-P(11)-C(111)$^{\#3}$	114.95(10)
Ag(1)-P(11)-C(111)$^{\#4}$	114.95(10)
Ag(1)-P(12)-C(211)	112.83(10)
Ag(1)-P(12)-C(221)	114.74(9)
Ag(1)-P(12)-C(231)	117.05(9)
Ag(2)-P(23)-C(311)	114.80(10)
Ag(2)-P(23)-C(311)$^{\#5}$	114.80(10)
Ag(2)-P(23)-C(311)$^{\#6}$	114.80(10)
Ag(2)-P(24)-C(411)	116.49(10)
Ag(2)-P(24)-C(421)	113.02(9)
Ag(2)-P(24)-C(431)	115.88(10)
P(11)-Ag(1)-P(12)	109.31(2)
P(11)-Ag(1)-P(12)$^{\#4}$	109.31(2)
P(11)-Ag(1)-P(12)$^{\#3}$	109.31(2)
P(12)-Ag(1)-P(12)$^{\#3}$	109.63(2)
P(12)-Ag(1)-P(12)$^{\#4}$	109.63(2)
P(12)$^{\#3}$-Ag(1)-P(12)$^{\#4}$	109.63(2)
P(23)-Ag(2)-P(24)	109.50(2)
P(23)-Ag(2)-P(24)$^{\#5}$	109.50(2)
P(23)-Ag(2)-P(24)$^{\#6}$	109.50(2)
P(24)-Ag(2)-P(24)$^{\#5}$	109.44(2)

P(24)-Ag(2)-P(24)$^{\#6}$	109.44(2)
P(24)$^{\#5}$-Ag(2)-P(24)$^{\#6}$	109.44(2)
F(11A)-P(01)-F(11A)$^{\#7}$	71.5(9)
F(11A)-P(01)-F(11A)$^{\#8}$	71.5(9)
F(11A)-P(01)-F(11B)	35.6(7)
F(11A)-P(01)-F(11B)$^{\#7}$	97.9(9)
F(11A)-P(01)-F(11B)$^{\#8}$	102.2(9)
F(11A)-P(01)-F(12)	93.7(6)
F(11A)-P(01)-F(12)$^{\#7}$	159.1(6)
F(11A) -P(01)-F(12)$^{\#8}$	90.1(5)
F(11A)$^{\#7}$-P(01)-F(11A)$^{\#8}$	71.5(9)
F(11A)$^{\#7}$-P(01)-F(11B)	102.2(9)
F(11A)$^{\#7}$-P(01)-F(11B)$^{\#7}$	35.6(7)
F(11A)$^{\#7}$-P(01)-F(11B)$^{\#8}$	97.9(9)
F(11A)$^{\#7}$-P(01)-F(12)	90.1(5)
F(11A)$^{\#7}$-P(01)-F(12)$^{\#7}$	93.7(6)
F(11A)$^{\#7}$-P(01)-F(12)$^{\#8}$	159.1(6)
F(11A)$^{\#8}$-P(01)-F(11B)	97.9(9)
F(11A)$^{\#8}$ -P(01)-F(11B)$^{\#7}$	102.2(9)
F(11A)$^{\#8}$-P(01)-F(11B)$^{\#8}$	35.6(7)
F(11A)$^{\#8}$-P(01)-F(12)	159.1(6)
F(11A)$^{\#8}$-P(01)-F(12)$^{\#7}$	90.1(6)
F(11A)$^{\#8}$-P(01)-F(12)$^{\#8}$	93.7(6)
F(11B)-P(01)-F(11B)$^{\#7}$	115.7(3)
F(11B)-P(01)-F(11B)$^{\#8}$	115.7(3)
F(11B)-P(01)-F(12)	75.9(6)
F(11B)-P(01)-F(12)$^{\#7}$	163.8(5)
F(11B)-P(01)-F(12)$^{\#8}$	64.4(6)
F(11B)$^{\#7}$-P(01)-F(11B)$^{\#8}$	115.7(3)
F(11B)$^{\#7}$-P(01)-F(12)	64.4(6)
F(11B)$^{\#7}$-P(01)-F(12)$^{\#7}$	75.9(6)
F(11B)$^{\#7}$-P(01)-F(12)$^{\#8}$	163.8(5)
F(11B)$^{\#8}$-P(01)-F(12)	163.8(5)
F(11B)$^{\#8}$-P(01)-F(12)$^{\#7}$	64.4(6)
F(11B)$^{\#8}$-P(01)-F(12)$^{\#8}$	75.9(6)
F(12)-P(01)-F(12)$^{\#7}$	101.2(3)
F(12)-P(01)-F(12)$^{\#8}$	101.2(3)

F(12)$^{\#7}$-P(01)-F(12)$^{\#8}$	101.2(3)
F(21)-P(02)-F(21)$^{\#1}$	90.4(2)
F(21)-P(02)-F(21)$^{\#2}$	90.4(2)
F(21)-P(02)-F(22)	87.7(2)
F(21)-P(02)-F(22)$^{\#1}$	177.3(2)
F(21)-P(02)-F(22)$^{\#2}$	91.5(2)
F(21)$^{\#1}$-P(02)-F(21)$^{\#2}$	90.4(2)
F(21)$^{\#1}$-P(02)-F(22)	91.5(2)
F(21)$^{\#1}$-P(02)-F(22)$^{\#1}$	87.7(2)
F(21)$^{\#1}$-P(02)-F(22)$^{\#2}$	177.3(2)
F(21)$^{\#2}$-P(02)-F(22)	177.3(2)
F(21)$^{\#2}$-P(02)-F(22)$^{\#1}$	91.5(2)
F(21)$^{\#2}$-P(02)-F(22)$^{\#2}$	87.7(2)
F(22)-P(02)-F(22)$^{\#1}$	90.3(3)
F(22)-P(02)-F(22)$^{\#2}$	90.3(3)
F(22)$^{\#1}$-P(02)-F(22)$^{\#2}$	90.3(3)
C(111)$^{\#3}$-P(11)-C(111)	103.48(12)
C(111)$^{\#3}$-P(11)-C(111)$^{\#4}$	103.48(12)
C(111)-P(11)-C(111)$^{\#4}$	103.48(12)
C(231)-P(12)-C(221)	105.02(13)
C(231)-P(12)-C(211)	103.57(14)
C(221)-P(12)-C(211)	101.94(14)
C(311)$^{\#5}$-P(23)-C(311)	103.66(12)
C(311)$^{\#5}$-P(23)-C(311)$^{\#6}$	103.66(12)
C(311)-P(23)-C(311)$^{\#6}$	103.66(12)
C(431)-P(24)-C(421)	104.09(13)
C(431)-P(24)-C(411)	103.36(14)
C(421)-P(24)-C(411)	102.30(13)
P(11)-C(111)-C(116)	117.7(2)
P(11)-C(111)-C(112)	123.3(3)
P(12)-C(211)-C(216)	117.8(2)
P(12)-C(211)-C(212)	123.4(2)
P(12)-C(221)-C(226)	116.4(2)
P(12)-C(221)-C(222)	124.7(2)
P(12)-C(231)-C(236)	122.5(2)
P(12)-C(231)-C(232)	119.3(2)
P(23)-C(311)-C(316)	123.4(3)

P(23)-C(311)-C(312)	117.8(2)
P(24)-C(411)-C(412)	119.4(2)
P(24)-C(411)-C(416)	122.1(2)
P(24)-C(421)-C(422)	125.3(2)
P(24)-C(421)-C(426)	116.8(2)
P(24)-C(431)-C(436)	123.3(2)
P(24)-C(431)-C(432)	118.4(2)
C(116)-C(111)-C(112)	119.0(3)
C(113)-C(112)-C(111)	120.0(4)
C(113)-C(112)-H(112)	120.0
C(111)-C(112)-H(112)	120.0
C(112)-C(113)-C(114)	121.5(3)
C(112)-C(113)-H(113)	119.3
C(114)-C(113)-H(113)	119.3
C(115)-C(114)-C(113)	118.0(3)
C(115)-C(114)-C(117)	119.8(4)
C(113)-C(114)-C(117)	122.2(4)
C(114)-C(115)-C(116)	121.1(3)
C(114)-C(115)-H(115)	119.4
C(116)-C(115)-H(115)	119.4
C(111)-C(116)-C(115)	120.4(3)
C(111)-C(116)-H(116)	119.8
C(115)-C(116)-H(116)	119.8
C(114)-C(117)-H(11A)	109.5
C(114)-C(117)-H(11B)	109.5
H(11A)-C(117)-H(11B)	109.5
C(114)-C(117)-H(11C)	109.5
H(11A)-C(117)-H(11C)	109.5
H(11B)-C(117)-H(11C)	109.5
C(216)-C(211)-C(212)	118.8(3)
C(211)-C(212)-C(213)	120.4(3)
C(211)-C(212)-H(212)	119.8
C(213)-C(212)-H(212)	119.8
C(214)-C(213)-C(212)	121.1(3)
C(214)-C(213)-H(213)	119.5
C(212)-C(213)-H(213)	119.5
C(213)-C(214)-C(215)	118.0(3)

C(213)-C(214)-C(217)	121.2(4)
C(215)-C(214)-C(217)	120.7(4)
C(214)-C(215)-C(216)	121.5(3)
C(214)-C(215)-H(215)	119.2
C(216)-C(215)-H(215)	119.2
C(211)-C(216)-C(215)	120.2(3)
C(211)-C(216)-H(216)	119.9
C(215)-C(216)-H(216)	119.9
C(214)-C(217)-H(21A)	109.5
C(214)-C(217)-H(21B)	109.5
H(21A)-C(217)-H(21B)	109.5
C(214)-C(217)-H(21C)	109.5
H(21A)-C(217)-H(21C)	109.5
H(21B)-C(217)-H(21C)	109.5
C(226)-C(221)-C(222)	118.8(3)
C(223)-C(222)-C(221)	119.8(3)
C(223)-C(222)-H(222)	120.1
C(221)-C(222)-H(222)	120.1
C(222)-C(223)-C(224)	122.0(3)
C(222)-C(223)-H(223)	119.0
C(224)-C(223)-H(223)	119.0
C(225)-C(224)-C(223)	117.1(3)
C(225)-C(224)-C(227)	121.6(3)
C(223)-C(224)-C(227)	121.3(3)
C(224)-C(225)-C(226)	121.5(3)
C(224)-C(225)-H(225)	119.3
C(226)-C(225)-H(225)	119.3
C(221)-C(226)-C(225)	120.8(3)
C(221)-C(226)-H(226)	119.6
C(225)-C(226)-H(226)	119.6
C(224)-C(227)-H(22A)	109.5
C(224)-C(227)-H(22B)	109.5
H(22A)-C(227)-H(22B)	109.5
C(224)-C(227)-H(22C)	109.5
H(22A)-C(227)-H(22C)	109.5
H(22B)-C(227)-H(22C)	109.5
C(236)-C(231)-C(232)	118.2(3)

C(233)-C(232)-C(231)	120.8(3)
C(233)-C(232)-H(232)	119.6
C(231)-C(232)-H(232)	119.6
C(232)-C(233)-C(234)	120.8(3)
C(232)-C(233)-H(233)	119.6
C(234)-C(233)-H(233)	119.6
C(235)-C(234)-C(233)	118.6(3)
C(235)-C(234)-C(237)	120.5(3)
C(233)-C(234)-C(237)	120.9(3)
C(234)-C(235)-C(236)	120.9(3)
C(234)-C(235)-H(235)	119.6
C(236)-C(235)-H(235)	119.6
C(235)-C(236)-C(231)	120.8(3)
C(235)-C(236)-H(236)	119.6
C(231)-C(236)-H(236)	119.6
C(234)-C(237)-H(23A)	109.5
C(234)-C(237)-H(23B)	109.5
H(23A)-C(237)-H(23B)	109.5
C(234)-C(237)-H(23C)	109.5
H(23A)-C(237)-H(23C)	109.5
H(23B)-C(237)-H(23C)	109.5
C(316)-C(311)-C(312)	118.8(3)
C(313)-C(312)-C(311)	120.8(3)
C(313)-C(312)-H(312)	119.6
C(311)-C(312)-H(312)	119.6
C(314)-C(313)-C(312)	121.2(3)
C(314)-C(313)-H(313)	119.4
C(312)-C(313)-H(313)	119.4
C(313)-C(314)-C(315)	117.7(3)
C(313)-C(314)-C(317)	120.6(4)
C(315)-C(314)-C(317)	121.7(4)
C(314)-C(315)-C(316)	121.6(4)
C(314)-C(315)-H(315)	119.2
C(316)-C(315)-H(315)	119.2
C(311)-C(316)-C(315)	119.9(3)
C(311)-C(316)-H(316)	120.1
C(315)-C(316)-H(316)	120.1

C(314)-C(317)-H(31A)	109.5
C(314)-C(317)-H(31B)	109.5
H(31A)-C(317)-H(31B)	109.5
C(314)-C(317)-H(31C)	109.5
H(31A)-C(317)-H(31C)	109.5
H(31B)-C(317)-H(31C)	109.5
C(412)-C(411)-C(416)	118.5(3)
C(411)-C(412)-C(413)	120.6(3)
C(411)-C(412)-H(412)	119.7
C(413)-C(412)-H(412)	119.7
C(414)-C(413)-C(412)	121.1(3)
C(414)-C(413)-H(413)	119.5
C(412)-C(413)-H(413)	119.5
C(413)-C(414)-C(415)	118.5(3)
C(413)-C(414)-C(417)	120.6(3)
C(415)-C(414)-C(417)	120.9(3)
C(414)-C(415)-C(416)	120.8(3)
C(414)-C(415)-H(415)	119.6
C(416)-C(415)-H(415)	119.6
C(415)-C(416)-C(411)	120.5(3)
C(415)-C(416)-H(416)	119.8
C(411)-C(416)-H(416)	119.8
C(414)-C(417)-H(41A)	109.5
C(414)-C(417)-H(41B)	109.5
H(41A)-C(417)-H(41B)	109.5
C(414)-C(417)-H(41C)	109.5
H(41A)-C(417)-H(41C)	109.5
H(41B)-C(417)-H(41C)	109.5
C(422)-C(421)-C(426)	117.9(3)
C(423)-C(422)-C(421)	120.2(3)
C(423)-C(422)-H(422)	119.9
C(421)-C(422)-H(422)	119.9
C(422)-C(423)-C(424)	121.7(3)
C(422)-C(423)-H(423)	119.2
C(424)-C(423)-H(423)	119.2
C(423)-C(424)-C(425)	118.2(3)
C(423)-C(424)-C(427)	122.2(3)

C(425)-C(424)-C(427)	119.5(3)
C(426)-C(425)-C(424)	120.3(3)
C(426)-C(425)-H(425)	119.9
C(424)-C(425)-H(425)	119.9
C(425)-C(426)-C(421)	121.7(3)
C(425)-C(426)-H(426)	119.2
C(421)-C(426)-H(426)	119.2
C(424)-C(427)-H(42A)	109.5
C(424)-C(427)-H(42B)	109.5
H(42A)-C(427)-H(42B)	109.5
C(424)-C(427)-H(42C)	109.5
H(42A)-C(427)-H(42C)	109.5
H(42B)-C(427)-H(42C)	109.5
C(436)-C(431)-C(432)	118.2(3)
C(433)-C(432)-C(431)	121.1(3)
C(433)-C(432)-H(432)	119.5
C(431)-C(432)-H(432)	119.5
C(434)-C(433)-C(432)	120.7(4)
C(434)-C(433)-H(433)	119.6
C(432)-C(433)-H(433)	119.6
C(435)-C(434)-C(433)	118.3(3)
C(435)-C(434)-C(437)	121.1(4)
C(433)-C(434)-C(437)	120.7(4)
C(434)-C(435)-C(436)	121.5(3)
C(434)-C(435)-H(435)	119.3
C(436)-C(435)-H(435)	119.3
C(431)-C(436)-C(435)	120.3(3)
C(431)-C(436)-H(436)	119.9
C(435)-C(436)-H(436)	119.9
C(434)-C(437)-H(43A)	109.5
C(434)-C(437)-H(43B)	109.5
H(43A)-C(437)-H(43B)	109.5
C(434)-C(437)-H(43C)	109.5
H(43A)-C(437)-H(43C)	109.5
H(43B)-C(437)-H(43C)	109.5

Appendix A

Symmetry transformations used to generate equivalent atoms:

#1 -y+1, z-1/2, -x+3/2 #2 -z+3/2, -x+1, y+1/2 #3 y, z, x #4 z, x, y #5 -z+1, x+1/2, -y+3/2

#6 y-1/2, -z+3/2, -x+1 #7 y+1/2, -z+3/2, -x+2 #8 -z+2, x-1/2, -y+3/2

Table A.3 Anisotropic displacement parameters (Å x 10^3) for $[Ag\{P(p\text{-}tol)_3\}_4]PF_6$. The anisotropic displacement factor exponent takes the form: $-2\pi^2[h^2a^{*2}U^{11} + ... + 2 h k a^* b^* U^{12}]$

	U11	U22	U33	U23	U13	U12
F(21)	66(2)	117(3)	50(2)	-19(2)	-22(2)	-15(2)
F(22)	81(2)	154(4)	95(3)	-5(3)	38(2)	-20(3)
P(02)	42(1)	42(1)	42(1)	2(1)	-2(1)	-2(1)
P(11)	20(1)	20(1)	20(1)	-3(1)	-3(1)	-3(1)
P(12)	15(1)	18(1)	23(1)	1(1)	1(1)	2(1)
P(23)	23(1)	23(1)	23(1)	5(1)	5(1)	-5(1)
P(24)	17(1)	19(1)	16(1)	-1(1)	-1(1)	0(1)
Ag(1)	16(1)	16(1)	16(1)	0(1)	0(1)	0(1)
Ag(2)	18(1)	18(1)	18(1)	1(1)	1(1)	-1(1)
P(01)	48(1)	48(1)	48(1)	-6(1)	-6(1)	6(1)
F(11A)	219(13)	131(10)	52(4)	22(4)	10(5)	16(7)
F(11B)	219(13)	131(10)	52(4)	22(4)	10(5)	16(7)
F(12)	95(3)	234(6)	112(4)	-14(4)	34(3)	62(4)
C(111)	24(1)	27(2)	22(1)	0(1)	-5(1)	-5(1)
C(112)	31(2)	43(2)	30(2)	-8(2)	-9(1)	-1(2)
C(113)	46(2)	66(3)	26(2)	-5(2)	-14(2)	-3(2)
C(114)	36(2)	44(2)	39(2)	5(2)	-17(2)	-5(2)
C(115)	27(2)	24(2)	40(2)	2(1)	-11(1)	-6(1)
C(116)	26(2)	24(2)	27(2)	3(1)	-6(1)	-4(1)
C(117)	55(3)	72(3)	50(3)	15(2)	-26(2)	8(2)
C(211)	23(2)	19(1)	21(2)	1(1)	3(1)	3(1)
C(212)	26(2)	27(2)	25(2)	1(1)	0(1)	4(1)
C(213)	38(2)	28(2)	31(2)	4(1)	-1(2)	9(2)
C(214)	46(2)	21(2)	33(2)	4(1)	10(2)	5(1)
C(215)	32(2)	22(2)	37(2)	-4(1)	4(1)	0(1)
C(216)	21(2)	26(2)	27(2)	-2(1)	1(1)	3(1)
C(217)	76(3)	26(2)	46(3)	10(2)	0(2)	-3(2)
C(221)	16(1)	18(1)	24(1)	1(1)	0(1)	3(1)

C(222)	22(2)	22(2)	28(2)	-3(1)	4(1)	5(1)
C(223)	16(1)	27(2)	33(2)	-2(1)	4(1)	-3(1)
C(224)	23(2)	21(2)	31(2)	-1(1)	-3(1)	1(1)
C(225)	24(2)	33(2)	27(2)	-5(1)	5(1)	3(1)
C(226)	18(1)	30(2)	29(2)	-3(1)	5(1)	-1(1)
C(227)	27(2)	44(2)	33(2)	-11(2)	-1(1)	-4(2)
C(231)	13(1)	23(1)	23(2)	1(1)	-3(1)	1(1)
C(232)	26(2)	25(2)	32(2)	3(1)	6(1)	3(1)
C(233)	31(2)	34(2)	31(2)	5(2)	3(1)	-1(2)
C(234)	21(2)	40(2)	26(2)	-7(1)	5(1)	-4(1)
C(235)	22(2)	32(2)	31(2)	-9(1)	1(1)	-1(1)
C(236)	19(1)	24(2)	25(2)	-3(1)	1(1)	-1(1)
C(237)	45(2)	58(3)	32(2)	-9(2)	13(2)	-4(2)
C(311)	26(2)	25(2)	23(2)	3(1)	4(1)	-5(1)
C(312)	27(2)	19(2)	28(2)	1(1)	6(1)	-5(1)
C(313)	28(2)	19(2)	35(2)	-3(1)	-1(1)	-2(1)
C(314)	47(2)	38(2)	30(2)	-4(2)	-7(2)	13(2)
C(315)	53(2)	68(3)	23(2)	8(2)	8(2)	24(2)
C(316)	34(2)	55(2)	28(2)	8(2)	10(2)	14(2)
C(317)	67(3)	76(3)	29(2)	-4(2)	-10(2)	30(3)
C(411)	23(2)	21(1)	17(1)	-2(1)	1(1)	2(1)
C(412)	29(2)	31(2)	24(2)	-6(1)	2(1)	-6(1)
C(413)	35(2)	41(2)	27(2)	-5(1)	11(1)	-8(2)
C(414)	48(2)	29(2)	23(2)	-7(1)	7(2)	-4(2)
C(415)	53(2)	29(2)	26(2)	-6(1)	3(2)	-18(2)
C(416)	35(2)	27(2)	20(2)	-2(1)	4(1)	-9(1)
C(417)	76(3)	45(2)	33(2)	-19(2)	21(2)	-18(2)
C(421)	17(1)	20(1)	18(1)	-2(1)	-1(1)	-1(1)
C(422)	21(1)	26(2)	24(2)	5(1)	-2(1)	3(1)
C(423)	19(2)	35(2)	36(2)	8(2)	-1(1)	-1(1)
C(424)	26(2)	31(2)	29(2)	6(1)	2(1)	-3(1)
C(425)	26(2)	27(2)	27(2)	6(1)	-2(1)	2(1)
C(426)	19(1)	26(2)	25(2)	1(1)	1(1)	1(1)
C(427)	33(2)	53(3)	74(3)	35(2)	4(2)	-6(2)
C(431)	18(1)	19(1)	23(1)	4(1)	0(1)	0(1)
C(432)	33(2)	26(2)	32(2)	0(1)	-4(1)	6(1)
C(433)	33(2)	27(2)	47(2)	-5(2)	-2(2)	7(1)

C(434)	26(2)	28(2)	57(2)	15(2)	-1(2)	3(1)
C(435)	25(2)	46(2)	37(2)	13(2)	-8(1)	4(2)
C(436)	21(2)	35(2)	26(2)	3(1)	-5(1)	1(1)
C(437)	40(2)	43(3)	79(3)	13(2)	0(2)	13(2)

Table A.4 Hydrogen coordinates (x 10^4) and isotropic displacement parameters ($Å^2$x 10^3) for [Ag{P(p-tol)$_3$}$_4$]PF_6.

	x	y	z	U(eq)
H(112)	8141	8011	9095	42
H(113)	8645	7501	9705	55
H(115)	9141	6527	8494	36
H(116)	8593	6998	7890	31
H(11A)	9686	6743	9479	88
H(11B)	9252	6261	9485	88
H(11C)	9210	6740	9919	88
H(212)	5743	8363	6430	31
H(213)	5829	9219	6039	39
H(215)	7120	9524	6987	37
H(216)	7039	8672	7382	30
H(21A)	6471	10289	6499	74
H(21B)	6276	10053	5927	74
H(21C)	6907	10059	6079	74
H(222)	5238	7347	7269	28
H(223)	4701	6892	6643	31
H(225)	5927	6900	5569	34
H(226)	6473	7334	6198	31
H(22A)	5108	6492	5303	52
H(22B)	4598	6829	5520	52
H(22C)	4743	6254	5783	52
H(232)	6045	7067	8112	33
H(233)	5599	7179	8932	38
H(235)	5406	8769	8612	34
H(236)	5857	8661	7793	27
H(23A)	5305	7788	9649	68
H(23B)	4786	8026	9342	68

H(23C)	5260	8424	9535	68
H(312)	2986	6524	8266	30
H(313)	3449	6190	9013	33
H(315)	2143	6470	9949	58
H(316)	1675	6812	9201	47
H(31A)	3200	5674	9984	86
H(31B)	2930	6124	10364	86
H(31C)	3493	6246	10067	86
H(412)	2681	7706	8876	34
H(413)	2507	8143	9690	41
H(415)	3709	9200	9384	43
H(416)	3887	8765	8568	33
H(41A)	2608	9161	10138	77
H(41B)	3240	9285	10209	77
H(41C)	2989	8736	10445	77
H(422)	4590	8049	7796	28
H(423)	5056	8698	7305	36
H(425)	3650	9414	6889	32
H(426)	3181	8748	7349	28
H(42A)	5074	9592	6881	80
H(42B)	4516	9909	6789	80
H(42C)	4715	9469	6356	80
H(432)	3859	6951	7434	36
H(433)	4440	6239	7631	43
H(435)	4578	6773	9160	43
H(436)	4011	7501	8962	33
H(43A)	5291	6032	8427	81
H(43B)	4786	5629	8376	81
H(43C)	4928	5899	8948	81

Table A.5 Hydrogen bonds for $[Ag\{P(p\text{-}tol)_3\}_4]PF_6$ (Å and °). Symmetry operations appear at the end of the table.

D-H...A	$d_{D\text{-}H}$	$d_{H\ldots A}$	$d_{D\ldots A}$	$<_{DHA}$
C(213)-H(213)...F(21)$^{\#9}$	0.95	2.54	3.439(4)	158.8

Appendix A

Symmetry transformations used to generate equivalent atoms:

#1 -y+1, z-1/2, -x+3/2 #2 -z+3/2, -x+1, y+1/2 #3 y, z, x #4 z, x, y #5 -z+1, x+1/2, -y+3/2

#6 y-1/2, -z+3/2, -x+1 #7 y+1/2, -z+3/2, -x+2 #8 -z+2, x-1/2, -y+3/2 #9 -x+1, y+1/2, -z+3/2

B Appendix - $[Ag\{P(p\text{-}tol)_3\}_3]ClO_4 \cdot CH_3COCH_3$

Table B.1 Atomic coordinates (x 10^4) and equivalent isotropic displacement parameters ($Å^2$x 10^3) for $[Ag\{P(p\text{-}tol)_3\}]ClO_4 \cdot CH_3COCH_3$. U(eq) is defined as one third of the trace of the orthogonalized U^{ij} tensor.

	x	y	z	U(eq)
Ag(1)	7707(1)	1285(1)	8087(1)	17(1)
Cl(1)	6112(1)	1370(1)	2740(1)	53(1)
P(1)	6833(1)	1936(1)	7527(1)	19(1)
P(2)	8877(1)	1576(1)	8417(1)	18(1)
P(3)	7338(1)	361(1)	7971(1)	16(1)
O(002)	8647(2)	903(2)	2722(3)	47(1)
O(1A)	6700(300)	1300(200)	3500(400)	104(3)
O(1B)	6700(300)	1300(200)	3500(400)	104(3)
O(2)	5987(4)	1916(2)	3033(6)	100(2)
O(3A)	5371(6)	1285(4)	3144(13)	81(3)
O(3B)	5743(7)	933(5)	2919(11)	81(3)
O(4A)	6389(7)	1377(6)	1553(14)	44(3)
O(4B)	6054(9)	1409(8)	1577(17)	71(5)
C(001)	7852(4)	804(4)	1253(6)	66(2)
C(002)	8220(3)	1117(3)	2149(5)	44(2)
C(003)	8067(4)	1687(3)	2268(7)	65(2)
C(111)	6646(2)	2416(2)	8646(4)	19(1)
C(112)	6662(2)	2246(2)	9773(4)	25(1)
C(113)	6517(2)	2591(2)	10662(4)	23(1)
C(114)	6360(2)	3117(2)	10450(4)	19(1)
C(115)	6344(2)	3286(2)	9305(4)	22(1)
C(116)	6484(2)	2942(2)	8414(4)	21(1)

C(117)	6187(3)	3491(2)	11411(5)	31(1)
C(121)	6019(2)	1652(2)	7149(4)	22(1)
C(122)	5476(2)	1681(2)	7902(4)	23(1)
C(123)	4873(2)	1430(2)	7640(5)	27(1)
C(124)	4798(2)	1151(2)	6627(5)	28(1)
C(125)	5335(2)	1124(2)	5870(5)	27(1)
C(126)	5950(2)	1365(2)	6139(4)	25(1)
C(127)	4145(3)	870(2)	6347(6)	39(1)
C(131)	7124(2)	2329(2)	6313(4)	22(1)
C(132)	6778(3)	2389(2)	5289(5)	29(1)
C(133)	7069(3)	2665(2)	4380(5)	36(1)
C(134)	7700(3)	2884(2)	4483(5)	35(1)
C(135)	8034(3)	2833(2)	5512(5)	33(1)
C(136)	7756(2)	2557(2)	6417(5)	27(1)
C(137)	8016(3)	3176(2)	3481(5)	47(2)
C(211)	8994(2)	2139(2)	9350(4)	19(1)
C(212)	9615(2)	2278(2)	9833(4)	23(1)
C(213)	9674(2)	2730(2)	10498(4)	25(1)
C(214)	9123(3)	3066(2)	10684(4)	29(1)
C(215)	8507(2)	2921(2)	10210(5)	28(1)
C(216)	8439(2)	2468(2)	9565(4)	24(1)
C(217)	9204(3)	3563(2)	11366(6)	42(2)
C(221)	9493(2)	1094(2)	8928(4)	18(1)
C(222)	9514(2)	972(2)	10087(4)	26(1)
C(223)	9937(2)	576(2)	10485(4)	26(1)
C(224)	10344(2)	294(2)	9738(4)	23(1)
C(225)	10329(2)	419(2)	8593(4)	23(1)
C(226)	9905(2)	814(1)	8179(5)	20(1)
C(227)	10801(2)	-135(2)	10192(5)	33(1)
C(231)	9185(2)	1781(2)	7016(4)	19(1)
C(232)	8964(2)	1499(2)	6058(4)	23(1)
C(233)	9176(2)	1640(2)	4972(4)	27(1)
C(234)	9593(3)	2069(2)	4804(4)	29(1)
C(235)	9804(2)	2353(2)	5764(5)	26(1)
C(236)	9609(2)	2202(2)	6855(4)	24(1)
C(237)	9812(3)	2220(3)	3621(5)	46(2)

C(311)	7806(2)	-119(2)	8817(4)	16(1)
C(312)	8499(2)	-140(2)	8677(4)	23(1)
C(313)	8877(2)	-505(2)	9280(5)	26(1)
C(314)	8576(2)	-851(2)	10051(4)	22(1)
C(315)	7883(2)	-827(2)	10187(4)	23(1)
C(316)	7493(3)	-465(2)	9583(4)	19(1)
C(317)	8986(3)	-1237(2)	10733(5)	34(1)
C(321)	7400(2)	97(2)	6531(4)	19(1)
C(322)	7371(2)	438(2)	5593(4)	24(1)
C(323)	7399(2)	244(2)	4486(5)	30(1)
C(324)	7476(2)	-291(2)	4276(4)	30(1)
C(325)	7507(2)	-629(2)	5202(5)	29(1)
C(326)	7468(3)	-444(2)	6323(4)	23(1)
C(327)	7528(3)	-497(3)	3074(6)	45(1)
C(331)	6463(2)	277(2)	8388(4)	18(1)
C(332)	6238(2)	543(2)	9358(4)	22(1)
C(333)	5571(2)	492(2)	9703(4)	27(1)
C(334)	5115(2)	188(2)	9086(4)	24(1)
C(335)	5346(2)	-77(2)	8126(5)	27(1)
C(336)	6021(2)	-37(2)	7784(4)	24(1)
C(337)	4383(2)	163(2)	9428(5)	37(1)

Table B.2 Bond lengths (Å) and angles (°) for $[Ag\{P(p\text{-}tol)_3\}]ClO_4 \cdot CH_3COCH_3$.

Atoms	Distance (Å)
Ag(1)-P(1)	2.485(1)
Ag(1)-P(2)	2.468(1)
Ag(1)-P(3)	2.461(1)
Cl(1)-O(1A)	1.4(5)
Cl(1)-O(1B)	1.4(5)
Cl(1)-O(2)	1.450(6)
Cl(1)-O(3A)	1.56(1)
Cl(1)-O(3B)	1.345(9)
Cl(1)-O(4A)	1.49(2)
Cl(1)-O(4B)	1.37(2)

P(1)-C(111)	1.825(5)
P(1)-C(121)	1.824(5)
P(1)-C(131)	1.827(5)
P(2)-C(211)	1.812(4)
P(2)-C(221)	1.831(4)
P(2)-C(231)	1.823(5)
P(3)-C(311)	1.825(4)
P(3)-C(321)	1.817(5)
P(3)-C(331)	1.817(4)
C(001)-C(002)	1.504(9)
C(001)-H(00A)	0.9800
C(001)-H(00B)	0.9800
C(001)-H(00C)	0.9800
C(002)-O(002)	1.209(8)
C(002)-C(003)	1.49(1)
C(003)-H(00D)	0.9800
C(003)-H(00E)	0.9800
C(003)-H(00F)	0.9800
C(232)-C(233)	1.383(7)
C(232)-C(231)	1.398(6)
C(232)-H(232)	0.9500
C(231)-C(236)	1.375(6)
C(236)-C(235)	1.386(7)
C(236)-H(236)	0.9500
C(237)-C(234)	1.499(7)
C(237)-H(23A)	0.9800
C(237)-H(23B)	0.9800
C(237)-H(23C)	0.9800
C(237)-H(23D)	0.9800
C(237)-H(23E)	0.9800
C(237)-H(23F)	0.9800
C(233)-C(234)	1.380(7)
C(233)-H(233)	0.9500
C(235)-C(234)	1.398(7)
C(235)-H(235)	0.9500
C(111)-C(112)	1.386(6)

C(111)-C(116)	1.399(6)
C(112)-C(113)	1.389(7)
C(112)-H(112)	0.9500
C(113)-C(114)	1.393(6)
C(113)-H(113)	0.9500
C(114)-C(115)	1.405(6)
C(114)-C(117)	1.509(7)
C(115)-C(116)	1.387(6)
C(115)-H(115)	0.9500
C(116)-H(116)	0.9500
C(117)-H(11A)	0.9800
C(117)-H(11B)	0.9800
C(117)-H(11C)	0.9800
C(121)-C(126)	1.393(7)
C(121)-C(122)	1.394(6)
C(122)-C(123)	1.391(6)
C(122)-H(122)	0.9500
C(123)-C(124)	1.388(8)
C(123)-H(123)	0.9500
C(124)-C(125)	1.387(7)
C(124)-C(127)	1.515(7)
C(125)-C(126)	1.401(7)
C(125)-H(125)	0.9500
C(126)-H(126)	0.9500
C(127)-H(12A)	0.9800
C(127)-H(12B)	0.9800
C(127)-H(12C)	0.9800
C(131)-C(132)	1.388(7)
C(131)-C(136)	1.389(7)
C(132)-C(133)	1.399(7)
C(132)-H(132)	0.9500
C(133)-C(134)	1.376(8)
C(133)-H(133)	0.9500
C(134)-C(135)	1.380(9)
C(134)-C(137)	1.520(7)
C(135)-C(136)	1.383(7)

C(135)-H(135)	0.9500
C(136)-H(136)	0.9500
C(137)-H(13A)	0.9800
C(137)-H(13B)	0.9800
C(137)-H(13C)	0.9800
C(211)-C(212)	1.402(6)
C(211)-C(216)	1.405(6)
C(212)-C(213)	1.390(6)
C(212)-H(212)	0.9500
C(213)-C(214)	1.403(7)
C(213)-H(213)	0.9500
C(214)-C(215)	1.393(7)
C(214)-C(217)	1.500(7)
C(215)-C(216)	1.381(7)
C(215)-H(215)	0.9500
C(216)-H(216)	0.9500
C(217)-H(21A)	0.9800
C(217)-H(21B)	0.9800
C(217)-H(21C)	0.9800
C(221)-C(222)	1.390(7)
C(221)-C(226)	1.394(6)
C(222)-C(223)	1.391(6)
C(222)-H(222)	0.9500
C(223)-C(224)	1.389(7)
C(223)-H(223)	0.9500
C(224)-C(225)	1.375(7)
C(224)-C(227)	1.513(6)
C(225)-C(226)	1.395(6)
C(225)-H(225)	0.9500
C(226)-H(226)	0.9500
C(227)-H(22A)	0.9800
C(227)-H(22B)	0.9800
C(227)-H(22C)	0.9800
C(311)-C(312)	1.388(6)
C(311)-C(316)	1.399(6)
C(312)-C(313)	1.385(6)

C(312)-H(312)	0.9500
C(313)-C(314)	1.392(7)
C(313)-H(313)	0.9500
C(314)-C(315)	1.387(6)
C(314)-C(317)	1.501(6)
C(315)-C(316)	1.393(6)
C(315)-H(315)	0.9500
C(316)-H(316)	0.9500
C(317)-H(31A)	0.9800
C(317)-H(31B)	0.9800
C(317)-H(31C)	0.9800
C(317)-H(31D)	0.9800
C(317)-H(31E)	0.9800
C(317)-H(31F)	0.9800
C(321)-C(322)	1.398(6)
C(321)-C(326)	1.399(7)
C(322)-C(323)	1.386(7)
C(322)-H(322)	0.9500
C(323)-C(324)	1.386(8)
C(323)-H(323)	0.9500
C(324)-C(325)	1.383(8)
C(324)-C(327)	1.502(8)
C(325)-C(326)	1.395(7)
C(325)-H(325)	0.9500
C(326)-H(326)	0.9500
C(327)-H(32A)	0.9800
C(327)-H(32B)	0.9800
C(327)-H(32C)	0.9800
C(331)-C(336)	1.380(6)
C(331)-C(332)	1.393(6)
C(332)-C(333)	1.390(6)
C(332)-H(332)	0.9500
C(333)-C(334)	1.391(7)
C(333)-H(333)	0.9500
C(334)-C(335)	1.386(7)
C(334)-C(337)	1.510(6)

C(335)-C(336)	1.403(6)
C(335)-H(335)	0.9500
C(336)-H(336)	0.9500
C(337)-H(33A)	0.9800
C(337)-H(33B)	0.9800
C(337)-H(33C)	0.9800

Atoms	Angles (º)
Ag(1)-P(1)-C(111)	113.4(1)
Ag(1)-P(1)-C(121)	114.9(1)
Ag(1)-P(1)-C(131)	110.3(1)
Ag(1)-P(1)-C(211)	116.8(2)
Ag(1)-P(1)-C(221)	118.7(1)
Ag(1)-P(1)-C(231)	105.1(1)
Ag(1)-P(1)-C(311)	117.1(1)
Ag(1)-P(1)-C(321)	112.5(2)
Ag(1)-P(1)-C(331)	112.5(1)
P(1)-Ag(1)-P(2)	120.01(4)
P(1)-Ag(1)-P(3)	114.25(4)
P(2)-Ag(1)-P(3)	125.06(3)
C(111)-P(1)-C(121)	104.9(2)
C(111)-P(1)-C(131)	104.9(2)
C(121)-P(1)-C(131)	107.9(2)
C(211)-P(2)-C(221)	104.2(2)
C(211)-P(2)-C(231)	105.9(2)
C(221)-P(2)-C(231)	105.0(2)
C(311)-P(3)-C(321)	102.7(2)
C(311)-P(3)-C(331)	105.3(2)
C(321)-P(3)-C(331)	105.7(2)
O(1A)-Cl(1)-O(1B)	0(10)
O(1A)-Cl(1)-O(2)	100(10)
O(1A)-Cl(1)-O(3A)	123(10)
O(1A)-Cl(1)-O(3B)	101(10)
O(1A)-Cl(1)-O(4B)	131(10)
O(1A)-Cl(1)-O(4A)	105(10)

O(1B)-Cl(1)-O(2)	100(10)
O(1B)-Cl(1)-O(3A)	123(10)
O(1B)-Cl(1)-O(3B)	101(10)
O(1B)-Cl(1)-O(4A)	105(10)
O(1B)-Cl(1)-O(4B)	131(10)
O(2)-Cl(1)-O(3A)	84.1(6)
O(2)-Cl(1)-O(3B)	131.1(8)
O(2)-Cl(1)-O(4A)	105.7(7)
O(2)-Cl(1)-O(4B)	98.6(9)
O(3A)-Cl(1)-O(3B)	47.6(6)
O(3A)-Cl(1)-O(4B)	103.3(9)
O(3A)-Cl(1)-O(4A)	129.1(8)
O(3B)-Cl(1)-O(4A)	110.8(9)
O(3B)-Cl(1)-O(4B)	99.7(10)
O(4A)-Cl(1)-O(4B)	26.7(8)
P(1)-C(111)-C(112)	118.0(3)
P(1)-C(111)-C(116)	123.0(3)
P(1)-C(121)-C(122)	120.8(4)
P(1)-C(121)-C(126)	119.9(4)
P(1)-C(131)-C(132)	124.9(4)
P(1)-C(131)-C(136)	116.5(4)
P(2)-C(211)-C(212)	123.6(3)
P(2)-C(211)-C(216)	118.4(3)
P(2)-C(221)-C(222)	119.1(3)
P(2)-C(221)-C(226)	121.9(4)
P(2)-C(231)-C(232)	118.0(3)
P(2)-C(231)-C(236)	123.4(4)
P(3)-C(311)-C(312)	117.9(3)
P(3)-C(311)-C(316)	122.7(3)
P(3)-C(321)-C(322)	119.6(4)
P(3)-C(321)-C(326)	122.0(4)
P(3)-C(331)-C(332)	117.9(3)
P(3)-C(331)-C(336)	122.6(3)
C(002)-C(001)-H(00A)	109.5
C(002)-C(001)-H(00B)	109.5
H(00A)-C(001)-H(00B)	109.5

C(002)-C(001)-H(00C)	109.5
H(00A)-C(001)-H(00C)	109.5
H(00B)-C(001)-H(00C)	109.5
O(002)-C(002)-C(003)	122.0(6)
O(002)-C(002)-C(001)	119.3(7)
C(003)-C(002)-C(001)	118.7(7)
C(002)-C(003)-H(00D)	109.5
C(002)-C(003)-H(00E)	109.5
H(00D)-C(003)-H(00E)	109.5
C(002)-C(003)-H(00F)	109.5
H(00D)-C(003)-H(00F)	109.5
H(00E)-C(003)-H(00F)	109.5
C(233)-C(232)-C(231)	120.5(4)
C(233)-C(232)-H(232)	119.8
C(231)-C(232)-H(232)	119.8
C(236)-C(231)-C(232)	118.7(4)
C(231)-C(236)-C(235)	120.8(4)
C(231)-C(236)-H(236)	119.6
C(235)-C(236)-H(236)	119.6
C(234)-C(237)-H(23A)	109.5
C(234)-C(237)-H(23B)	109.5
H(23A)-C(237)-H(23B)	109.5
C(234)-C(237)-H(23C)	109.5
H(23A)-C(237)-H(23C)	109.5
H(23B)-C(237)-H(23C)	109.5
C(234)-C(237)-H(23D)	109.5
H(23A)-C(237)-H(23D)	141.1
H(23B)-C(237)-H(23D)	56.3
H(23C)-C(237)-H(23D)	56.3
C(234)-C(237)-H(23E)	109.5
H(23A)-C(237)-H(23E)	56.3
H(23B)-C(237)-H(23E)	141.1
H(23C)-C(237)-H(23E)	56.3
H(23D)-C(237)-H(23E)	109.5
C(234)-C(237)-H(23F)	109.5
H(23A)-C(237)-H(23F)	56.3

H(23B)-C(237)-H(23F)	56.3
H(23C)-C(237)-H(23F)	141.1
H(23D)-C(237)-H(23F)	109.5
H(23E)-C(237)-H(23F)	109.5
C(234)-C(233)-C(232)	121.1(5)
C(234)-C(233)-H(233)	119.5
C(232)-C(233)-H(233)	119.5
C(236)-C(235)-C(234)	120.8(4)
C(236)-C(235)-H(235)	119.6
C(234)-C(235)-H(235)	119.6
C(233)-C(234)-C(235)	118.2(5)
C(233)-C(234)-C(237)	120.5(5)
C(235)-C(234)-C(237)	121.3(5)
C(112)-C(111)-C(116)	119.0(4)
C(111)-C(112)-C(113)	120.7(4)
C(111)-C(112)-H(112)	119.7
C(113)-C(112)-H(112)	119.7
C(112)-C(113)-C(114)	121.1(4)
C(112)-C(113)-H(113)	119.4
C(114)-C(113)-H(113)	119.4
C(113)-C(114)-C(115)	117.8(4)
C(113)-C(114)-C(117)	121.3(4)
C(115)-C(114)-C(117)	120.8(4)
C(116)-C(115)-C(114)	121.2(4)
C(116)-C(115)-H(115)	119.4
C(114)-C(115)-H(115)	119.4
C(115)-C(116)-C(111)	120.1(4)
C(115)-C(116)-H(116)	119.9
C(111)-C(116)-H(116)	119.9
C(114)-C(117)-H(11A)	109.5
C(114)-C(117)-H(11B)	109.5
H(11A)-C(117)-H(11B)	109.5
C(114)-C(117)-H(11C)	109.5
H(11A)-C(117)-H(11C)	109.5
H(11B)-C(117)-H(11C)	109.5
C(126)-C(121)-C(122)	119.1(4)

C(123)-C(122)-C(121)	120.2(4)
C(123)-C(122)-H(122)	119.9
C(121)-C(122)-H(122)	119.9
C(124)-C(123)-C(122)	120.9(5)
C(124)-C(123)-H(123)	119.5
C(122)-C(123)-H(123)	119.5
C(125)-C(124)-C(123)	119.1(4)
C(125)-C(124)-C(127)	119.8(5)
C(123)-C(124)-C(127)	121.1(5)
C(124)-C(125)-C(126)	120.4(5)
C(124)-C(125)-H(125)	119.8
C(126)-C(125)-H(125)	119.8
C(121)-C(126)-C(125)	120.3(4)
C(121)-C(126)-H(126)	119.9
C(125)-C(126)-H(126)	119.9
C(124)-C(127)-H(12A)	109.5
C(124)-C(127)-H(12B)	109.5
H(12A)-C(127)-H(12B)	109.5
C(124)-C(127)-H(12C)	109.5
H(12A)-C(127)-H(12C)	109.5
H(12B)-C(127)-H(12C)	109.5
C(132)-C(131)-C(136)	118.5(4)
C(131)-C(132)-C(133)	120.3(5)
C(131)-C(132)-H(132)	119.8
C(133)-C(132)-H(132)	119.8
C(134)-C(133)-C(132)	120.9(5)
C(134)-C(133)-H(133)	119.6
C(132)-C(133)-H(133)	119.6
C(133)-C(134)-C(135)	118.4(5)
C(133)-C(134)-C(137)	120.3(6)
C(135)-C(134)-C(137)	121.2(5)
C(134)-C(135)-C(136)	121.5(5)
C(134)-C(135)-H(135)	119.3
C(136)-C(135)-H(135)	119.3
C(135)-C(136)-C(131)	120.3(5)
C(135)-C(136)-H(136)	119.8

C(131)-C(136)-H(136)	119.8
C(134)-C(137)-H(13A)	109.5
C(134)-C(137)-H(13B)	109.5
H(13A)-C(137)-H(13B)	109.5
C(134)-C(137)-H(13C)	109.5
H(13A)-C(137)-H(13C)	109.5
H(13B)-C(137)-H(13C)	109.5
C(212)-C(211)-C(216)	117.9(4)
C(213)-C(212)-C(211)	120.5(4)
C(213)-C(212)-H(212)	119.7
C(211)-C(212)-H(212)	119.7
C(212)-C(213)-C(214)	121.4(5)
C(212)-C(213)-H(213)	119.3
C(214)-C(213)-H(213)	119.3
C(215)-C(214)-C(213)	117.6(4)
C(215)-C(214)-C(217)	121.8(5)
C(213)-C(214)-C(217)	120.6(5)
C(216)-C(215)-C(214)	121.5(4)
C(216)-C(215)-H(215)	119.2
C(214)-C(215)-H(215)	119.2
C(215)-C(216)-C(211)	121.0(4)
C(215)-C(216)-H(216)	119.5
C(211)-C(216)-H(216)	119.5
C(214)-C(217)-H(21A)	109.5
C(214)-C(217)-H(21B)	109.5
H(21A)-C(217)-H(21B)	109.5
C(214)-C(217)-H(21C)	109.5
H(21A)-C(217)-H(21C)	109.5
H(21B)-C(217)-H(21C)	109.5
C(222)-C(221)-C(226)	118.8(4)
C(221)-C(222)-C(223)	120.3(4)
C(221)-C(222)-H(222)	119.9
C(223)-C(222)-H(222)	119.9
C(224)-C(223)-C(222)	121.0(4)
C(224)-C(223)-H(223)	119.5
C(222)-C(223)-H(223)	119.5

C(225)-C(224)-C(223)	118.7(4)
C(225)-C(224)-C(227)	121.3(5)
C(223)-C(224)-C(227)	119.9(5)
C(224)-C(225)-C(226)	121.0(4)
C(224)-C(225)-H(225)	119.5
C(226)-C(225)-H(225)	119.5
C(221)-C(226)-C(225)	120.2(5)
C(221)-C(226)-H(226)	119.9
C(225)-C(226)-H(226)	119.9
C(224)-C(227)-H(22A)	109.5
C(224)-C(227)-H(22B)	109.5
H(22A)-C(227)-H(22B)	109.5
C(224)-C(227)-H(22C)	109.5
H(22A)-C(227)-H(22C)	109.5
H(22B)-C(227)-H(22C)	109.5
C(312)-C(311)-C(316)	119.4(4)
C(313)-C(312)-C(311)	120.2(4)
C(313)-C(312)-H(312)	119.9
C(311)-C(312)-H(312)	119.9
C(312)-C(313)-C(314)	121.2(4)
C(312)-C(313)-H(313)	119.4
C(314)-C(313)-H(313)	119.4
C(315)-C(314)-C(313)	118.1(4)
C(315)-C(314)-C(317)	120.4(4)
C(313)-C(314)-C(317)	121.4(4)
C(314)-C(315)-C(316)	121.6(4)
C(314)-C(315)-H(315)	119.2
C(316)-C(315)-H(315)	119.2
C(315)-C(316)-C(311)	119.4(4)
C(315)-C(316)-H(316)	120.3
C(311)-C(316)-H(316)	120.3
C(314)-C(317)-H(31A)	109.5
C(314)-C(317)-H(31B)	109.5
H(31A)-C(317)-H(31B)	109.5
C(314)-C(317)-H(31C)	109.5
H(31A)-C(317)-H(31C)	109.5

H(31B)-C(317)-H(31C)	109.5
C(314)-C(317)-H(31D)	109.5
H(31A)-C(317)-H(31D)	141.1
H(31B)-C(317)-H(31D)	56.3
H(31C)-C(317)-H(31D)	56.3
C(314)-C(317)-H(31E)	109.5
H(31A)-C(317)-H(31E)	56.3
H(31B)-C(317)-H(31E)	141.1
H(31C)-C(317)-H(31E)	56.3
H(31D)-C(317)-H(31E)	109.5
C(314)-C(317)-H(31F)	109.5
H(31A)-C(317)-H(31F)	56.3
H(31B)-C(317)-H(31F)	56.3
H(31C)-C(317)-H(31F)	141.1
H(31D)-C(317)-H(31F)	109.5
H(31E)-C(317)-H(31F)	109.5
C(322)-C(321)-C(326)	118.4(4)
C(323)-C(322)-C(321)	120.6(5)
C(323)-C(322)-H(322)	119.7
C(321)-C(322)-H(322)	119.7
C(324)-C(323)-C(322)	121.2(5)
C(324)-C(323)-H(323)	119.4
C(322)-C(323)-H(323)	119.4
C(325)-C(324)-C(323)	118.3(5)
C(325)-C(324)-C(327)	120.8(5)
C(323)-C(324)-C(327)	120.9(5)
C(324)-C(325)-C(326)	121.5(5)
C(324)-C(325)-H(325)	119.2
C(326)-C(325)-H(325)	119.2
C(325)-C(326)-C(321)	120.0(5)
C(325)-C(326)-H(326)	120.0
C(321)-C(326)-H(326)	120.0
C(324)-C(327)-H(32A)	109.5
C(324)-C(327)-H(32B)	109.5
H(32A)-C(327)-H(32B)	109.5
C(324)-C(327)-H(32C)	109.5

H(32A)-C(327)-H(32C)	109.5
H(32B)-C(327)-H(32C)	109.5
C(336)-C(331)-C(332)	119.5(4)
C(333)-C(332)-C(331)	119.8(4)
C(333)-C(332)-H(332)	120.1
C(331)-C(332)-H(332)	120.1
C(332)-C(333)-C(334)	121.4(4)
C(332)-C(333)-H(333)	119.3
C(334)-C(333)-H(333)	119.3
C(335)-C(334)-C(333)	118.2(4)
C(335)-C(334)-C(337)	120.8(5)
C(333)-C(334)-C(337)	120.9(5)
C(334)-C(335)-C(336)	120.8(4)
C(334)-C(335)-H(335)	119.6
C(336)-C(335)-H(335)	119.6
C(331)-C(336)-C(335)	120.2(4)
C(331)-C(336)-H(336)	119.9
C(335)-C(336)-H(336)	119.9
C(334)-C(337)-H(33A)	109.5
C(334)-C(337)-H(33B)	109.5
H(33A)-C(337)-H(33B)	109.5
C(334)-C(337)-H(33C)	109.5
H(33A)-C(337)-H(33C)	109.5
H(33B)-C(337)-H(33C)	109.5

Table B.3 Anisotropic displacement parameters ($Å^2$ x 10^3) for $[Ag\{P(p\text{-}tol)_3\}]ClO_4.CH_3COCH_3$. The anisotropic displacement factor exponent takes the form: $-2\pi^2[h^2a^{*2}U^{11} + ... + 2\ h\ k\ a^*\ b^*\ U^{12}]$

	U^{11}	U^{22}	U^{33}	U^{23}	U^{13}	U^{12}
Ag(1)	16(1)	13(1)	22(1)	2(1)	-1(1)	1(1)
Cl(1)	75(1)	61(1)	23(1)	8(1)	-5(1)	-20(1)
P(1)	17(1)	16(1)	24(1)	4(1)	0(1)	4(1)
P(2)	16(1)	16(1)	21(1)	0(1)	-1(1)	1(1)
P(3)	16(1)	13(1)	19(1)	0(1)	1(1)	0(1)
O(002)	61(3)	51(3)	30(2)	-6(2)	-7(2)	-8(2)

Appendix B

O(1A)	129(6)	140(8)	42(4)	12(4)	2(4)	84(5)
O(1B)	129(6)	140(8)	42(4)	12(4)	2(4)	84(5)
O(2)	176(6)	65(3)	59(4)	-2(3)	27(5)	45(4)
O(3A)	110(8)	81(6)	54(5)	35(6)	-21(6)	-62(5)
O(3B)	110(8)	81(6)	54(5)	35(6)	-21(6)	-62(5)
O(4A)	70(9)	41(6)	22(5)	3(4)	12(7)	-9(6)
O(4B)	116(15)	67(8)	31(6)	8(5)	22(11)	10(11)
C(001)	63(4)	103(7)	31(3)	-7(4)	-2(3)	-47(4)
C(002)	52(4)	60(4)	21(3)	6(3)	-1(3)	-24(3)
C(003)	77(5)	49(4)	71(5)	15(4)	-36(4)	-22(4)
C(232)	20(2)	22(2)	27(2)	-2(2)	-4(2)	0(2)
C(231)	18(2)	17(2)	20(2)	1(2)	-2(2)	2(2)
C(236)	23(2)	22(2)	27(2)	-4(2)	-2(2)	0(2)
C(237)	52(4)	57(4)	29(3)	3(3)	12(3)	1(3)
C(233)	27(2)	30(2)	24(2)	-6(2)	-2(2)	3(2)
C(235)	21(2)	27(2)	30(3)	1(2)	2(2)	-2(2)
C(234)	27(2)	36(3)	23(2)	0(2)	7(2)	6(2)
C(111)	16(2)	20(2)	22(2)	5(2)	1(2)	2(2)
C(112)	25(2)	22(2)	28(2)	8(2)	-3(2)	2(2)
C(113)	25(2)	25(2)	19(2)	8(2)	-3(2)	1(2)
C(114)	15(2)	21(2)	22(2)	1(2)	0(2)	-3(2)
C(115)	23(2)	19(2)	26(2)	4(2)	-3(2)	2(2)
C(116)	23(2)	17(2)	22(2)	7(2)	1(2)	2(2)
C(117)	35(3)	30(3)	28(3)	-5(2)	0(2)	-1(2)
C(121)	19(2)	18(2)	28(2)	4(2)	-2(2)	6(2)
C(122)	25(2)	20(2)	25(3)	4(2)	1(2)	2(2)
C(123)	25(2)	23(2)	34(3)	3(2)	4(2)	-1(2)
C(124)	24(2)	21(2)	38(3)	6(2)	-4(2)	0(2)
C(125)	22(2)	25(2)	35(3)	-2(2)	0(2)	4(2)
C(126)	24(2)	23(2)	27(2)	1(2)	2(2)	3(2)
C(127)	28(3)	33(3)	56(4)	-2(3)	-1(3)	-10(2)
C(131)	20(2)	20(2)	25(2)	4(2)	8(2)	8(2)
C(132)	29(3)	30(3)	28(3)	6(2)	6(2)	4(2)
C(133)	42(3)	37(3)	28(3)	7(2)	5(2)	3(2)
C(134)	40(3)	25(2)	39(3)	7(2)	17(2)	10(2)
C(135)	27(3)	24(2)	47(3)	10(2)	11(2)	1(2)

C(136)	26(2)	22(2)	34(3)	9(2)	2(2)	4(2)
C(137)	58(4)	44(3)	39(3)	15(3)	25(3)	4(3)
C(211)	24(2)	18(2)	17(2)	-2(2)	3(2)	0(2)
C(212)	22(2)	21(2)	25(2)	-2(2)	-1(2)	2(2)
C(213)	26(2)	26(2)	24(2)	-6(2)	6(2)	-4(2)
C(214)	40(3)	19(2)	26(2)	-7(2)	15(2)	-6(2)
C(215)	32(3)	17(2)	35(3)	-1(2)	11(2)	8(2)
C(216)	22(2)	20(2)	32(3)	0(2)	2(2)	3(2)
C(217)	54(3)	23(2)	49(4)	-14(2)	29(3)	-12(2)
C(221)	15(2)	15(2)	24(2)	-1(2)	-3(2)	3(2)
C(222)	26(2)	27(2)	24(2)	0(2)	1(2)	5(2)
C(223)	27(2)	30(3)	21(2)	3(2)	-3(2)	2(2)
C(224)	16(2)	15(2)	37(3)	4(2)	-6(2)	-2(2)
C(225)	18(2)	18(2)	32(2)	-5(2)	1(2)	2(2)
C(226)	18(2)	19(2)	22(2)	0(2)	-2(2)	-1(1)
C(227)	24(2)	26(2)	49(3)	11(2)	-5(2)	2(2)
C(311)	17(2)	11(2)	20(2)	-1(2)	-1(2)	0(1)
C(312)	24(2)	18(2)	27(2)	7(2)	2(2)	1(2)
C(313)	16(2)	20(2)	42(3)	5(2)	-6(2)	2(2)
C(314)	24(2)	16(2)	25(2)	-2(2)	-7(2)	3(2)
C(315)	30(2)	19(2)	21(2)	4(2)	2(2)	-4(2)
C(316)	20(2)	18(2)	18(2)	1(2)	0(2)	-3(2)
C(317)	35(3)	24(2)	42(3)	7(2)	-12(2)	1(2)
C(321)	14(2)	21(2)	22(2)	0(2)	2(2)	-2(2)
C(322)	20(2)	26(2)	25(2)	8(2)	1(2)	3(2)
C(323)	19(2)	45(3)	25(2)	6(2)	-1(2)	2(2)
C(324)	19(2)	47(3)	22(2)	-7(2)	1(2)	2(2)
C(325)	26(2)	32(3)	29(3)	-12(2)	3(2)	0(2)
C(326)	22(2)	24(2)	22(2)	2(2)	3(2)	-2(2)
C(327)	37(3)	72(4)	25(2)	-14(3)	4(3)	1(2)
C(331)	20(2)	15(2)	19(2)	2(2)	2(2)	0(1)
C(332)	19(2)	19(2)	28(2)	-4(2)	2(2)	2(2)
C(333)	31(2)	24(2)	25(2)	-4(2)	8(2)	5(2)
C(334)	19(2)	22(2)	30(3)	5(2)	6(2)	5(2)
C(335)	18(2)	32(2)	32(2)	-2(3)	1(2)	-2(2)
C(336)	22(2)	27(2)	22(2)	-8(2)	2(2)	-3(2)

C(337)	22(2)	42(3)	47(3)	1(3)	13(2)	4(2)

Table B.4 Hydrogen coordinates (x 10^4) and isotropic displacement parameters ($Å^2$x 10^3) for [Ag{P(p-tol)$_3$}]ClO_4.CH_3COCH_3.

	x	y	z	U(eq)
H(00A)	8067	459	1165	98
H(00B)	7867	993	522	98
H(00C)	7383	756	1487	98
H(00D)	8364	1842	2848	98
H(00E)	7597	1731	2503	98
H(00F)	8140	1864	1533	98
H(232)	8667	1209	6153	27
H(236)	9770	2393	7499	29
H(23A)	10104	2531	3662	69
H(23B)	9415	2302	3156	69
H(23C)	10059	1927	3273	69
H(23D)	9614	1976	3065	69
H(23E)	10304	2204	3572	69
H(23F)	9660	2580	3454	69
H(233)	9032	1439	4332	33
H(235)	10086	2652	5667	31
H(112)	6773	1890	9939	30
H(113)	6524	2466	11429	28
H(115)	6235	3642	9138	27
H(116)	6471	3063	7646	25
H(11A)	5706	3461	11590	46
H(11B)	6288	3853	11177	46
H(11C)	6452	3401	12090	46
H(122)	5518	1872	8597	28
H(123)	4507	1450	8162	32
H(125)	5286	941	5166	33
H(126)	6321	1333	5630	30
H(12A)	4160	511	6654	58

H(12B)	4086	856	5515	58
H(12C)	3768	1061	6692	58
H(132)	6341	2241	5206	35
H(133)	6828	2702	3682	43
H(135)	8465	2991	5601	39
H(136)	8000	2523	7113	33
H(13A)	8174	2921	2912	70
H(13B)	8397	3386	3755	70
H(13C)	7680	3408	3132	70
H(212)	9998	2062	9705	27
H(213)	10096	2813	10834	30
H(215)	8125	3139	10333	34
H(216)	8010	2378	9263	29
H(21A)	9527	3795	10983	63
H(21B)	9369	3476	12133	63
H(21C)	8768	3742	11426	63
H(222)	9237	1160	10610	31
H(223)	9948	497	11280	31
H(225)	10612	234	8075	27
H(226)	9897	891	7384	23
H(22A)	10974	-345	9552	49
H(22B)	10547	-363	10712	49
H(22C)	11179	25	10605	49
H(312)	8715	96	8166	28
H(313)	9350	-520	9166	31
H(315)	7670	-1062	10704	28
H(316)	7019	-454	9690	22
H(31A)	9462	-1200	10530	51
H(31B)	8836	-1596	10563	51
H(31C)	8927	-1165	11551	51
H(31D)	8688	-1441	11233	51
H(31E)	9315	-1045	11200	51
H(31F)	9223	-1476	10212	51
H(322)	7333	807	5716	28
H(323)	7366	481	3859	35
H(325)	7555	-997	5071	35

H(326)	7488	-684	6945	27
H(32A)	7175	-338	2602	67
H(32B)	7473	-881	3079	67
H(32C)	7971	-407	2759	67
H(332)	6539	758	9783	26
H(333)	5424	668	10375	32
H(335)	5043	-288	7695	33
H(336)	6174	-227	7133	29
H(33A)	4163	497	9242	56
H(33B)	4349	98	10253	56
H(33C)	4161	-124	9012	56

Table B.5 Hydrogen bonds for $[Ag\{P(p\text{-}tol)_3\}_3]ClO_4 \cdot CH_3COCH_3$ (Å and °).

D-H...A	d_{D-H}	$d_{H...A}$	$d_{D...A}$	$<_{DHA}$
C(001)-H(00C)...O(4A)	0.98	2.53	3.27(2)	132.4
C(003)-H(00E)...O(1A)	0.98	2.44	3.3(5)	141.6
C(217)-H(21B)...O(3A)$^{\#1}$	0.98	2.39	3.14(2)	132.3
C(112)-H(112)...O(4A)$^{\#2}$	0.95	2.42	3.08(2)	126.8
C(113)-H(113)...O(2)$^{\#2}$	0.95	2.57	3.423(8)	149.6
C(125)-H(125)...O(3A)	0.95	2.52	3.21(2)	129.4
C(233)-H(233)...O(002)	0.95	2.45	3.395(6)	178.3
C(323)-H(323)...O(1A)	0.95	2.45	3.2(5)	134.5

Symmetry transformations used to generate equivalent atoms:

#1 x+1/2,-y+1/2,z+1 #2 x,y,z+1

C Appendix - $[Ag_4\{P(p\text{-}tol)_3\}_4Br_4]\cdot CH_3COCH_3$

Table C.1 Atomic coordinates (x 10^4) and equivalent isotropic displacement parameters ($Å^2$x 10^3) for $[Ag_4\{P(p\text{-}tol)_3\}_4Br_4]$. U(eq) is defined as one third of the trace of the ortogonalized U^{ij} tensor.

	x	y	z	U(eq)
C(211)	5753(3)	3461(3)	2043(1)	22(1)
C(216)	5854(3)	3921(3)	2277(1)	26(1)
C(215)	5133(3)	3998(3)	2378(1)	28(1)
C(214)	4301(3)	3623(3)	2251(1)	26(1)
C(212)	4922(3)	3103(3)	1910(1)	29(1)
C(213)	4204(3)	3173(3)	2015(1)	33(1)
C(127)	3756(4)	-1765(4)	-9(1)	47(1)
C(217)	3527(3)	3718(4)	2362(1)	38(1)
Ag(1)	6400(1)	1955(1)	934(1)	30(1)
Ag(2)	6667	3333	1429(1)	31(1)
Br(2)	6667	3333	590(1)	24(1)
Br(1)	8031(1)	3111(1)	1211(1)	26(1)
P(21)	6667	3333	1898(1)	21(1)
P(11)	6634(1)	735(1)	789(1)	23(1)
C(111)	7728(3)	1140(3)	626(1)	24(1)
C(121)	5801(3)	-22(3)	551(1)	24(1)
C(115)	9005(3)	979(4)	487(1)	34(1)
C(131)	6608(3)	-21(3)	1046(1)	24(1)
C(116)	8185(3)	651(3)	621(1)	29(1)
C(114)	9383(3)	1806(4)	353(1)	35(1)
C(112)	8116(3)	1979(3)	496(1)	32(1)
C(124)	4471(3)	-1152(3)	186(1)	33(1)
C(126)	4998(3)	8(3)	519(1)	31(1)
C(134)	6530(3)	-1088(3)	1477(1)	32(1)

C(133)	5868(4)	-1431(3)	1286(1)	39(1)
C(132)	5898(3)	-914(3)	1072(1)	35(1)
C(135)	7242(3)	-201(3)	1449(1)	32(1)
C(113)	8926(3)	2295(3)	361(1)	37(1)
C(136)	7282(3)	338(3)	1238(1)	30(1)
C(137)	6467(4)	-1652(4)	1714(1)	44(1)
C(123)	5272(4)	-1185(4)	218(1)	37(1)
C(122)	5929(3)	-626(3)	398(1)	35(1)
C(125)	4346(3)	-551(3)	339(1)	37(1)
C(117)	10279(4)	2171(5)	206(1)	52(2)

Table C.2 Bond lengths (Å) and angles (°) for $[Ag_4\{P(p\text{-}tol)_3\}_4Br_4]$. Symmetry operations appear at the end of the table.

Atoms	Distance (Å)
Ag(1)-P(11)	2.400(1)
Ag(1)-Br(1)$^{\#1}$	2.6516(6)
Ag(1)-Br(2)	2.7748(6)
Ag(1)-Br(1)	2.8335(5)
Ag(1)$^{\#1}$-Ag(2)	3.3163(6)
Ag(1)$^{\#1}$-Br(2)	2.7748(6)
Ag(1)$^{\#2}$-Ag(2)	3.3163(6)
Ag(1)$^{\#2}$-Br(1)	2.6516(6)
Ag(1)$^{\#2}$-Br(2)	2.7748(6)
Ag(2)-P(21)	2.407(2)
Ag(2)-Br(1)	2.7491(5)
Ag(2)-Br(1)$^{\#1}$	2.7491(5)
Ag(2)-Br(1)$^{\#2}$	2.7491(5)
P(11)-C(111)	1.822(4)
P(11)-C(121)	1.818(4)
P(11)-C(131)	1.821(4)
P(21)-C(211)	1.821(4)
P(21)-C(211)$^{\#1}$	1.821(4)
P(21)-C(211)$^{\#2}$	1.821(4)
C(211)-C(216)	1.393(6)

C(211)-C(212)	1.394(6)
C(216)-C(215)	1.387(6)
C(216)-H(216)	0.9300
C(215)-C(214)	1.382(6)
C(215)-H(215)	0.9300
C(214)-C(213)	1.393(6)
C(214)-C(217)	1.505(6)
C(212)-C(213)	1.385(6)
C(212)-H(212)	0.9300
C(213)-H(213)	0.9300
C(127)-C(124)	1.512(7)
C(127)-H(12A)	0.9600
C(127)-H(12B)	0.9600
C(127)-H(12C)	0.9600
C(217)-H(21A)	0.9600
C(217)-H(21B)	0.9600
C(217)-H(21C)	0.9600
C(111)-C(116)	1.382(6)
C(111)-C(112)	1.400(6)
C(121)-C(122)	1.389(6)
C(121)-C(126)	1.392(6)
C(115)-C(116)	1.388(7)
C(115)-C(114)	1.391(7)
C(115)-H(115)	0.9300
C(131)-C(132)	1.385(6)
C(131)-C(136)	1.393(6)
C(116)-H(116)	0.9300
C(114)-C(113)	1.383(8)
C(114)-C(117)	1.520(7)
C(112)-C(113)	1.379(7)
C(112)-H(112)	0.9300
C(124)-C(125)	1.380(7)
C(124)-C(123)	1.390(7)
C(126)-C(125)	1.382(7)
C(126)-H(126)	0.9300
C(134)-C(133)	1.377(7)

C(134)-C(135)	1.381(7)
C(134)-C(137)	1.516(7)
C(133)-C(132)	1.389(7)
C(133)-H(133)	0.9300
C(132)-H(132)	0.9300
C(135)-C(136)	1.392(6)
C(135)-H(135)	0.9300
C(113)-H(113)	0.9300
C(136)-H(136)	0.9300
C(137)-H(13A)	0.9600
C(137)-H(13B)	0.9600
C(137)-H(13C)	0.9600
C(123)-C(122)	1.388(7)
C(123)-H(123)	0.9300
C(122)-H(122)	0.9300
C(125)-H(125)	0.9300
C(117)-H(11A)	0.9600
C(117)-H(11B)	0.9600
C(117)-H(11C)	0.9600

Atoms	Angle (°)
Br(1)-Ag(1)-Br(1)$^{\#1}$	104.93(2)
Br(1)-Ag(1)-Br(2)	92.71(2)
Br(1)-Ag(1)-P(11)	103.06(3)
Br(1)$^{\#1}$-Ag(1)-Br(2)	96.80(2)
Br(1)$^{\#1}$-Ag(1)-P(11)	132.31(3)
Br(2)-Ag(1)-P(11)	119.60(3)
Ag(1)$^{\#1}$-Ag(2)-Ag(1)$^{\#2}$	67.87(14)
Ag(1)$^{\#1}$-Ag(2)-Br(1)	106.11(2)
Ag(1)$^{\#1}$-Ag(2)-Br(1)$^{\#1}$	54.74(1)
Ag(1)$^{\#1}$-Ag(2)-Br(1)$^{\#2}$	50.80(1)
Ag(1)$^{\#1}$-Ag(2)-P(21)	139.866(9)
Ag(1)$^{\#2}$-Ag(2)-Br(1)	50.80(13)
Ag(1)$^{\#2}$-Ag(2)-Br(1)$^{\#1}$	106.11(2)
Ag(1)$^{\#2}$-Ag(2)-Br(1)$^{\#2}$	54.73(1)

Ag(1)$^{\#2}$-Ag(2)-P(21)	139.866(9)
Br(1)-Ag(2)-Br(1)$^{\#1}$	104.62(2)
Br(1)-Ag(2)-Br(1)$^{\#2}$	104.62(2)
Br(1)-Ag(2)-P(21)	113.97(1)
Br(1)$^{\#1}$-Ag(2)-Br(1)$^{\#2}$	104.62(2)
Br(1)$^{\#1}$-Ag(2)-P(21)	113.97(1)
Br(1)$^{\#2}$-Ag(2)-P(21)	113.97(1)
Ag(1)-Br(1)-Ag(1)$^{\#2}$	84.84(2)
Ag(1)-Br(1)-Ag(2)	72.87(2)
Ag(1)$^{\#2}$-Br(1)-Ag(2)	75.74(2)
Ag(1)-Br(2)-Ag(1)$^{\#1}$	83.70(2)
Ag(1)-Br(2)-Ag(1)$^{\#2}$	83.70(2)
Ag(1)$^{\#1}$-Br(2)-Ag(1)$^{\#2}$	83.70(2)
Ag(1)-P(11)-C(111)	113.1(1)
Ag(1)-P(11)-C(121)	114.2(1)
Ag(1)-P(11)-C(111)	114.8(1)
C(111)-P(11)-C(121)	103.7(2)
C(111)-P(11)-C(131)	105.1(2)
C(121)-P(11)-C(131)	104.8(2)
Ag(2)-P(21)-C(211)	114.2(1)
Ag(2)-P(21)-C(211)$^{\#1}$	114.2(1)
Ag(2)-P(21)-C(211)$^{\#2}$	114.2(1)
C(211)-P(21)-C(211)$^{\#1}$	104.4(2)
C(211)-P(21)-C(211)$^{\#2}$	104.4(2)
C(211)$^{\#1}$-P(21)-C(211)$^{\#2}$	104.4(2)
P(11)-C(111)-C(112)	118.2(3)
P(11)-C(111)-C(116)	123.4(3)
P(11)-C(121)-C(122)	123.3(3)
P(11)-C(121)-C(126)	118.7(3)
P(11)-C(131)-C(132)	122.4(3)
P(11)-C(131)-C(136)	118.6(3)
P(21)-C(221)-C(222)	118.5(3)
P(21)-C(221)-C(226)	122.9(3)
C(216)-C(211)-C(212)	118.5(4)
C(215)-C(216)-C(211)	120.3(4)
C(215)-C(216)-H(216)	119.8

C(211)-C(216)-H(216)	119.8
C(214)-C(215)-C(216)	121.3(4)
C(214)-C(215)-H(215)	119.4
C(216)-C(215)-H(215)	119.4
C(215)-C(214)-C(213)	118.3(4)
C(215)-C(214)-C(217)	120.7(4)
C(213)-C(214)-C(217)	121.0(4)
C(213)-C(212)-C(211)	120.6(4)
C(213)-C(212)-H(212)	119.7
C(211)-C(212)-H(212)	119.7
C(212)-C(213)-C(214)	120.9(4)
C(212)-C(213)-H(213)	119.6
C(214)-C(213)-H(213)	119.6
C(124)-C(127)-H(12A)	109.5
C(124)-C(127)-H(12B)	109.5
H(12A)-C(127)-H(12B)	109.5
C(124)-C(127)-H(12C)	109.5
H(12A)-C(127)-H(12C)	109.5
H(12B)-C(127)-H(12C)	109.5
C(214)-C(217)-H(21A)	109.5
C(214)-C(217)-H(21B)	109.5
H(21A)-C(217)-H(21B)	109.5
C(214)-C(217)-H(21C)	109.5
H(21A)-C(217)-H(21C)	109.5
H(21B)-C(217)-H(21C)	109.5
C(116)-C(111)-C(112)	118.4(4)
C(122)-C(121)-C(126)	118.0(4)
C(116)-C(115)-C(114)	120.6(5)
C(116)-C(115)-H(115)	119.7
C(114)-C(115)-H(115)	119.7
C(132)-C(131)-C(136)	118.6(4)
C(111)-C(116)-C(115)	121.0(4)
C(111)-C(116)-H(116)	119.5
C(115)-C(116)-H(116)	119.5
C(113)-C(114)-C(115)	118.2(4)
C(113)-C(114)-C(117)	120.7(5)

C(115)-C(114)-C(117)	121.1(5)
C(113)-C(112)-C(111)	120.1(4)
C(113)-C(112)-H(112)	120.0
C(111)-C(112)-H(112)	120.0
C(125)-C(124)-C(123)	118.2(4)
C(125)-C(124)-C(127)	121.2(5)
C(123)-C(124)-C(127)	120.6(5)
C(125)-C(126)-C(121)	120.8(4)
C(125)-C(126)-H(126)	119.6
C(121)-C(126)-H(126)	119.6
C(133)-C(134)-C(135)	117.7(4)
C(133)-C(134)-C(137)	121.3(5)
C(135)-C(134)-C(137)	121.0(5)
C(134)-C(133)-C(132)	122.0(5)
C(134)-C(133)-H(133)	119.0
C(132)-C(133)-H(133)	119.0
C(131)-C(132)-C(133)	120.0(4)
C(131)-C(132)-H(132)	120.0
C(133)-C(132)-H(132)	120.0
C(134)-C(135)-C(136)	121.4(4)
C(134)-C(135)-H(135)	119.3
C(136)-C(135)-H(135)	119.3
C(112)-C(113)-C(114)	121.7(5)
C(112)-C(113)-H(113)	119.2
C(114)-C(113)-H(113)	119.2
C(135)-C(136)-C(131)	120.2(4)
C(135)-C(136)-H(136)	119.9
C(131)-C(136)-H(136)	119.9
C(134)-C(137)-H(13A)	109.5
C(134)-C(137)-H(13B)	109.5
H(13A)-C(137)-H(13B)	109.5
C(134)-C(137)-H(13C)	109.5
H(13A)-C(137)-H(13C)	109.5
H(13B)-C(137)-H(13C)	109.5
C(122)-C(123)-C(124)	120.8(4)
C(122)-C(123)-H(123)	119.6

C(124)-C(123)-H(123)	119.6
C(123)-C(122)-C(121)	120.8(4)
C(123)-C(122)-H(122)	119.6
C(121)-C(122)-H(122)	119.6
C(124)-C(125)-C(126)	121.3(5)
C(124)-C(125)-H(125)	119.4
C(126)-C(125)-H(125)	119.4
C(114)-C(117)-H(11A)	109.5
C(114)-C(117)-H(11B)	109.5
H(11A)-C(117)-H(11B)	109.5
C(114)-C(117)-H(11C)	109.5
H(11A)-C(117)-H(11C)	109.5
H(11B)-C(117)-H(11C)	109.5

Symmetry transformations used to generate equivalent atoms:

#1 -x+y+1, -x+1, z #2 -y+1, x-y, z

Table C.3 Anisotropic displacement parameters ($Å^2 x\ 10^3$) for $[Ag_4\{P(p\text{-}tol)_3\}_4Br_4]$. The anisotropic displacement factor exponent takes the form: $-2\pi^2[\ h^2a^{*2}U^{11} + ... + 2\ h\ k\ a^*\ b^*\ U^{12}\ ]$

	U^{11}	U^{22}	U^{33}	U^{23}	U^{13}	U^{12}
Ag(1)	38(1)	26(1)	32(1)	-6(1)	-3(1)	19(1)
Ag(2)	36(1)	36(1)	20(1)	0	0	18(1)
Br(1)	26(1)	31(1)	26(1)	-1(1)	-3(1)	16(1)
Br(2)	27(1)	27(1)	19(1)	0	0	14(1)
P(11)	24(1)	21(1)	24(1)	-3(1)	-3(1)	12(1)
P(21)	22(1)	22(1)	18(1)	0	0	11(1)
C(111)	22(2)	24(2)	22(2)	-1(2)	-3(2)	9(2)
C(112)	33(2)	23(2)	36(2)	4(2)	-4(2)	12(2)
C(113)	36(3)	31(2)	32(2)	6(2)	1(2)	7(2)
C(114)	26(2)	41(3)	25(2)	-3(2)	-1(2)	8(2)
C(115)	29(2)	41(3)	33(2)	-2(2)	-2(2)	19(2)
C(116)	29(2)	29(2)	30(2)	3(2)	-1(2)	14(2)
C(117)	38(3)	61(4)	43(3)	5(3)	14(2)	15(3)
C(121)	25(2)	24(2)	22(2)	-2(2)	-1(2)	12(2)

C(122)	28(2)	37(2)	40(3)	-13(2)	-4(2)	17(2)
C(123)	36(3)	37(3)	34(3)	-15(2)	1(2)	14(2)
C(124)	34(2)	32(2)	25(2)	-3(2)	-6(2)	11(2)
C(125)	30(2)	33(2)	48(3)	-7(2)	-12(2)	16(2)
C(126)	29(2)	28(2)	37(2)	-6(2)	-2(2)	16(2)
C(127)	45(3)	40(3)	40(3)	-9(2)	-15(2)	10(2)
C(131)	28(2)	26(2)	22(2)	-1(2)	1(2)	15(2)
C(132)	36(2)	26(2)	36(3)	-1(2)	-9(2)	10(2)
C(133)	44(3)	27(2)	38(3)	5(2)	-3(2)	12(2)
C(134)	43(3)	34(2)	26(2)	2(2)	5(2)	25(2)
C(135)	37(2)	38(2)	22(2)	-2(2)	-2(2)	20(2)
C(136)	31(2)	28(2)	27(2)	0(2)	0(2)	13(2)
C(137)	59(3)	46(3)	32(3)	7(2)	5(2)	30(3)
C(211)	23(2)	22(2)	22(2)	1(1)	1(2)	12(2)
C(212)	27(2)	30(2)	29(2)	-7(2)	-4(2)	14(2)
C(213)	25(2)	35(2)	37(2)	-8(2)	-6(2)	14(2)
C(214)	24(2)	23(2)	32(2)	0(2)	2(2)	11(2)
C(215)	30(2)	27(2)	27(2)	-3(2)	0(2)	15(2)
C(216)	25(2)	28(2)	25(2)	-4(2)	-3(2)	13(2)
C(217)	29(2)	41(3)	46(3)	-8(2)	3(2)	19(2)

Table C.4 Hydrogen coordinates (x 10^4) and isotropic displacement parameters (Å^{2}x 10^3) for [Ag_4{P(p-tol)$_3$}$_4$Br$_4$].

	x	y	z	U(eq)
H(216)	6408	4178	2366	31
H(215)	5211	4307	2534	33
H(212)	4851	2815	1751	35
H(213)	3648	2916	1927	39
H(12A)	3399	-2368	63	70
H(12B)	4051	-1795	-166	70
H(12C)	3363	-1522	-49	70
H(21A)	3052	3133	2421	57
H(21B)	3288	3944	2229	57

H(21C)	3748	4140	2505	57
H(115)	9305	643	487	40
H(116)	7939	95	708	35
H(112)	7826	2325	499	38
H(126)	4898	409	619	37
H(133)	5385	-2029	1301	47
H(132)	5442	-1166	946	42
H(135)	7704	42	1573	38
H(113)	9172	2850	273	45
H(136)	7761	938	1225	35
H(13A)	6075	-1607	1842	65
H(13B)	7066	-1425	1787	65
H(13C)	6220	-2280	1664	65
H(123)	5369	-1587	117	45
H(122)	6462	-656	415	42
H(125)	3814	-521	321	44
H(11A)	10179	2230	25	78
H(11B)	10507	1755	225	78
H(11C)	10717	2759	275	78